The Multi-Regge Limit from the Wilson Loop OPE

TILL BARGHEER,[a,b] VSEVOLOD CHESTNOV,[b] VOLKER SCHOMERUS[b]

[a] *Institut für Theoretische Physik, Leibniz Universität Hannover,*
Appelstraße 2, 30167 Hannover, Germany

[b] *DESY Theory Group, DESY Hamburg,*
Notkestraße 85, D-22603 Hamburg, Germany

{till.bargheer,vsevolod.chestnov,volker.schomerus}@desy.de

Abstract

The finite remainder function for planar, color-ordered, maximally helicity violating scattering processes in $\mathcal{N} = 4$ super Yang–Mills theory possesses a non-vanishing multi-Regge limit that depends on the choice of a Mandelstam region. We analyze the combined multi-Regge collinear limit in all Mandelstam regions through an analytic continuation of the Wilson loop OPE. At leading order, the former is determined by the gluon excitation of the Gubser–Klebanov–Polyakov string. We illustrate the general procedure at the example of the heptagon remainder function at two loops. In this case, the continuation of the leading order terms in the Wilson loop OPE suffices to determine the two-loop multi-Regge heptagon functions in all Mandelstam regions from their symbols. The expressions we obtain are fully consistent with recent results by Del Duca et al.

Contents

1 Introduction

Constructing the scattering amplitudes of a four-dimensional quantum field theory beyond a few orders of perturbation theory has been a long-term challenge for theoretical physics. Back in the 1960s/70s, it gave rise to the analytic S-matrix program, which aimed at reconstructing scattering amplitudes from their analytic properties in the space of complexified kinematic invariants. At that time there existed few tools to make precision predictions at high loop orders, or even at finite coupling. This has changed during the last two decades, in which our understanding of gauge theories in general, and of the maximally supersymmetric $\mathcal{N} = 4$ Yang–Mills (SYM) theory in particular, has advanced significantly. Many new calculational techniques are now available, so that for the first time scattering amplitudes in a 4d gauge theory are accessible even beyond perturbation theory. In the case of $\mathcal{N} = 4$ SYM theory, a concrete one-dimensional model could be identified that describes the corresponding flux tube. This model turned out to be integrable, and its solution allows us to compute scattering amplitudes at any coupling [1–5], though far from the collinear limit many flux tube excitations must be summed, which often restricts practical applications to near-collinear kinematics.

A particularly interesting kinematic limit of scattering theory is the multi-Regge limit. Roughly, it concerns regions in the space of kinematic variables that are probed by particle

colliders, in which the collision of two highly energetic particles produces many new particles of much lower energies which escape the scattering region, along with two particles that carry away most of initial energy. The multi-Regge regime is not only experimentally relevant, but also of significant theoretical interest. First of all, while the limit entails remarkable simplifications, it still has a very rich structure that has been studied extensively in the context of the analytic S-matrix program. In Regge theory, whole classes of Feynman diagrams resum into the exchange of effective particles called Reggeons, which give rise to the famous Regge trajectories. Pole terms in the scattering amplitudes can be associated with single-Reggeon exchange, while the exchange of multi-Reggeon states is seen in cut terms.

The fundamental assumptions Regge theory makes about the analytic structure of partial waves are rooted in fundamental properties of the theory, such as confinement. Hence Regge theory applies to large classes of models, including supersymmetric Yang–Mills theories. These possess the same multi-Regge behavior as their bosonic cousins, at least in the leading logarithmic approximation (LLA). Indeed, over the last decade, Regge theory has been pivotal in pushing the perturbative expansion in $\mathcal{N} = 4$ supersymmetric Yang–Mills theory. When Bern, Dixon, and Smirnov (BDS) proposed their celebrated all-loop formula for color-ordered, maximally helicity violating (MHV) scattering amplitudes of n gluons [6], the mismatch with the expected analytic structure of the S-matrix was clearly demonstrated in the multi-Regge regime [7]. Along with independent evidence from holography [8], this showed that the BDS formula was incomplete beyond five external gluons, and required a finite correction term that is known as the remainder function. In constructing the finite remainder for generic kinematics, predictions of Regge theory have been used as essential boundary data for the perturbative amplitude bootstrap to high loop orders, see [9] and references therein.

In spite of all the simplifications and integrability, constructing the finite remainder function in multi-Regge kinematics remains a challenging problem. For six external gluons, the problem was solved in [10] to all orders, completing a program that was initiated by Bartels et al. [11], who determined the leading logarithmic approximation (LLA) to all orders in the gauge coupling, with extensions to next-to-LLA (NLLA), and next-to-NLLA (NNLLA) in [12] and [13]. The loop expansion of these expressions was studied in [14]. In the strong-coupling limit, the multi-Regge limit of the hexagon remainder function was calculated in [15, 16]. For a larger number of external gluons, results are sparse. The first expressions for the multi-Regge limit of the heptagon remainder function in LLA and in all Mandelstam regions were proposed by Bartels et al. in [17, 18]. All other results to date are restricted to two loops. The symbol of the two-loop remainder function in the multi-Regge limit for any number of external gluons was discussed in [19, 20], and the upgrade to functions was completed in [21–23].

In comparison, the collinear limit that we mentioned in the introductory paragraph is much better understood. In this case, the Wilson loop operator product expansion (OPE) [1–5] allows to obtain exact results that are based on the complete solution of the relevant flux tube, which turns out be quantum integrable. Extracting the analytic structure in general kinematics requires a resummation of all flux-tube excitations, which is very difficult in general. Here, we pursue a different, somewhat indirect route: We exploit the leading collinear behavior of the flux-tube OPE to explore the weak-coupling expansion of Regge theory. While this is certainly much less ambitious than the beautiful all-order derivation of the hexagon remainder in multi-Regge kinematics by Basso et al. [10], the structure of the remainder function becomes richer for higher numbers of gluons. In particular, there exist several disjoint Mandelstam regions, and more cuts that can contribute to the multi-Regge limit of the remainder function.

The main goal here is to obtain constraints on the finite remainder function of $\mathcal{N} = 4$ supersymmetric Yang–Mills theory in multi-Regge kinematics in all Mandelstam regions from the Wilson loop OPE. The Wilson loop OPE allows to compute the remainder function in collinear asymptotics for completely spacelike polygon Wilson loops. Such completely spacelike

configurations define the main sheet of the remainder function. On this sheet, the multi-Regge limit of the remainder function is trivial, since the BDS amplitude is multi-Regge exact. In order to go to non-trivial Mandelstam regions, in which the remainder function possesses a non-vanishing multi-Regge limit, we need to analytically continue the OPE data. Through these analytic continuations, we can obtain the remainder function in a collinear limit of the multi-Regge regime. We shall refer to this limit as a combined multi-Regge collinear limit. A priori, it may not be entirely clear that the collinear limit sees enough of the branch cuts to reach the relevant Mandelstam regions, but we shall provide evidence that this is the case. At the example of the two-loop heptagon remainder function, which is known in all four non-trivial Mandelstam regions, we shall show that our analysis fixes correctly all parameters that cannot be determined from general consistency requirements when we perform the lift from symbols to functions.

Let us briefly outline the content of the following sections. In Section 2, we shall provide some of the kinematical background. In particular, we introduce appropriate coordinates to describe and parametrize multi-Regge kinematics. Then we turn to the collinear limit. We introduce a special set of variables that is particularly well suited in the combined multi-Regge collinear limit, and explain how to perform analytic continuations in the collinear regime. Section 3 contains a lightning review of the flux tube and the Wilson loop OPE. The latter is used to compute leading terms in the collinear limit of the heptagon remainder function. The remaining two sections address the analytic continuation from the main sheet to the various Mandelstam regions. For pedagogical reasons, we start with the hexagon case (Section 4) before turning to the more elaborate heptagon, which admits four Mandelstam regions in which the remainder function does not vanish (Section 5). For all these regions, we perform the analytic continuation. It turns out that the continuation of the leading-order terms in the Wilson loop OPE, along with a few standard requirements, suffice to lift the symbols of the two-loop multi-Regge heptagon to functions. The expressions we obtain for the two-loop heptagon remainders in the multi-Regge regime are fully consistent with recent results by Del Duca et al. [21–23]. We conclude with an extensive outlook to further directions and open problems in Section 6. The paper also includes several technical appendices, in particular on tessellations of the Wilson loop and associated variables for the Wilson loop OPE and multi-Regge limits for all multiplicities (Appendix A). Appendix C provides an extensive analysis of the multi-Regge limit of the two-loop symbol and its lift to the two-loop heptagon function. We show that for the two most interesting Mandelstam regions, single-valuedness, symmetry, and collinear behavior determine the multi-Regge limit of the heptagon remainder up to four parameters. The latter are fixed by our continuation in Section 5.

2 The Multi-Regge Limit

Our ultimate goal is to compute the multi-Regge limit of the finite remainder function for color ordered maximally helicity violating (MHV) amplitudes in the planar limit of $\mathcal{N} = 4$ super Yang–Mills theory from the Wilson loop operator product expansion (OPE). This section contains some background material. After a short reminder on Mandelstam regions and multi-Regge kinematics, we turn to collinear kinematics and introduce a variant of the cross ratios introduced in [1] that is particularly appropriate to discuss the combined multi-Regge collinear limit. The final subsection outlines how we calculate remainder functions in the combined multi-Regge collinear limit from the Wilson loop OPE by summing relevant cut contributions, see (2.23) and (2.24) below.
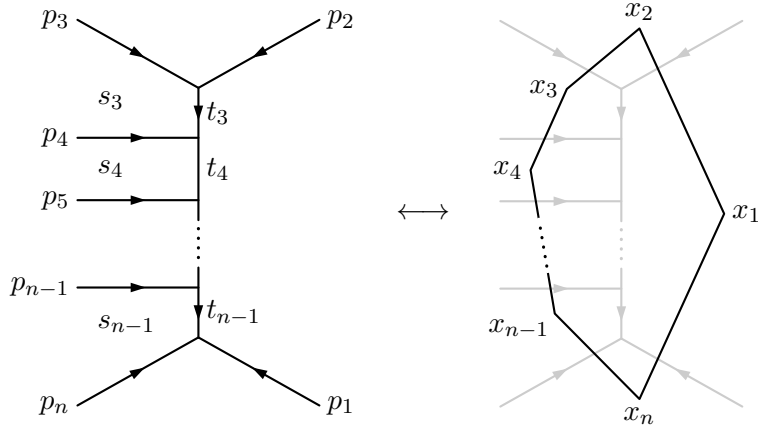
Figure 1: Kinematics of the scattering process $2 \to n - 2$. Forward energies are labeled by s_i, momentum transfers by t_i. On the right-hand side we show a graphical representation of the dual variables x_i.

2.1 Multi-Regge Regime and Mandelstam Regions

We consider the scattering of n gluons. With later kinematical limits in mind we shall think of two incoming particles whose momenta we denote by p_1, p_2 and $n - 2$ outgoing particles of momentum $-p_3, ..., -p_n$, as shown in Figure 1. It will be convenient to label momenta p_i by arbitrary integers i such that $p_{i+n} \equiv p_i$. In the context of $\mathcal{N} = 4$ supersymmetric Yang–Mills theory, it is advantageous to pass to a set of dual variables x_i such that

$$p_i = x_i - x_{i-1}. \tag{2.1}$$

The variables x_i inherit their periodicity $x_{i+n} = x_i$ from the periodicity of the p_i and momentum conservation. Let us also introduce the notation $x_{ij} = x_i - x_j$. The x_{ij}^2 provide a large set of Lorentz invariants $x_{ij}^2 = x_{ji}^2$. Throughout this note, we use a Lorentzian metric with signature $(-, +, +, +)$. When expressed in terms of the momenta, the invariants read

$$x_{ij}^2 = (p_{i+1} + \cdots + p_j)^2. \tag{2.2}$$

Lorentz symmetry along with the mass-shell conditions $p_i^2 = 0$ imply that only $3n - 10$ of these variables are independent. We will not make any specific choice here. On the main sheet, all the energies p_i^0 are assumed to be positive. We will refer to the Mandelstam invariants x_{ij}^2 that are negative on the main sheet as s-like (e. g. forward energies, see Figure 1). Those that obey $x_{ij}^2 \geq 0$ on the main sheet are called t-like (e. g. momentum transfers).

The finite remainder function R for an n-gluon scattering amplitude is invariant under dual conformal symmetry [24], and hence it can only depend on cross ratios of the form

$$U_{ij} \equiv \frac{x_{i+1,j}^2 x_{i,j+1}^2}{x_{ij}^2 x_{i+1,j+1}^2}, \qquad 3 \leq |i - j| < n - 2. \tag{2.3}$$

Since the conformal group in four dimensions has 15 generators, only $3n - 15$ of these cross ratios are independent. For the discussion of the multi-Regge limit, we adopt the following choice [15, 25]

$$u_{j,1} = U_{j-3,j}, \qquad u_{j,2} = U_{j-2,n}, \qquad u_{j,3} = U_{1,j-1}, \tag{2.4}$$

where $j = 5, ..., n - 1$. Note that for $n < 6$ one cannot form any cross ratios, and hence the remainder functions R_n must be trivial for $n = 4, 5$. In the case of $n = 6$ external gluons, however, there exits 3 independent cross ratios, which we shall simply denote by u_1, u_2, u_3. And indeed it

has been argued in [7] that R_6 must be a non-vanishing function of the cross ratios u_i in order to correct for the unphysical analytical structure of the Bern-Dixon-Smirnov (BDS) Ansatz [6].

In the multi-Regge limit, the absolute values of the s-like variables are much larger than the t-like ones, which are kept finite. The precise characterization of the limit in terms of Mandelstam invariants can be found in [25]. Here, we shall mostly focus on the multi-Regge limit of the remainder functions R_n, which depend on the Mandelstam invariants only through the cross ratios u, of which a complete independent set is given in (2.4). In the multi-Regge limit, the so-called "large" cross ratios $u_{j,1}$ tend to $u_{j,1} \sim 1$ while the remaining "small" ones tend to zero, i.e. $u_{j,2}, u_{j,3} \sim 0$. Cross ratios with the same index j approach their limit values such that the following ratios remain finite:

$$\left[\frac{u_{j,2}}{1 - u_{j,1}} \right]^{\mathrm{MRL}} =: \frac{1}{|1 + w_j|^2} \quad , \quad \left[\frac{u_{j,3}}{1 - u_{j,1}} \right]^{\mathrm{MRL}} =: \frac{|w_j|^2}{|1 + w_j|^2} \,, \tag{2.5}$$

These expressions are parametrized by $n - 5$ pairs of so-called "anharmonic ratios" $(w_j, \bar{w}_j)$, $j = 5, \ldots, n - 1$. In the above formulas, $|f(w)|^2$ means $|f(w)|^2 = f(w)f(\bar{w})$, even if w and $\bar{w}$ are not complex conjugates of each other. Our conventions concerning the enumeration of gluons are shown in Figure 1. Here and in the following, the superscript "MRL" instructs us to evaluate the expression in square brackets in multi-Regge kinematics.

We are going to evaluate the multi-Regge limit for functions which possess branch cuts, and so in order to make it well-defined, we need to specify the sheet on which the limit is actually performed. There exist 2^{n-4} different Mandelstam regions that are distinguished by the signs of the energies p_i^0 for $i = 4, \ldots, n - 1$. These regions are reached by continuing the energies p_j^0 of outgoing particles with indices $j \in I \subset \{4, \ldots, n - 1\}$ to negative values. The choice of the subset I labels the different Mandelstam regions.

To each such Mandelstam region I, we associate an n-component object $\varrho^I = (\varrho_j^I)$ such that

$$\varrho_j^I = \begin{cases} -1 & \text{if } j \in I \,, \\ 0 & \text{if } j \in \{1 \equiv n + 1, 2\} \,, \\ +1 & \text{otherwise} \,. \end{cases} \tag{2.6}$$

Since the first and last two entries of ϱ are fixed to take the values $\varrho_2 = 0 = \varrho_{n+1}$ and $\varrho_3 = 1 = \varrho_n$, we will also use the $n - 4$ component $\varrho = (\varrho_i, i = 4, \ldots, n - 1)$ to label Mandelstam regions. When we go into a region $\varrho = (\varrho_i)$, our curve in the space of kinematic invariants may wind around the endpoints of some branch cuts of the remainder function. Physical branch points are typically located at the points $U_{ij} = 0$. The winding numbers of the variables U_{ij} around the points $U_{ij} = 0$ for the various Mandelstam regions are [26][1]

$$n_{ij}(\varrho) = \frac{1}{4} (\varrho_{i+2} - \varrho_{i+1})(\varrho_{j+1} - \varrho_j) \,. \tag{2.7}$$

Let us point out that the numbers n_{ij} take values in the set of half-integers, i.e. $n_{ij} \in \mathbb{Z}/2$. The so-called large cross-ratios that become $u_{ij} \to 1$ in multi-Regge kinematics, however, possess integer winding numbers for all choices of ϱ.

If we perform the multi-Regge limit of the remainder functions R_n in the region in which all the energies are positive (i.e. on the main sheet, which is accessible to the Wilson loop OPE), the result turns out to vanish,

$$[R_n(u, a)]_{++\cdots+}^{\mathrm{MRL}} = 0 \,. \tag{2.8}$$

In other words, in the region $\varrho_0 = (+, +, \ldots, +)$, the BDS formula is actually multi-Regge exact. If it was only for this region, the multi-Regge limit would not be able to see the difference between a vanishing and non-vanishing remainder function.

---

[1]Our conventions here differ from those used in [26] by an overall sign.

As we have anticipated in the introduction, however, there exists other regions in which the Regge limit of the remainder function does not vanish. Of course, the non-vanishing terms must be associated with the cut contributions that are picked up when we analytically continue from the region ϱ_0 into a new region ϱ. Hence, the multi-Regge limit is able to detect that the remainder functions are non-zero, in spite of (2.8).

2.2 Collinear Kinematics and Multi-Regge Limit

In order to be able to study the combined multi-Regge collinear limit, we need to introduce a new parametrization of the null-polygons with cusps at x_i. Natural variables for such polygons arose in the construction of the OPE for null polygon Wilson loops [1,27–29]. We will describe a slightly modified parametrization that features a canonical multi-Regge limit for any number n of edges.

The kinematic variables we shall use in the remainder function depend on the choice of a tessellation of the null-polygon that encodes the kinematic data of the scattering process. Our choice of tessellation is adapted to the $2 \to n-2$ multi-Regge limit we want to investigate below. It differs from the tessellation used in [1,2]. We will tessellate the n-gon into $(n-5)$ internal tetragons and two boundary tetragons by drawing the (unique) null lines from cusps $x_4, \ldots, x_{n-1}$ to line x_{12}, intersecting the line x_{12} at points $x'_4, \ldots, x'_{n-1}$, see Figure 1 and Figure 2 (left). For our tessellation, the variables τ_j, σ_j, ϕ_j, $j = 5, \ldots, n-1$, parametrize the three conformal transformations that stabilize the internal tetragon $(x_{j-1}, x_j, x'_j, x'_{j-1})$. Acting with these conformal transformations on all cusps x_j that lie above that internal tetragon generates all conformally inequivalent configurations.[2] The tetragon variables τ_j, σ_j, ϕ_j can be expressed in terms of the cross ratios $u'_{j,1}$, $u'_{j,2}$, and $u'_{j,3}$ of the surrounding internal hexagon (see Figure 2),

$$
\begin{aligned}
u'_{j,1} &= U_{(j-2)',j,j-2,j+1}\,, \\
u'_{j,2} &= U_{j-2,j+1,j-1,(j+1)'}\,, \qquad U_{i,j,k,l} = \frac{x_{il}^2 x_{jk}^2}{x_{ij}^2 x_{kl}^2}\,, \qquad x_{ij} \equiv |x_i - x_j|\,, \\
u'_{j,3} &= U_{(j+1)',j-1,(j-2)',j}\,,
\end{aligned}
\tag{2.9}
$$

via

$$
u'_{j,1} = \frac{1 - e^{-2\tau_j}}{1 + e^{2\sigma_j} + 2\,e^{\sigma_j - \tau_j}\cos\phi_j}\,, \qquad \frac{u'_{j,2}}{u'_{j,1}} = e^{2\sigma_j}\,, \qquad u'_{j,3} = e^{-2\tau_j}\,.
\tag{2.10}
$$

We shall also use

$$
T_j = e^{-\tau_j}\,, \quad S_j = e^{\sigma_j}\,, \quad F_j = e^{i\phi_j}\,.
\tag{2.11}
$$

See Appendix A for more details and explicit definitions of the variables τ_j, σ_j, ϕ_j.

The limit in which all τ_i are large, that is $T_i \ll 1$, is a multi-collinear limit. This is the limit in which it is easiest to evaluate the Wilson loop OPE formula for the remainder function that we will spell out below. The multi-Regge regime, on the other hand, corresponds to a double scaling limit where $T_i \ll 1$ and $S_j \ll 1$ while the ratios $S_i/T_i \equiv r_i$ are kept finite.

The arguments of large logarithms in the multi-Regge limit are given by

$$
\varepsilon_j = u_{j,2} u_{j,3}\,, \qquad j = 5, \ldots, n-1\,.
\tag{2.12}
$$

Our choice of tessellation is such that each triple of cross ratios $\{u_{j,1}, u_{j,2}, u_{j,3}\}$ is associated to one inner null tetragon, namely the tetragon that is invariant under τ_j, σ_j, and ϕ_j. This is illustrated in Figure 3: in the limit $T_j \to 0$, the upper part of the polygon is flattened to the top of the tetragon, which sends $u_{j,3} \to 0$. In this limit, the variable S_j controls the positions of all cusps on the upper line of the tetragon. Upon sending $S_j \to 0$, all cusps on that line

---

[2]Of course, one can alternatively act with the inverse conformal transformations on the bottom part of the polygon. These two choices are related by a global conformal transformation and hence conformally equivalent.
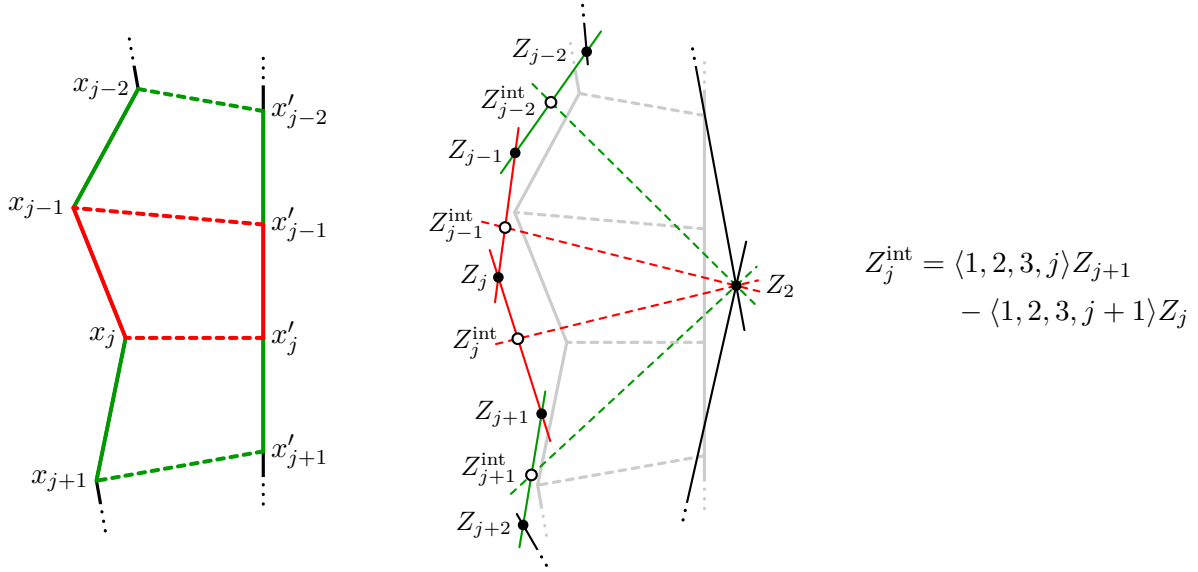
Figure 2: *Left:* Inner tetragon (red) stabilized by τ_j, σ_j, and ϕ_j, together with the surrounding hexagon (green) that defines the cross ratios (2.9). The primed coordinates all lie on the line x_{12}. *Middle:* The corresponding momentum-twistor configuration. *Right:* Formula for the "internal" momentum twistors Z_j^{int} that define the primed coordinates x_j'.

$$Z_j^{\text{int}} = \langle 1, 2, 3, j \rangle Z_{j+1} - \langle 1, 2, 3, j+1 \rangle Z_j$$
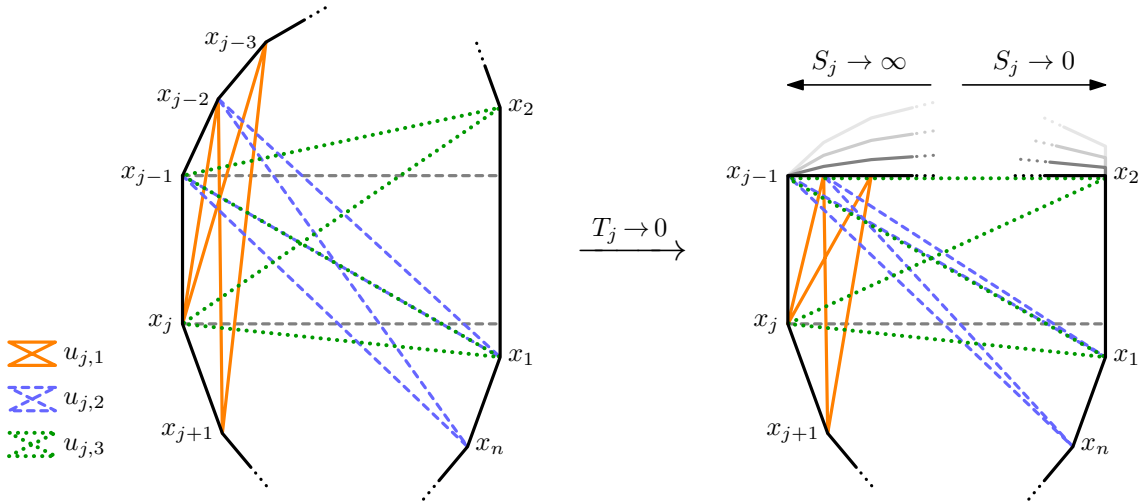
Figure 3: One inner null tetragon (gray dashed lines) with the associated "large" cross ratio $u_{j,1}$ (orange, solid) and "small" cross ratios $u_{j,2}$ (blue, dashed) and $u_{j,3}$ (green, dotted). Upon sending $T_j \to 0$, the upper part of the polygon flattens to the top of the tetragon, implying $u_{j,3} \sim T_j^2 \to 0$. Further sending $S_j \to 0$ shifts all points on the upper null line to the right. Conversely, sending $S_j \to \infty$ shifts all points to the left. One can easily see that $u_{j,1} \to 1$, $u_{j,2} \to 0$ when $S_j \to 0$, as required by the multi-Regge limit.

approach the point x_2 on the right, which implies that $u_{j,1} \to 1$ and $u_{j,2} \to 0$, as required by the multi-Regge limit.[3] More precisely, for fixed j we have

$$u_{j,1} \to 1 + \mathcal{O}(T_j^2)\,, \qquad u_{j,2} \to \mathcal{O}(T_j^2)\,, \tag{2.13}$$

$$u_{j,3} \to \mathcal{O}(T_j^2) \qquad \text{for} \ \ T_j \to 0 \ \text{with} \ S_j/T_j \ \text{fixed.} \tag{2.14}$$

Even though not apparent in Figure 3, all other cross ratios $u_{i,k}$, $i \neq j$, remain finite in this limit. The exact expression of $u_{j,k}$ in terms of $r_j = S_j/T_j$ and F_j depend on the normalizations of τ_j, σ_j, and ϕ_j, as well as on the choice of "reference polygon" obtained when $\tau_j, \sigma_j, \phi_j = 0$. We found it possible to choose normalizations and reference polygons such that with

$$r_i^2 = \frac{S_i^2}{T_i^2} = \frac{1}{w_i \bar{w}_i}\,, \qquad F_i^2 = \frac{w_i}{\bar{w}_i}\,, \qquad S_i^2 T_i^2 = r_i^2 T_i^4 = \varepsilon_i\,, \tag{2.15}$$

the cross ratios satisfy the wanted Regge limit relations (2.5) and (2.12), namely

$$\frac{u_{j,2}}{1 - u_{j,1}} = \frac{1}{|1 + w_j|^2} + \sum_i \mathcal{O}(T_i^2)\,, \qquad \frac{u_{j,3}}{1 - u_{j,1}} = \frac{|w_j|^2}{|1 + w_j|^2} + \sum_i \mathcal{O}(T_i^2)\,,$$

$$u_{j,2}\, u_{j,3} = \varepsilon_j \left(1 + \sum_{i \neq j} \mathcal{O}(T_i^2) \right) + \mathcal{O}(T_j^5)\,, \qquad j = 5, \ldots, n - 1 \tag{2.16}$$

when $T_j \to 0$ with $r_j = S_j/T_j$ fixed for all j. On the other hand, in the multi-collinear limit $T_j \to 0$ with S_j finite for all j, the relevant cross ratios become

$$u_{j,1} = \frac{1 + S_{j-1}^2 (1 + S_j^2)}{(1 + S_{j-1}^2)(1 + S_j^2)} + \sum_i \mathcal{O}(T_i)\,,$$

$$u_{j,2} = \frac{A_j}{1 + A_j} + \sum_i \mathcal{O}(T_i)\,, \qquad u_{j,3} = T_j^2 \left(1 + \sum_{i \neq j} \mathcal{O}(T_i^2) \right)\,, \tag{2.17}$$

where

$$S_j^2 = \frac{A_j}{1 + A_{j+1}}\,. \tag{2.18}$$

In these formulas, the index j runs through $j = 5, \ldots, n - 1$ and we need to supply the boundary conditions

$$A_n = S_4 = 0 \tag{2.19}$$

to make our formulas well defined and give the correct behavior of the cross ratios in the collinear limit. See Appendix A for more details and higher-order expansions.

When discussing the combined multi-Regge collinear limit, the parametrization of the multi-Regge cross ratios (2.4) in general kinematics in terms of the tetragon variables T_j, S_j, F_j that were introduced through eq. (2.10) is well adapted for any number n of external gluons. We do not state general formulas for the $u_{j,a}$ in terms of the tetragon variables here, but will do so for $n = 6, 7$ below. All this requires us to work out relations between the $u'_{j,a}$ defined in eq. (2.9) and the cross ratios (2.4) we use in the multi-Regge limit.

---

[3]Conversely, all points on the upper line approach x_{j-1} on the left when sending $S_j \to \infty$.

2.3 Analytic Continuation in the Collinear Limit

Our goal is to recover the combined multi-Regge collinear limit of the remainder function in all Mandelstam or multi-Regge regions from the Wilson loop OPE. The latter is computed on the main sheet $\varrho = (+, \ldots, +)$ and must be continued into the non-trivial Mandelstam regions along some curve γ. The main goal of this subsection is to set up some notation that allows to evaluate the result of such analytical continuations in collinear kinematics. Since we are only interested in the combined multi-Regge collinear limit, we shall implement the multi-Regge limit throughout.

As we will see in the next section, it is not too difficult to construct the finite remainder function to leading order in the T_i at low number of loops from the Wilson loop OPE. The explicit expressions $R_{n,(l)}^{\text{ope}}$ turn out to contain several functions of the variables S_i which possess branch cuts ending at r hypersurfaces $\sigma_\nu, \nu = 1, \ldots, r$ of co-dimension two in the space of complexified S-variables. We shall choose a set of generators p_ν for the fundamental group π_1 of the complement, i.e. $p_\nu \in \pi_1(\mathbb{C}^{n-5} \setminus \{\sigma_\nu \,|\, \nu = 1, \ldots, r\})$. If we continue the remainder function along a curve $\mathcal{C}_\nu$ associated to the generator p_ν, we may pick up a cut contribution whose multi-Regge limit may or may not vanish.

$$[\mathcal{C}_\nu R_{n,(l)}^{\text{ope}}]^{\text{MRL}} \equiv (1 + 2\pi i \Delta_\nu) R_{n,(l)}^{\text{ope}} . \tag{2.20}$$

Let us now pick an arbitrary element $\gamma \in \pi_1$ in our fundamental group. By construction, γ can be written as a product of p_ν, i.e. it is a finite product of the form $\gamma = \prod_k p_{\nu_k}^{n_k} = p_{\nu_1}^{n_1} p_{\nu_2}^{n_2} \cdots$ with $\nu_k \in \{1, \ldots, r\}$ and $n_k \in \{\pm 1\}$. Note that the fundamental group is not abelian so that the order matters. Continuation along a curve $\mathcal{C}_\gamma$ that is associated to the element γ gives

$$[\mathcal{C}_\gamma R_{n,(l)}^{\text{ope}}]^{\text{MRL}} = \prod_k (1 + 2\pi i \Delta_{\nu_k})^{n_k} R_{n,(l)}^{\text{ope}} = (1 + 2\pi i \Delta_{\nu_1})^{n_1} (1 + 2\pi i \Delta_{\nu_2})^{n_2} \cdots R_{n,(l)}^{\text{ope}} . \tag{2.21}$$

Here, $(1 + 2\pi i \Delta)^{-1}$ is defined as a formal geometric series expansion in $2\pi i \Delta$. Let us make a few comments. First of all, our symbols $(1 + 2\pi i \Delta_\nu)$ are a bit formal. One should first expand all the terms with $n_k = -1$, and then write the right hand side as a sum of 'products' of the Δ_ν. Each of the terms in this sum then stands for *the multi-Regge limit* of a particular multiple cut contribution. We drop the leading term $1 \cdot R_{n,(l)}^{\text{ope}}$, since it vanishes in the multi-Regge limit. We stress that taking the multi-Regge limit does not commute with evaluating cut contributions, i.e. even if the multi-Regge limit $\Delta_\nu R$ of a cut contribution vanishes, the multi-Regge limit $\Delta_\mu \Delta_\nu R$ of a double-cut contribution may not vanish. We shall see examples later on.

The right hand side of eq. (2.21) can now be expanded in the number of cut contributions, starting with those terms that contain a single cut Δ_ν,

$$[\mathcal{C}_\gamma R_{n,(l)}^{\text{ope}}]^{\text{MRL}} = \left(2\pi i \sum_\nu c_\nu \Delta_\nu + (2\pi i)^2 \sum_{\mu,\nu} c_{\mu,\nu} \Delta_\mu \Delta_\nu + \ldots \right) R_{n,(l)}^{\text{ope}} \tag{2.22}$$

Let us point out that the sum on the right hand side is finite at any given loop order l since the maximal number of non-vanishing discontinuities at l loops is $2l - 1$.

In principle, there is a unique curve γ_ϱ associated to each Mandelstam region, and if this curve was known, we could simply compute the combined multi-Regge collinear limit in all regions

$$[R_{n,(l)}^\varrho]^{\text{CL}} = [\mathcal{C}_{\gamma_\varrho} R_{n,(l)}^{\text{ope}}]^{\text{MRL}} \tag{2.23}$$

and obtain strong constraints on the remainder function in multi-Regge kinematics. In practice, however, the curve γ_ϱ is not known, and the equality (2.23),

$$[R_{n,(l)}^\varrho]^{\text{CL}} = \left(2\pi i \sum_\nu c_\nu \Delta_\nu + (2\pi i)^2 \sum_{\mu,\nu} c_{\mu,\nu} \Delta_\mu \Delta_\nu + \ldots \right) R_{n,(l)}^{\text{ope}} \tag{2.24}$$

imposes constraints on both sides of the equation, i.e. on the remainder function in multi-Regge kinematics and on the curve γ_ϱ (through the coefficients c_μ, $c_{\mu,\nu}$ etc.). Eqs. (2.23) or (2.24) are our key to constraining the multi-Regge limits of the remainder function in subsequent sections.

Even though the curve γ_ϱ is not known in general, the coefficients $c_\bullet$ that characterize the discontinuity expansion are not entirely free. The first set of constraints comes from the winding numbers $n_{ij}(\varrho)$ we defined in eq. (2.7). Let us recall that there exists a famous projection from the fundamental or first homotopy group π_1 to the first homology group H_1 of our space $\mathbb{C}^{n-5} \setminus \{\sigma_\nu \mid \nu = 1, \ldots, r\}$. Elements of the latter are characterized by the winding numbers of the former around the endpoints σ_ν of our branch points. Recall that H_1 is an abelian group that is obtained from the non-abelian fundamental group π_1 by equating all commutators to the unit element. This set of winding numbers is clearly not sufficient to determine the associated curve, but it allows us to compute the leading coefficients c_ν. In fact, for each generator p_ν of the fundamental group, one can compute the winding numbers n_{ij}^ν of the cross ratio U_{ij}. These allow to constrain the coefficients $c_\nu = c_\nu(\varrho)$ as

$$\sum_\nu n_{ij}^\nu c_\nu(\varrho) = n_{ij}(\varrho)\,, \tag{2.25}$$

where $n_{ij}(\varrho)$ are the known winding numbers (2.7) of the cross ratios U_{ij} as one continues into the Mandelstam region ϱ. As we will see below, there are as many independent cross ratios U_{ij} as there are generators p_ν, and hence (2.25) completely fixes the coefficients c_ν. In addition to these constraints on the coefficients of single discontinuities, we can also constrain the coefficients of multiple discontinuities. As an example, let us consider the following statement

$$d_{\mu,\nu}(\gamma) := c_{\mu,\nu}(\gamma) + c_{\nu,\mu}(\gamma) = c_\mu(\gamma)c_\nu(\gamma) = c_\mu c_\nu\,, \tag{2.26}$$

which allows to determine the coefficient $c_{\nu,\mu}$ from $c_{\mu,\nu}$ along with the coefficients c_ν of the single discontinuities.

In order to prove this equality, we first note that it is safe to ignore all generators $\mathcal{C}_k$ with $k \neq \mu, \nu$ that may appear in the expression for our curve γ. Hence, for the purpose of computing $c_{\mu,\nu}$ and $c_{\nu,\mu}$ we can think of the curve as a product of p_μ, p_ν and their inverses. Of course, the order in which these factors appear in the curve does matter for the individual coefficients, but not for the anti-commutator $d_{\mu,\nu}$ we defined in eq. (2.26). In fact, since $d_{\mu,\nu}$ is computed from coefficients of double discontinuities, we obtain

$$(1 + 2\pi i \Delta_\mu)^n (1 + 2\pi i \Delta_\nu)^m - (1 + 2\pi i \Delta_\nu)^m (1 + 2\pi i \Delta_\mu)^n$$
$$\sim (1 + 2\pi i\, n\Delta_\mu)(1 + 2\pi i\, m\Delta_\nu) - (1 + 2\pi i\, m\Delta_\nu)(1 + 2\pi i\, n\Delta_\mu) = (2\pi i)^2 nm(\Delta_\mu\Delta_\nu - \Delta_\nu\Delta_\mu).$$

Consequently, in calculating the anti-commutator we do not have to worry about the order of p_μ and p_ν. It is therefore straightforward to compute the anti-commutator from the coefficients of the single discontinuities,

$$d_{\mu,\nu}(\gamma) = d_{\mu,\nu}((1 + \Delta_\mu)^{c_\mu}(1 + \Delta_\nu)^{c_\nu} + \ldots) = d_{\mu,\nu}(c_\mu c_\nu \Delta_\mu \Delta_\nu + \ldots) = c_\mu c_\nu. \tag{2.27}$$

Here, the ellipses stand for terms with $d_{\mu,\nu}(\ldots) = 0$, and c_μ, c_ν are overall numbers of Δ_μ, Δ_ν respectively. This completes the proof of eq. (2.26).

In all this discussion, we have ignored one detail that will start to appear from $n = 7$ external gluons. As we pointed out in Section 2.1, some of the winding numbers of small cross ratios may fail to be integer. The meaning of half-integer winding numbers is simple: We need to allow cross ratios to become negative by going above (winding number $+1/2$) or below (winding number $-1/2$) the origin. Without loss of generality, we choose to append such continuations to the very end of our curves. We shall explain this in more detail below when be discuss the heptagon.

11

3 OPE Expansion to Two Loops

In this section we want to construct the collinear limit of the two-loop heptagon remainder function from the Wilson loop OPE. The result is spelled out in the third subsection. Its derivation needs some background about the flux tube in four-dimensional $\mathcal{N} = 4$ SYM theory and the Wilson loop OPE, which we provide in the first two subsections in order to keep our discussion self-contained. While some parts of the leading collinear terms in the two-loop heptagon remainder function had been computed before, the complete result also contains new terms which we derive in the final subsection, after a short warm-up with a one-loop calculation.

3.1 The Flux Tube or GKP String

The formula for the remainder function that we spell out in the next subsection realizes an old idea in quantum field theory, namely to construct the four-dimensional amplitudes in terms of a one-dimensional quantum system that describes the famous flux tube and its excitations. In the case of $\mathcal{N} = 4$ super Yang–Mills theory, this flux tube is also known as Gubser–Klebanov–Polyakov (GKP) string, referring to the incarnation of the flux tube in the dual AdS_5 geometry [30]. Let us describe some facts about this one-dimensional quantum systems that will become relevant below.

The excitations of the GKP string can be considered as multi-particle states that are built up from a set of single-particle excitations. The set of single-particle excitations is known [31] to consist of six 'scalars' ϕ, eight 'fermions' $\psi, \bar{\psi}$, two 'gluons' $F, \bar{F}$, and so-called 'gluon bound states' $D^k F$ and $D^k \bar{F}$, where k can be any positive integer $k = 1, 2, 3, \ldots$. The names of these excitations refer to their four-dimensional origin. They carry an action of the four-dimensional R-symmetry group SO(6) under which the scalars transform in the vector representations, while fermions ψ and $\bar{\psi}$ are spinors. All gluon bound states, finally, transform as scalars under SO(6). In the one-dimensional system, all the elementary particles can move with some rapidity u. As a consequence of integrability, their dispersion law is known for any value of the coupling parameter g. In fact, these quantities are determined by the famous Beisert–Eden–Staudacher (BES) equation [32], which can be solved to any desired order, both at weak and strong coupling. For us, only the gluon and gluon bound state excitations are relevant. For these, the leading order terms of the energy $E = E(u)$ and the momentum $p(u)$ take the form [31]

$$E_{D^k F}(u) = E_{D^k \bar{F}}(u) = 1 + k + 2g^2 \left(\psi\left(\frac{k+3}{2} + iu \right) + \psi\left(\frac{k+3}{2} - iu \right) - 2\psi(1) \right) + O(g^4) \,, \quad (3.1)$$

and

$$p_{D^k F}(u) = p_{D^k \bar{F}}(u) = 2u + 2ig^2 \left(\psi\left(\frac{k+1}{2} + iu \right) - \psi\left(\frac{k+1}{2} - iu \right) \right) + O(g^4) \,. \quad (3.2)$$

Here, we allow for k to be $k = 0$, in which case the formulas give the dispersion law of the gluon excitations. Let us also mention that the one-particle excitations possess a conserved U(1) charge m, which we shall refer to as helicity. For the gluon bound states, this is simply given by

$$m_{D^k F} = 1 + k \,, \qquad m_{D^k \bar{F}} = -1 - k \,. \quad (3.3)$$

Being a discrete quantum number, m neither depends on the coupling g nor on the rapidity u. To complete the description of single-particle excitations, let us note that the one-particle wave functions $\Psi(u)$ are integrated with a measure that depends on the rapidity. Once again, this measure is known for all one-particle excitations and any coupling. In the case of gluons and gluon bound states, it reads

$$\mu_{D^k F}(u) = \mu_{D^k \bar{F}}(u) = (-1)^{k+1} g^2 \frac{\Gamma(\frac{k+1}{2} + iu)\Gamma(\frac{k+1}{2} - iu)}{\Gamma(k+1)(u^2 + (k+1)^2/4)} + O(g^4) \,. \quad (3.4)$$

Similar formulas also exist for the other one-particle excitations, i.e. the scalars and fermions. Since we won't need them below, we refrain from spelling them out here. Let us only mention that all one-particle excitations satisfy $E_X^{g=0}(u) \geq 1$. Equality holds only for scalars, fermions and gluons, but obviously not for non-trivial gluon bound states.

From the one-particle states, one can now build up multi-particle excitations. These can contain any number N of single-particle excitations, each with its own rapidity $u_a, a = 1, \ldots, N$. Since the GKP string is integrable, the energy E, momentum p and helicity m of such multi-particle states can be computed as the sum of their single-particle constituents. The interaction between the single-particle excitations is described by a factorizable S-matrix, i.e. it can be built from the two-particle S-matrix. The latter is also known explicitly, but since we will not need it here, at least not directly, we will not give explicit formulas.

3.2   Wilson Loop OPE and Finite Remainder

After this preparation, we are now able to state the main result from [1–3,5]. According to Basso et al., the finite remainder function of a color ordered planar MHV n-gluon amplitude in $\mathcal{N} = 4$ super Yang–Mills theory is given by

$$R_g(\tau_i, \sigma_i, \varphi_i) = \log \mathcal{W}_g(\tau_i, \sigma_i, \varphi_i) - \log \mathcal{W}_g^{\mathrm{BDS}}(\tau_i, \sigma_i, \varphi_i) \qquad (3.5)$$

where the first term takes the form[4]

$$\mathcal{W}_g(\tau_i, \sigma_i, \varphi_i) = \sum_{\Psi_i} \left[\prod_{i=1}^{n-5} e^{E_i^g \tau_i \pm i p_i^g \sigma_i + i m_i \varphi_i} \right] P_g(0|\Psi_1) P_g(\Psi_1|\Psi_2) \ldots P_g(\Psi_{n-5}|0) \ . \qquad (3.6)$$

Let us explain the individual pieces of this formula. First of all, we need to discuss the summation. The $n - 5$ objects $\Psi_i, i = 1, \ldots n - 5$ that we sum over are $n - 5$ multi-particle excitations of the GKP string. Hence the sum consists of a discrete (but infinite) summation over the single-particle content of the multi-particle states, along with an integration over the rapidity variables. The rapidity integration must be performed with the appropriate measure $\mu^g(u)$. To be quite precise, it should also contain appropriate symmetry factors that depend on the exact multi-particle content, but we will not need these below.

E_i, p_i, and m_i denote the energy, momentum, and helicity of these multi-particle states. Recall that these are simply obtained by summing the energy, momentum, and helicity of the single-particle constituents. The kinematic invariants τ_i, σ_i, and φ_i of our scattering process multiply the energies, momenta, and helicities. Finally, the factors P are known as pentagon transitions. One should think of them as being determined uniquely by the S-matrix of the GKP string. For gluon excitations, the pentagon transitions are

$$P_{FF}(u|v) = P_{\bar{F}\bar{F}}(u|v) = -\frac{1}{g^2} \frac{\Gamma(iu - iv)}{\Gamma(-\frac{1}{2} + iu)\Gamma(-\frac{1}{2} - iv)} + O(g^0) \,, \qquad (3.7)$$

$$P_{F\bar{F}}(u|v) = P_{\bar{F}F}(u|v) = \frac{\Gamma(2 + iu - iv)}{\Gamma(\frac{3}{2} + iu)\Gamma(\frac{3}{2} - iv)} + O(g^2) \,, \qquad (3.8)$$

and $P_F(0|u) = 1 = P_{\bar{F}}(0|u)$. The formulas can be extended to any pair of multi-particle excitations, and in particular to gluon bound states and their multi-particle composites. We will not need these formulas below. Let us only mention that $P(\Psi_1|\Psi_2)$ satisfies an important selection

---

[4]The expression we display here differs from the one in [1] by the $\pm$ in front of the σ_i. In our formula, the sign alternates depending on whether i is even or odd. The difference is caused by the different orientations of the internal squares in the tessellation we adopted to describe the combined multi-Regge collinear limit, see Section 2.2.

rule. As we pointed out above, all single-particle excitations transform under the space-time R-symmetry SO(6). The action on single-particle states induces an action on the multi-particle states Ψ_1 and Ψ_2. The pentagon transition $P(\Psi_1|\Psi_2)$ intertwines this action. Since the vacuum 0 of the GKP string is SO(6) invariant, the transition $P(0|\Psi)$ can only be non-zero if the action of SO(6) on Ψ contains a trivial subrepresentation. If Ψ is a single-particle state, it must be a gluon or gluon bound state in order for $P(0|\Psi)$ to be non-trivial.

It remains to describe the second term in eq. (3.5), namely the functions $\mathcal{W}^{\mathrm{BDS}}$. It is given by

$$\log \mathcal{W}_g^{\mathrm{BDS}}(\tau_i, \sigma_i, \varphi_i) = \frac{\Gamma_{\mathrm{cusp}}(g)}{4g^2} (\log \mathcal{W}_g)^{(1)}(\tau_i, \sigma_i, \varphi_i) \,, \tag{3.9}$$

where $(\log \mathcal{W}_g)^{(1)}$ denotes the one-loop part of the function $\log \mathcal{W}_g$ defined in eq. (3.6). We divide by $4g^2$ in order to remove the dependence on the coupling from the one-loop result, and then multiply with the so-called cusp anomalous dimension Γ_{cusp}. The latter describes the vacuum energy of the GKP string, and it is also known for any value of the coupling. Its weak coupling expansion reads

$$\Gamma_{\mathrm{cusp}}(g) = 4g^2 - \frac{4\pi^2}{3}g^4 + O(g^6) \,. \tag{3.10}$$

It is not too difficult to work out explicit formulas for the function $\mathcal{W}^{\mathrm{BDS}}$ for any number of external gluons.

3.3 The Heptagon Remainder Function

We now describe the hexagon and heptagon remainder functions in the collinear limit at two loops. We first discuss the general structure of the collinear expansion in a bit more detail, mainly to fix our notation. Then, we state our results on the two-loop heptagon remainder function. We restrict ourselves to the first non-trivial terms in the collinear expansion of eq. (3.6): For $n \in \{6, 7\}$ we consider the two-loop term proportional to g^4 with only the lowest corrections to the asymptotic expansion in $T_i \to 0$. As it was shown in [2], only the one-gluon excitation can contribute to these terms, which makes the problem much more manageable.

Let us start with putting more structure to eqs. (3.5) and (3.6), following [2]. For the hexagon, the collinear ($T_5 \to 0$) expansion at weak coupling takes the form (see eq. (35) in [2])

$$\mathcal{W}_{\mathrm{hex}} = 1 + 2T_5 \cos(\phi_5)\, \tilde{f}_5(T_5, S_5) + \mathcal{O}(T^2) \,, \tag{3.11}$$

where the second term proportional to $\tilde{f}_5$ comes form the propagation of a one-gluon excitation through the only internal square of hexagon (see also Section 2.1). Similarly, the leading term in the collinear ($T_i \to 0$) expansion of the heptagon is (see eq. (38) in [2]):

$$\begin{aligned} \mathcal{W}_{\mathrm{hep}} = 1 &+ 2T_5 \cos(\phi_5)\, \tilde{f}_5(T_5, S_5) + 2T_6 \cos(\phi_6)\, \tilde{f}_6(T_6, S_6) \\ &+ 2T_5 T_6 \cos(\phi_5 + \phi_6)\, h_{56}(T_5, T_6, S_5, S_6) \\ &+ 2T_5 T_6 \cos(\phi_5 - \phi_6)\, \bar{h}_{56}(T_5, T_6, S_5, S_6) + \mathcal{O}(T^2) \,. \end{aligned} \tag{3.12}$$

Here, the first line comes from the one-gluon excitation in either of the internal squares of the heptagon, and the second and third lines from excitations in both of the squares. The hexagon functions $\tilde{f}_5$ and $\tilde{f}_6$ are identical up to an inversion of S_6:

$$\tilde{f}_5(T, S) \equiv \tilde{f}(T, S) \,, \quad \tilde{f}_6(T, S) \equiv \tilde{f}(T, 1/S) \,, \tag{3.13}$$

where $\tilde{f}(T, S)$ is the usual hexagon function of [2]. The heptagon functions $h_{56} \equiv h$ and $\bar{h}_{56} \equiv \bar{h}$ are also defined in [2]. The inversion of the S-variable in the hexagon function $\tilde{f}_6$ comes about because one of the two internal squares in the tessellation employed by [1, 2] is horizontally

14

flipped with respect to the other, whereas in our tessellation, all internal squares are oriented the same way (see Section 2 and Appendix A). For the same reason, the argument S_6 in the heptagon functions is inverted with respect to [2]:

$$h^{\text{here}}(T_5, T_6, S_5, S_6) = h^{\text{BSV}}(T_5, T_6, S_5, 1/S_6),$$
$$\bar{h}^{\text{here}}(T_5, T_6, S_5, S_6) = \bar{h}^{\text{BSV}}(T_5, T_6, S_5, 1/S_6). \tag{3.14}$$

The hexagon and heptagon functions are graded in powers of $\log(T_i)$:

$$\tilde{f}(T, S) = \sum_{L \geq 1} \sum_{p=0}^{L-1} \tilde{f}_L^{(p)} (\log(T))^p, \tag{3.15}$$

$$h(T_5, T_6, S_5, S_6) = \sum_{L \geq 1} \sum_{p_5, p_6} h_L^{(p_5, p_6)} (\log(T_5))^{p_5} (\log(T_6))^{p_6}, \tag{3.16}$$

$$\bar{h}(T_5, T_6, S_5, S_6) = \sum_{L \geq 1} \sum_{p_5, p_6} \bar{h}_L^{(p_5, p_6)} (\log(T_5))^{p_5} (\log(T_6))^{p_6}, \tag{3.17}$$

where the inner sum on the second line covers the $0 \leq p_5 + p_6 \leq L - 1$ domain, whereas the inner sum in the last line covers $0 \leq p_5 + p_6 \leq L - 2$. The components $\tilde{f}_L^{(p)}$, $h_L^{(p_5, p_6)}$, and $\bar{h}_L^{(p_5, p_6)}$ are proportional to g^{2L}. The relevant terms in this grading up to two-loop order are

$$\tilde{f}(T, S) = \tilde{f}_1^{(0)}(S) + \tilde{f}_2^{(0)}(S) + \log(T) \tilde{f}_2^{(1)}(S) + \dots, \tag{3.18}$$

$$h(T_5, T_6, S_5, S_6) = h_1^{(0,0)}(S_5, S_6) + h_2^{(0,0)}(S_5, S_6)$$
$$+ \log(T_5) h_2^{(1,0)}(S_5, S_6) + \log(T_6) h_2^{(0,1)}(S_5, S_6) + \dots, \tag{3.19}$$

$$\bar{h}(S_5, S_6) = \bar{h}_2^{(0,0)}(S_5, S_6) + \dots. \tag{3.20}$$

The component functions $\tilde{f}_L^{(0)}$, $\tilde{f}_L^{(1)}$, $h_L^{(0,0)}$, and $\bar{h}_L^{(0,0)}$ to two loop order can be found in the literature, see the discussion around eqs. (118), (125) and (126) in [2] as well as the file `Functionshf.nb` accompanying that paper, and eq. (62) in [33] together with the file `MHV_full.m` there. For $\tilde{f}_2^{(0)}$ and $\tilde{f}_2^{(1)}$, see also (4.14) and (4.15) below. The only missing pieces that we need to compute ourselves are the functions $h_2^{(1,0)}$ and $h_2^{(0,1)}$ that appear at two loops. As we shall show below, the first of these functions is given by

$$h_2^{(1,0)}(S_5, S_6) = \frac{2g^4}{S_5 S_6} \Big[(1 + S_5^2) \log(1 + S_5^2) \Big(\log(1 + S_5^2) - \log(S_5^2) - 2 \Big) - 2S_5^2 S_6^2 \log(S_5^2)$$
$$- 2S_5^2(1 + S_6^2) \log(1 + S_6^2) + (1 + S_5^2 + S_5^2 S_6^2) \log(1 + S_5^2 + S_5^2 S_6^2) \cdot$$
$$\cdot \Big(2 + \log(S_5^2) + \log(1 + S_6^2) - \log(1 + S_5^2 + S_5^2 S_6^2) \Big) \Big]. \tag{3.21}$$

The second function is then obtained by an inversion of the S-variables, i.e.

$$h_2^{(0,1)}(S_5, S_6) = h_2^{(1,0)}(1/S_6, 1/S_5). \tag{3.22}$$

The general one-gluon contribution to the OPE of the heptagon remainder function is given in eq. (39) of [2][5]

$$h = \int \frac{du_5 du_6}{4\pi^2} \mu(u_5) P(-u_5 | u_6) \mu(u_6) e^{-\tau_5 E(u_5) + ip(u_5)\sigma_5 - \tau_6 E(u_6) - ip(u_6)\sigma_6}. \tag{3.23}$$

The helicity-breaking transition $\bar{h}$ has the same form with $P \to \bar{P}$. In the following two subsections, we will describe how one can obtain explicit results for all of the building blocks in eqs. (3.18, 3.19, 3.20) from the OPE integral (3.23).

---

[5]Note the change of sign in σ_6 with respect to the conventions in [2]. This is caused by our choice of tessellation, see the comments above.

3.4 Evaluation of the Collinear Remainder Function

The goal of this final subsection is to provide a brief sketch of the methods that allow to evaluate the remainder function in the collinear limit. Before we dive into the full complexity of the two-loop integral (3.19), we first calculate the function $h_1^{(0,0)}$ at one loop in order to illustrate the main steps in a more pedagogical setting.

3.4.1 One-loop Remainder Function

The one-loop contribution $h_1^{(0,0)}$ comes from the first term in the g^2 expansion of the integral (3.23)

$$h_1^{(0,0)} = g^2 \int \frac{du_5 \, du_6}{4\pi^2} e^{2i(\sigma_5 u_5 - \sigma_6 u_6)} \frac{\Gamma(\frac{3}{2} + iu_5)\Gamma(-iu_5 - iu_6)\Gamma(\frac{3}{2} + iu_6)}{(u_5^2 + \frac{1}{4})(u_6^2 + \frac{1}{4})} . \tag{3.24}$$

We compute this integral via the residue theorem. The u_5–contour of integration can be closed in the upper half-plane so that only the poles at $u_{5,\text{pole}} = i(\frac{1}{2} + k_5)$, $k_5 \in \mathbb{Z}_{\geq 0}$ contribute. Following [33] we take $u_5 = u_{5,\text{pole}} + \varepsilon$ and pick the ε^{-1}–term in the series expansion $\varepsilon \to 0$ to compute the residue. We then repeat the same procedure for u_6 and arrive at the following double sum over poles,

$$h_1^{(0,0)} = g^2 \frac{S_6}{S_5} \Bigg[\sum_{k_5,6 \in \mathbb{Z}_{\geq 1}} \frac{(-S_5^{-2})^{k_5}(-S_6^2)^{k_6}}{(k_5+1)(k_6+1)k_5 k_6} \times \frac{\Gamma(1 + k_5 + k_6)}{\Gamma(k_5)\Gamma(k_6)}$$
$$+ \sum_{k_5 \in \mathbb{Z}_{\geq 1}} \frac{(-S_5^{-2})^{k_5} + (-S_6^2)^{k_5}}{k_5 + 1} + 1 \Bigg], \tag{3.25}$$

where in the second line we combined the $k_5 = 0$ and $k_6 = 0$ residues together into one separate term. These sums turn out to be very easy to perform, and in Appendix B we explain how one can express them in terms of simple logarithms, so that the helicity-preserving function $h_1^{(0,0)}$ takes the form

$$h_1^{(0,0)} = g^2 \left(\frac{S_5}{2S_6} \log \frac{1 + S_5^2 + S_5^2 S_6^2}{(1 + S_5^2)(1 + S_6^2)} + S_5 S_6 \log \frac{1 + S_5^2 + S_5^2 S_6^2}{S_5^2(1 + S_6^2)} + (S_5 \leftrightarrow 1/S_6) \right). \tag{3.26}$$

Let us furthermore note that the helicity-breaking transition starts only at g^4, i.e. the one-loop contribution $\bar{h}_1^{(0,0)} = 0$ vanishes, see eq. (124) of [2]. After this preparation, we can proceed to higher loops.

3.4.2 Higher-Loop Remainder Function

Here we describe the procedure to compute the higher terms in the g^2-expansion of the 1-gluon contribution to the remainder function in terms of multiple polylogarithms, which mostly follows [33] and [34]. The idea is exactly the same as we applied in the previous Section 3.4.1: First we need to extract the desired loop contribution from the integral (3.23), then we apply the residue theorem to convert the integrals into sums over poles. These sums can finally be expressed in terms of multiple polylogarithms.

When expanded to higher loops, the schematic structure of the integrand in eq. (3.23) becomes:

$$\frac{e^{2i(\sigma_5 u_5 - \sigma_6 u_6)}}{\prod_{j=5,6} (u_j + \frac{i}{2})^{r_j}(u_j - \frac{i}{2})^{p_j}} \cdot \Gamma(\tfrac{3}{2} + iu_5)\Gamma(-iu_5 - iu_6)\Gamma(\tfrac{3}{2} + iu_6) \times$$
$$\times \mathcal{Q}\Big(\Big\{ u_j, \psi^{(m_j)}(\tfrac{1}{2} \pm iu_j), \psi^{(n_j)}(\tfrac{3}{2} \pm iu_j) \Big\}_{j=5,6} \Big). \tag{3.27}$$

Compared to our discussion in the previous Section 3.4.1, the Γ-functions do not change, the denominators acquire integer exponents r_j and p_j, and a polynomial $\mathcal{Q}$ of the rapidities u_j and ψ-functions of various weight appear. The location of the relevant poles stays the same, only the residues become more complicated. Therefore, we use the same procedure as above to convert the integral (3.27) into a sum over residues. As in [33], a few basic relations for Γ- and ψ-functions turn out to be very useful in this step,

$$\Gamma(z)\Gamma(1-z) = \frac{\pi}{\sin \pi z}\,,$$

$$\psi^{(n)}(z+1) = \psi^{(n)}(z) + (-1)^n n! z^{-n-1}\,,$$

$$\psi^{(n)}(z) = (-1)^n \psi^{(n)}(1-z) - \pi \partial_z^n \cot(\pi z)\,.$$

After some processing, we arrive at the following L-loop analogue of eq. (3.25):

$$h_L^{(p_5,p_6)} = \sum_{k_{5,6}\in\mathbb{Z}_{\geq 1}} \frac{(-S_5^{-2})^{k_5}(-S_6^2)^{k_6}}{\prod_{j=5,6}(k_j)^{p_j}(1+k_j)^{r_j}} \cdot \frac{\Gamma(1+k_5+k_6)}{\Gamma(k_5)\Gamma(k_6)} \times \mathcal{P}\Big(\big\{k_j, \psi_{k_j}^{(m_j)}, \psi_{1+k_j}^{(n_j)}\big\}_{j=5,6}\Big)\,, \quad (3.28)$$

where we have introduced shorthands $\psi_k^{(m)} := \psi^{(m)}(k)$ for polygamma functions of integer arguments. On the right hand side of eq. (3.28), the polynomial $\mathcal{P}$ depends on both the summation indices k_5, k_6 and ψ-functions of weight $m_j, n_j < 2L$, the powers of common denominators p_j, r_j are bounded by the number of loops as well. This double sum cannot be done in full generality for arbitrary loop number, but for every fixed number of loops, we can make use of algorithms developed in [35]. In order to do so, we replace the Γ-functions with a binomial $\binom{k_5+k_6}{k_5}$, introduce a new variable $j = k_5 + k_6$, and express ψ-functions in terms of so-called S-sums (see eq. (3) in [35])

$$S(n; m_1, \ldots, m_k; x_1, \ldots, x_k) = \sum_{i=1}^{n} \frac{x_1^i}{i_1^m} S(i; m_2, \ldots, m_k; x_2, \ldots, x_k)\,. \quad (3.29)$$

The ψ-functions of integer arguments are related to these objects via

$$\psi_k = -\gamma_{\mathrm{E}} + S(k-1,1,1) \quad (3.30)$$

$$\psi_k^{(m)} = (-1)^{m+1} m! \left(\zeta_{m+1} - S(k-1, m+1, 1)\right)\,. \quad (3.31)$$

After all these conversions, we make use of the XSUMMER package [36] for FORM [37] that rewrites these sums over residues in terms of multiple polylogarithms (see also [35] for a description of the algorithm). Since the only missing pieces at two loops are the functions $h_2^{(1,0)}$ and $h_2^{(0,1)}$ in eq. (3.21), we can just filter the corresponding terms with $\tau_i \equiv \log(T_i)$ that come from the g^2 corrections to the gluon energy (3.1) in the two-loop expansion of eq. (3.23), perform the residue resummation, and convert the produced answer to classical polylogarithms using the package [38], which finally yields (3.21) and (3.22).

With all this, we are finally able to write the full expression (3.12) for the two-loop remainder function in collinear kinematics in terms of only classical polylogarithms $\{\log, \mathrm{Li}_2, \mathrm{Li}_3\}$. This form of the answer makes it easy to understand the analytical structure, and hence it provides an ideal starting point for our discussion in the next sections.

4 Continuation and Regge Limit: The Hexagon

In this section, we now turn to the central theme of this work, namely the continuation of the collinear remainder function from the main sheet into non-trivial Mandelstam regions. Our goal

here is to illustrate the general procedure at the simplest example, namely the hexagon.[6] After a brief review of the relevant coordinates and limits, we will discuss existing results for the only Mandelstam region in which the Regge limit of the hexagon remainder function is non-vanishing and can be computed to any desired order. We will state the known results for two loops in the combined multi-Regge collinear limit. Then we turn to the continuation in collinear kinematics. Starting from the main sheet, we discuss how to reach the Mandelstam region and compute the relevant cut contributions. We shall show how the continuation allows to recover the two-loop result for the combined multi-Regge collinear limit of the remainder function from the leading terms in the Wilson loop OPE.

4.1 Variables and Limits

Let us now specialize the discussion of kinematics in Section 2.2 to the case of $n = 6$ external gluons, for which the finite remainder function depends on just three cross ratios, which we denote as

$$u_1 = U_{25} , \quad u_2 = U_{36} , \quad u_3 = U_{14} ,$$

omitting the first index $j = 5$ in eqs. (2.4). According to the general prescription, the multi-Regge regime is reached when the "large" cross ratio u_1 approaches $u_1 = 1$, while the "small" cross ratios go to zero, i. e.

$$u_1 \to 1 , \qquad u_2 \to 0 , \qquad u_3 \to 0 . \tag{4.1}$$

The ratios of vanishing terms remain finite, and are used to define a single pair of anharmonic ratios $w = w_5$ and $\bar{w} = \bar{w}_5$ as

$$\frac{u_2}{1 - u_1} \to \frac{1}{|1 + w|^2} , \qquad \frac{u_3}{1 - u_1} \to \frac{|w|^2}{|1 + w|^2} . \tag{4.2}$$

For $n = 6$ the approach to the Regge regime is controlled through a single parameter,[7]

$$\varepsilon = u_2 u_3 . \tag{4.3}$$

that tends to zero in the limit.

Next we want to discuss the relation with the kinematic variables we have used in our discussion of the Wilson loop OPE. We can express the three cross ratios u_i through the kinematical variables $T \equiv T_5$, $S \equiv S_5$ and $F \equiv F_5 = \exp(i\varphi)$ we have introduced above as,

$$u_1 = U_{2,5} = \frac{1 - T^2}{1 + S^2 + 2ST \cos \varphi} , \quad u_2 = U_{3,6} = \frac{S^2(1 - T^2)}{1 + S^2 + 2ST \cos \varphi} , \quad u_3 = U_{1,4} = T^2 . \tag{4.4}$$

When comparing with our expressions in eq. (2.10), we use the identifications $x_3' = x_2$ and $x_6' = x_1$ for $n = 6$ to show that

$$u_1' = U_{3',5,3,6} = U_{2,5,3,6} = U_{2,5} = u_1 , \qquad u_2' = U_{3,6,4,6'} = U_{3,6,4,1} = U_{3,6} = u_2 ,$$

$$u_3' = U_{6',4,3',5} = U_{1,4,2,5} = U_{1,4} = u_3 .$$

---

[6]The analytic continuation of the perturbative expansion of the hexagon Wilson loop OPE has been explored before: Using a specific choice of continuation path, Hatsuda [39] could match the analytically continued collinear expansion against known Regge-limit data up to the next-to-next-to-leading logarithmic approximation (N²LLA) at five loops, and produced predictions for N³LLA and N⁴LLA. That work preceded the all-order continuation of the hexagon carried out in [10].

[7]Note that our normalization of the parameter ε differs from the one used by Dixon et al. [40], see footnote 2 in [20], but it is consistent with eqs. (4.8) and (4.9).

In the collinear limit, the relations (4.4) read

$$u_1 = \frac{1}{1+S^2} + \mathcal{O}(T), \quad u_2 = \frac{S^2}{1+S^2} + \mathcal{O}(T^3), \quad u_3 = T^2. \tag{4.5}$$

This coincides with our claim in eqs. (2.17) if we take into account that $S_4 = 0$ and $S^2 = S_5^2 = A_5$ for $n = 6$. When parametrized in terms of S, T, and $F = \exp(i\varphi)$, the Regge limit is taken by sending both T and S to zero, while keeping $r = S/T$ finite, i.e. in the Regge limit, the remainder function depends on the finite variables r and F along with the quantity T that vanishes in the limit. These are related to $w, \bar{w}$ and ε through

$$r^2 = \frac{1}{w\bar{w}}, \qquad F^2 = \frac{w}{\bar{w}}, \qquad S^2 T^2 = r^2 T^4 = \varepsilon, \tag{4.6}$$

as in (2.15). This concludes our brief summary of the relevant variables and limits that are used in the subsequent analysis of the hexagon remainder function.

4.2 The Remainder Function in Multi-Regge Kinematics

For the hexagon $n = 6$, the remainder function is well known to possess only one Mandelstam region with a non-trivial Regge limit, namely the region $\varrho = (--)$. In this region, the two-loop contribution to the finite remainder function in multi-Regge kinematics reads

$$R_{6,(2)}^{--}(\varepsilon, w) = 2\pi i\, f(\varepsilon; w) = 2\pi i \big(f_1(w) \log \varepsilon + f_0(w) \big), \tag{4.7}$$

where the leading logarithmic term contains the coefficient

$$f_1(w) = \frac{1}{2} \log |1+w|^2 \log \left| \frac{1+w}{w} \right|^2, \tag{4.8}$$

while the next-to-leading logarithmic term is given by

$$f_0(w) = -4\,\mathrm{Li}_3(-w) - 4\,\mathrm{Li}_3(-\bar{w}) + 2 \log |w|^2 \big(\mathrm{Li}_2(-w) + \mathrm{Li}_2(-\bar{w}) \big)$$

$$+ \frac{1}{3} \log^2 |1+w|^2 \log \frac{|w|^6}{|1+w|^4} - \frac{1}{2} \log |1+w|^2 \log \left| \frac{1+w}{w} \right|^2 \log \frac{|w|^2}{|1+w|^4}. \tag{4.9}$$

We use the variables that were introduced in the previous subsection. This formula can be derived from the general expression for the six-gluon remainder function due to [11] that in its original version encodes at least the leading logarithmic (LL) terms to all loop orders. The result of Bartels et al. parametrizes the multi-Regge limit of the remainder function in terms of two functions of the coupling g, the impact factor and the so-called BFKL eigenvalue. These possess a power series expansion in g. In order to construct the LL contributions of the remainder function at any loop order, it is sufficient to know the leading terms in these expansions. It is not too difficult to reconstruct the LLA in eq. (4.7) from the results in [11], and in fact to carry out these computations to higher loop orders, and even beyond the leading logarithmic order, see [14] for an extensive discussion. Explicit expressions for the impact factor and BFKL eigenvalue in NLLA were first given in [12].

If we apply the combined multi-Regge collinear limit, i.e. send $r^2 = 1/(w\bar{w})$ to infinity while keeping the ratio $w/\bar{w} = F^2$ finite, these formulas reduce to

$$\left[\tfrac{1}{2\pi i} R_{6,(2)}^{--} \right]^{\mathrm{CL}} = C\, 2 \log(r) \log(\varepsilon) + C \big(8 + 8 \log(r) + 4 \log(r)^2 \big), \tag{4.10}$$

with

$$C = \frac{\cos(\phi)}{r}. \tag{4.11}$$

Let us stress that our formulas for the remainder function in multi-Regge kinematics and the combined multi-Regge collinear limit contain terms from LLA and NLLA. At this order in the weak-coupling expansion, the expression we state is complete. At higher orders, the multi-Regge limit of the remainder function is also known exactly from the amplitude bootstrap [13] and ultimately to all loops due to the work by Basso et al. [10]. We will not need such extensions here.

4.3 Analytic Continuation

Let us now see how we can recover the results we reviewed in the previous subsection, and in particular eq. (4.10), through analytic continuation from the collinear $n = 6$ remainder function on the main sheet. The relevant Mandelstam region $\varrho = (--)$ is reached by some curve along which only the large cross ratio $u_1 = U_{2,5}$ has non-trivial winding number

$$n_{25} = \frac{1}{4}(\varrho_4 - \varrho_3)(\varrho_6 - \varrho_5) = \frac{1}{4}(-1-1)(1+1) = -1 \tag{4.12}$$

around $u_1 = 0$, see eq. (2.7). In order to initiate our analysis, let us display the collinear limit of the two-loop remainder function on the main sheet. From the Wilson loop OPE one finds

$$R_{6,(2)}(S,T,F) = 2T\cos(\phi)\tilde{f}_2^{(0)}(S) + 2T\cos(\phi)\log(T)\tilde{f}_2^{(1)}(S) - (\log\mathcal{W}_g^{\mathrm{BDS}})^{(2)} + \mathcal{O}(T^2) \,, \tag{4.13}$$

where

$$\tilde{f}_2^{(0)}(S) = g^4(S + S^{-1})\left[\frac{(12+\pi^2)\log S^2}{3(1+S^2)} + \log(1+S^{-2})(4-2\log(S^2))\right.$$
$$\left. + (\log(S^2)-2)\log^2(1+S^{-2}) + \frac{2}{3}\log^3(1+S^{-2}) - 2\mathrm{Li}_3(-S^{-2})\right] \tag{4.14}$$

and

$$\tilde{f}_2^{(1)}(S) = 2g^4(S + S^{-1})\left[-\frac{2\log(S^2)}{1+S^2} + (\log(S^2)-2)\log(1+S^{-2}) + \log(1+S^{-2})\right]. \tag{4.15}$$

The BDS part is given by

$$(\log\mathcal{W}_g^{\mathrm{BDS}})^{(2)} = g^4\frac{2\pi^2}{3}T(S+S^{-1})\left[\frac{\log(S^2)}{1+S^2} + \log(1+S^{-2})\right]. \tag{4.16}$$

There are a number of comments we would like to make about these expressions. First of all, a closer look at the arguments of the (poly-)logarithms reveals that the remainder function possesses $r = 2$ branch points in the complex S^2-plane. These are the points $S^2 = 0$ and $S^2 + 1 = 0$. Of course we see this here only to the given order of the expansion, but the statement remains true for higher loops, see e.g. the explicit three-loop expression in [41]. It is important to note that, to leading order in the collinear limit, the cross ratios u_i we listed in the previous subsection can be built as products of the two functions S^2 and $1 + S^2$ and their inverses. This makes it particularly easy to switch between curves in the S^2-plane and in the space of cross ratios. Let us also note that the remainder function vanishes in the multi-Regge limit $S \to 0$ before we analytically continue from the main sheet into other Mandelstam regions.

Our task is to derive the eqs. (4.10) from the formula (4.13) through analytic continuation along some specific curve in the space of kinematic variables. Since we will focus on the collinear limit, our paths will remain in this limit, i.e. we will not vary T. This is justified by the fact that, by eq. (4.5), u_1 and u_2 only depend on S^2 in the collinear limit, whereas $u_3 = U_{1,4} = T^2$ has winding number $n_{1,4} \sim (\varrho_5 - \varrho_4) = 0$ by eq. (2.7). As we can see from the explicit formulas

generator	S^2
$\mathcal{C}_1$	
$\mathcal{C}_2$	

Table 1: Path generators for the hexagon.

above, the two-loop contributions to the collinear limit are analytic in φ. This statement actually remains true at any finite loop order. Hence, we can restrict to paths along which φ is kept constant. It remains to study paths in the complex S^2-plane that start and end in the region where $S^2 > 0$. As we pointed out before, the remainder function possesses branch points at $S^2 = -1$ and $S^2 = 0$. Equivalence classes of paths are therefore parametrized by the fundamental group $\pi_1(\mathbb{C} \setminus \{0, -1\})$. This group is generated by two elements p_1 and p_2. The precise choice is a matter of convention. Let us agree that the generator p_1 is associated with a curve $\mathcal{C}_1$ that starts at some point $S^2 > 0$, runs slightly above the real axis, surrounds $S^2 = 0$ in counterclockwise direction before running back to its starting point where $S^2 > 0$. As for p_2, we make a similar choice, except that now the curve $\mathcal{C}_2$ runs from $S^2 > 0$ towards $S^2 = -1$ above the real axis, surrounds the point $S^2 = -1$ in counterclockwise direction and runs back *below* the real axis to its starting point. The two curves are depicted in Table 1.

Since the cross ratios are rational functions of S^2, they acquire corresponding phase shifts which are easy to work out,

$$
\begin{aligned}
\mathcal{C}_1 u_1 &= u_1\,, & \mathcal{C}_1 u_2 &= e^{2\pi i} u_2\,, & \mathcal{C}_1 u_3 &= u_3 \\
\mathcal{C}_2 u_1 &= e^{-2\pi i} u_1\,, & \mathcal{C}_2 u_2 &= u_2\,, & \mathcal{C}_2 u_3 &= u_3\,.
\end{aligned}
\tag{4.17}
$$

Here and in the following, the symbol $\mathcal{C}_i f(u)$ means the value of a function f of the cross ratios at the endpoint of an analytic continuation along the curve $\mathcal{C}_i$. The value of the cross ratio u_3 is unaffected by the continuation as it does not depend on S^2.

Now we can study the behavior of the remainder function upon continuation. For the continuation along the curves $\mathcal{C}_1$ and $\mathcal{C}_2$ one finds

$$
\left[\mathcal{C}_i R^{\mathrm{ope}}_{6,(2)}\right]^{\mathrm{MRL}} = (1 + 2\pi i \Delta_i) R^{\mathrm{ope}}_{6,(2)}
\tag{4.18}
$$

with

$$
\Delta_2 R^{\mathrm{ope}}_{6,(2)} = C\big(8 + 8\log(r) + 4\log(r)^2\big) + C\,2\log(r)\log(\varepsilon)\,,
\tag{4.19}
$$

and $\Delta_1 R^{\mathrm{ope}}_{6,(2)} = 0$. Non-vanishing cut contributions for more general elements $g \in \pi_1$ in our fundamental group can also be worked out by combining the following building blocks

$$
\begin{aligned}
\Delta_2 \Delta_1 R^{\mathrm{ope}}_{6,(2)} &= C\big(4 - 4i\pi + 2\log(r)\big) - C\,\log(\varepsilon)\,, \\
\Delta_1 \Delta_2 R^{\mathrm{ope}}_{6,(2)} &= C\big(4 + 4i\pi + 6\log(r)\big) + C\,\log(\varepsilon)\,, \\
\Delta_2 \Delta_2 \Delta_1 R^{\mathrm{ope}}_{6,(2)} &= -\Delta_1 \Delta_1 \Delta_2 R^{\mathrm{ope}}_{6,(2)} = -4C\,.
\end{aligned}
\tag{4.20}
$$

All other discontinuities, and in particular those beyond triple discontinuities, vanish at this loop order. Let us stress once again that our symbols Δ_i combine an analytic continuation with taking the Regge limit. Before taking the Regge limit, a continuation along $\mathcal{C}_1$ produces a nontrivial cut

contribution, which vanishes only in the Regge limit. If, on the other hand, we continue this cut contribution along $\mathcal{C}_2$, new terms appear that possess a non-trivial Regge limit.

Our first and most important observation is that continuation of the collinear remainder function along the curve $\mathcal{C}_2$ gives a single non-vanishing cut contribution, namely $\Delta_2 R_{6,(2)}^{\mathrm{ope}}$, which agrees exactly with the expected formula (4.10) for the collinear limit of the remainder function in the Mandelstam region $\varrho = (--)$. This is fully consistent with the kinematics, as the cross ratio u_1 has winding number -1 under the generator $\mathcal{C}_2$ of eq. (4.17), as required for the $\varrho = (--)$ region by eq. (4.12).

We can carry the analysis a bit further and ask to which extent the expression (4.10) determines the curve. In order to investigate this issue, let us first write the collinear limit of the hexagon remainder in the non-trivial Mandelstam region in terms of cut contributions,

$$\left[R_{6,(2)}^{--}\right]^{\mathrm{CL}} = \left(2\pi i \sum_i c_i \Delta_i + (2\pi i)^2 \sum_{i,j} c_{i,j} \Delta_i \Delta_j + (2\pi i)^3 \sum_{i,j,k} c_{i,j,k} \Delta_i \Delta_j \Delta_k\right) R_{6,(2)}^{\mathrm{ope}} . \qquad (4.21)$$

Using our list (4.20) one may infer the following four constraints on the coefficients

$$c_2 = 1, \quad c_{1,2} = 0 = c_{2,1}, \quad c_{1,1,2} = c_{2,2,1} . \qquad (4.22)$$

It is now easy to see that curves of the form $\mathcal{C}_1^{\alpha_1} \mathcal{C}_2^{\alpha_2} \mathcal{C}_1^{\alpha_3}$ are consistent with eq. (4.10) if and only if $\alpha_1 = \alpha_3 = 0$ and $\alpha_2 = 1$, i.e. within this family of curves, $\mathcal{C}_2$ is the only solution. On the other hand, there do exist other curves that give rise to the same cut contributions, e.g.

$$\mathcal{C}_1^k \mathcal{C}_2^{1-k} \mathcal{C}_1^{-1} \mathcal{C}_2^k \mathcal{C}_1^{1-k} \qquad (4.23)$$

for any value of $k \in \mathbb{Z}$. For $k \neq 0$, these curves are not the same as $\mathcal{C}_2$, even though they have the same winding numbers around $u_1 = 0$ and $u_2 = 0$. It would be interesting to investigate whether these curves are excluded by higher-order corrections in the loop or collinear expansion. The curve of eq. (4.23) is actually unique in the class of curves that involve only two powers of $\mathcal{C}_2$ generators that are separated by some power of $\mathcal{C}_1$, if we impose both the LLA and NLLA constraints by matching formula (4.21) against (4.10). The conditions from LLA alone (i.e. $\log \varepsilon$ terms) dictate only $c_{1,2} = c_{2,1}$ and $c_{1,1,2} = c_{2,2,1}$. Eq. (4.22) is a consequence of the anticommutator lemma (2.26) together with the total winding conditions $c_1 = 1 - c_2 = 0$, which follow from eq. (4.17). If we allow elements of the fundamental group that involve three powers of $\mathcal{C}_2$, separated by some powers of $\mathcal{C}_1$, the LLA and NLLA constraints can be solved by

$$\mathcal{C}_1^{\alpha_1} \mathcal{C}_2^{\alpha_2} \mathcal{C}_1^{-\alpha_1-\alpha_2} \mathcal{C}_2^{\alpha_1} \mathcal{C}_1^{\alpha_2} \mathcal{C}_2^{1-\alpha_1-\alpha_2} \qquad (4.24)$$

for $\alpha_1, \alpha_2 < -1$. We conclude that the two-loop formulas in LLA and NLLA impose strong constraints on the curve of continuation, but in order to fix the curve completely, one needs additional assumptions on its form.

5 Continuation and Multi-Regge Limit: The Heptagon

We now approach the main goal of this work, namely to repeat the analysis outlined in the previous section for the heptagon. In this case, the analysis is richer because there exist four Mandelstam regions in which the remainder function possesses a non-trivial multi-Regge limit. After a short discussion of the relevant kinematical variables, we will review known results about the multi-Regge limit of the heptagon remainder function in all four Mandelstam regions. In the final subsections, their collinear limit will be reproduced by analytic continuation from the Wilson loop OPE.

5.1 Variables and Limits

Before we start our analysis, it is again useful to review some of the formulas we derived in Section 2 for the heptagon. When $n = 7$, there are six independent cross ratios (2.4), two of which approach $u_{5,1} = u_{6,1} = 1$ while the other four vanish in multi-Regge kinematics. Consequently, the approach to the multi-Regge limit is now controlled by two small ε parameters

$$\varepsilon_5 = u_{5,2}u_{5,3}\,, \qquad \varepsilon_6 = u_{6,2}u_{6,3}\,, \tag{5.1}$$

while the limit itself is parametrized by four anharmonic ratios w_5, $\bar{w}_5$ and w_6, $\bar{w}_6$.

Once again, we can parametrize the heptagons in general kinematics in terms of the variables introduced in Section 2.1 and Appendix A as

$$\{T_j, S_j, F_j\} = \{e^{-\tau_j}, e^{\sigma_j}, e^{i\phi_j}\}\,, \qquad j = 5, \ldots, n-1\,. \tag{5.2}$$

The precise relation between these variables and our set of heptagon cross ratios (2.4) may be worked out from the formulas in Section 2.2,

$$u_{5,3} = U_{1,4} = \frac{T_5^2}{1 - T_6^2}\,,$$

$$u_{5,1} = U_{2,5} = \frac{1 - T_5^2}{1 + S_5^2 + 2c_5 S_5 T_5}\,,$$

$$u_{5,2} = U_{3,7} = \frac{S_5^2 \left(1 - T_5^2 - T_6^2\right)}{\left(1 - T_6^2\right)\left(1 + S_5^2 + 2c_5 S_5 T_5\right)} \cdot \frac{1}{U_{3,6}}\,,$$

$$u_{6,1} = U_{3,6} = \frac{S_5^2 S_6^2(1 - T_5^2) + (1 - T_6^2) + S_5^2 + 2c_5 S_5 T_5 + 2c_6 S_6^2 S_6 T_6 + 2c_+ S_5 T_5 S_6 T_6}{\left(1 + S_5^2 + 2c_5 S_5 T_5\right)\left(1 + S_6^2 + 2c_6 S_6 T_6\right)}\,,$$

$$U_{2,6} = \frac{\left(1 - T_5^2 - T_6^2\right)}{\left(1 - T_5^2\right)\left(1 + S_6^2 + 2c_6 S_6 T_6\right)} \cdot \frac{1}{U_{3,6}}\,,$$

$$u_{6,2} = U_{4,7} = \frac{S_6^2(1 - T_6^2)}{1 + S_6^2 + 2c_6 S_6 T_6}\,,$$

$$u_{6,3} = U_{1,5} = \frac{T_6^2}{1 - T_5^2}\,, \tag{5.3}$$

with the shorthand notation

$$c_5 = \cos(\phi_5)\,, \qquad c_6 = \cos(\phi_6)\,, \quad c_+ = \cos(\phi_5 + \phi_6)\,. \tag{5.4}$$

Besides the six cross ratios $u_{j,i}$, we have also listed $U_{2,6}$. The latter is not independent, but related to the set $u_{j,i}$ through a non-rational Gram determinant relation. Together, the seven cross ratios (5.3) constitute a multiplicative basis for the set of all conformal cross ratios of the heptagon. For the purpose of understanding analytic continuation paths in the space of cross ratios, it is therefore sufficient to consider these seven.

Given the formulas (5.3), it is straightforward to obtain the following expressions for the leading terms in the cross ratios as T_5 and T_6 are sent to zero,

$$u_{5,1} = U_{25} = \frac{1}{1 + S_5^2} + \mathcal{O}(T)$$

$$u_{5,2} = U_{37} = \frac{S_5^2(1 + S_6^2)}{1 + S_5^2 + S_5^2 S_6^2} + \mathcal{O}(T)\,, \qquad u_{5,3} = U_{14} = T_5^2 + \mathcal{O}(T^3)\,,$$

$$u_{6,1} = U_{36} = \frac{1 + S_5^2 + S_5^2 S_6^2}{(1 + S_5^2)(1 + S_6^2)} + \mathcal{O}(T) \tag{5.5}$$

$$u_{6,2} = U_{47} = \frac{S_6^2}{1 + S_6^2} + \mathcal{O}(T) \,, \qquad u_{6,3} = U_{15} = T_6^2 + \mathcal{O}(T^3)$$

$$U_{26} = \frac{1 + S_5^2}{1 + S_5^2 + S_5^2 S_6^2} + \mathcal{O}(T) \,.$$

Setting $S_j = r_j T_j$, the multi-Regge limit is attained for $T_j \to 0$, keeping r_j finite. For the heptagon, one finds

$$r_5^2 = \frac{1}{w_5 \bar{w}_5} \,, \qquad F_5^2 = \frac{w_5}{\bar{w}_5} \,, \qquad \frac{T_5^2}{S_5^2} = r_5^2 T_5^4 = \varepsilon_5 \,,$$

$$r_6^2 = \frac{1}{w_6 \bar{w}_6} \,, \qquad F_6^2 = \frac{w_6}{\bar{w}_6} \,, \qquad \frac{T_6^2}{S_6^2} = r_6^2 T_6^4 = \varepsilon_6 \,. \tag{5.6}$$

Note that the equations for F_i require to expand the expressions (5.3) for the cross ratios to higher orders in small T_i, beyond the terms stated in eq. (5.5). One way to derive eq. (5.6) is to solve the system of quadratic equations (2.5) for $\{w_5, \bar{w}_5, w_6, \bar{w}_6\}$ in terms of $\{T_i, S_i, F_i = \exp(i\phi_i)\}$ using eqs. (2.4) and (5.3). Once this is done, one can insert the result into the right hand side of eq. (5.6) (after picking appropriate branches of square roots) to obtain the left hand side as leading terms in the collinear $T_i \to 0$ expansion.

From the multi-Regge limit, the combined multi-Regge collinear limit is attained for $r_5, r_6 \to \infty$. If we start in general kinematics $\{T_j, S_j, F_j\}$, we reach the collinear limit when we send $T_j \to 0$ while keeping S_j and F_j finite. We can then continue to the combined multi-Regge collinear limit by letting $S_j \to 0$, keeping $S_j/T_j \gg 1$. In practice, we set $S_j = T_j r_j$ and take the limit $r_j \to \infty$, keeping $T_j \ll 1/r_j$.

5.2 The Remainder Function in Multi-Regge Kinematics

The heptagon remainder function is known to possess a non-trivial multi-Regge limit in four Mandelstam regions. These regions are associated with the four different sign choices of the energies p_i^0, $i = 4, 5, 6$, in which at least two energies are flipped. At least for three of these regions, the remainder function in multi-Regge kinematics at two loops is known.[8] As in the case of the hexagon, the two-loop result receives contributions from both LLA and NLLA. The regions $\varrho = (--+)$ and $\varrho = (+--)$ are the easiest, because the answer involves exactly the same information that appears for the multi-Regge limit of the hexagon, i.e. using the variables defined in eqs. (5.2) and (5.6), the multi-Regge limit of the remainder function reads [18]

$$R_{7,(2)}^{--+} = f(\varepsilon_5; w_5) \,, \qquad R_{7,(2)}^{+--} = f(\varepsilon_6; w_6) \,, \tag{5.7}$$

where f is the function we defined in eq. (4.7). For $\varrho = (---)$, the two-loop remainder function is also known in the Regge limit, but it involves a new function g [18–20],

$$R_{7,(2)}^{---} = f(\varepsilon_5; v_5) + f(\varepsilon_6; v_6) + g(v_5, v_6) \,, \tag{5.8}$$

where the variables

$$v_5 = \frac{w_5 w_6}{1 + w_6} \equiv -1/y \,, \qquad v_6 = (1 + w_5) w_6 \equiv -x \tag{5.9}$$

combine pairs of adjacent particles into clusters [20, 42]. The symbol of the function g was determined in [20], and it can be used to constraint the function g. Based on symmetry arguments,

---

[8]For the last region $(-+-)$, the remaining free coefficients where fixed in [23], see below.

it was fixed up to 25 unfixed rational coefficients in [20]. If additional constraints from single-valuedness, symmetries and collinear limits are taken into account, the function g can be shown to take the following form, see Appendix C and [22],

$$g(x,y) = -1/2\,G_0^{\mathbf{s},x}G_0^{\mathbf{s},\breve{y}}G_1^{\mathbf{s},\breve{y}} + 1/2\,G_0^{\mathbf{s},x}G_1^{\mathbf{s},x}G_1^{\mathbf{s},\breve{y}} + 1/2\,G_0^{\mathbf{s},\breve{y}}G_1^{\mathbf{s},x}G_1^{\mathbf{s},\breve{y}} - 1/2\,G_0^{\mathbf{s},x}G_1^{\mathbf{s},x}G_x^{\mathbf{s},\breve{y}}$$

$$+ 1/2\,G_0^{\mathbf{s},\breve{y}}G_1^{\mathbf{s},\breve{y}}G_x^{\mathbf{s},\breve{y}} - G_1^{\mathbf{s},\breve{y}}G_{0,1}^{\mathbf{s},x} + G_x^{\mathbf{s},\breve{y}}G_{0,1}^{\mathbf{s},x} + G_0^{\mathbf{s},x}G_{0,1}^{\mathbf{s},\breve{y}} - G_1^{\mathbf{s},x}G_{0,1}^{\mathbf{s},\breve{y}} - G_x^{\mathbf{s},\breve{y}}G_{0,1}^{\mathbf{s},\breve{y}}$$

$$+ G_1^{\mathbf{s},x}G_{0,x}^{\mathbf{s},\breve{y}} - G_0^{\mathbf{s},\breve{y}}G_{1,x}^{\mathbf{s},\breve{y}} - G_1^{\mathbf{s},x}G_{1,x}^{\mathbf{s},\breve{y}} + G_1^{\mathbf{s},\breve{y}}G_{1,x}^{\mathbf{s},\breve{y}} + 2\,G_{0,1,x}^{\mathbf{s},\breve{y}} - 2\,G_{1,1,x}^{\mathbf{s},\breve{y}}$$

$$+ \kappa_0\zeta_2\,G_x^{\mathbf{s},\breve{y}} + 2\pi i\big[\kappa_1\big((G_0^{\mathbf{s},x} - G_1^{\mathbf{s},x})G_1^{\mathbf{s},x} + (G_0^{\mathbf{s},\breve{y}} - G_1^{\mathbf{s},\breve{y}})G_1^{\mathbf{s},\breve{y}}\big)$$

$$+ \kappa_2(G_0^{\mathbf{s},x} - G_1^{\mathbf{s},x})G_1^{\mathbf{s},\breve{y}} + \kappa_3(G_0^{\mathbf{s},x} - G_0^{\mathbf{s},\breve{y}})G_x^{\mathbf{s},\breve{y}}\big]\,. \tag{5.10}$$

Here and in the following, we use the condensed notation $G_{a_1,\dots,a_n}^{\mathbf{s},z} \equiv G^{\mathbf{s}}(a_1,\dots,a_n;z)$, and $\breve{y} \equiv 1/y$. The functions $G^{\mathbf{s}}$ are obtained by applying the single-valued map [43] to multiple or Goncharov polylogarithms [44], which can be defined recursively as iterated integrals

$$G(a_1,\dots,a_n;z) \equiv \begin{cases} \dfrac{1}{n!}\log^n z & \text{if } a_1 = \dots = a_n = 0\,, \\[2mm] \displaystyle\int_0^z \dfrac{dt}{t-a_1}G(a_2,\dots,a_n;t) & \text{otherwise,} \end{cases} \tag{5.11}$$

with $G(;z) = 1$. The expansion of this function in the collinear limit takes the form

$$[g(v_5,v_6)]^{\text{CL}} = C_-\Big(2\log(r_6) + 4\pi i(\kappa_1 - \kappa_3)\Big)$$

$$+ C_+\Big((-6 - 8\pi i(2\kappa_1 + \kappa_2))\log(r_6) - 8\pi i(\kappa_1 - \kappa_3)\log(r_5)$$

$$+ 4\pi i(\kappa_1 - \kappa_3) + \frac{\pi^2\kappa_0}{3} - 4\log^2(r_6) - 4\log(r_5)\log(r_6) - 4\Big)$$

$$+ C_5\Big(-\frac{\pi^2\kappa_0}{3} - 8\pi i\kappa_3\log(r_5)\Big) - 8\pi i\kappa_1 C_6\log(r_6)\,, \tag{5.12}$$

where we have used the abbreviated notation

$$C_5 = \frac{\cos(\phi_5)}{r_5}\,, \quad C_6 = \frac{\cos(\phi_6)}{r_6}\,, \quad C_+ = \frac{\cos(\phi_5 + \phi_6)}{r_5 r_6}\,, \quad C_- = \frac{\cos(\phi_5 - \phi_6)}{r_5 r_6}\,. \tag{5.13}$$

We see that all remaining coefficients $\kappa_0,\dots,\kappa_3$ in the function g survive the collinear limit, and that they can be fixed by collinear data. In [22], the values of the coefficients for the function g were determined to be[9]

$$\kappa_0 = \kappa_1 = \kappa_2 = \kappa_3 = 0\,. \tag{5.14}$$

There is one more Mandelstam region we need to discuss, namely the region $\varrho = (-+-)$. In this case, the multi-Regge limit of the remainder function is known to take the form [18, 20],

$$R_{7,(2)}^{-+-} = f(\varepsilon_5, v_5) + f(\varepsilon_6, v_6) - f(\varepsilon_5, w_5) - f(\varepsilon_6, w_6) + \tilde{g}(v_5, v_6)\,. \tag{5.15}$$

Here, f is the same function (4.7) that appears for the hexagon. The function $\tilde{g}$ was not known until quite recently [23]. Our analysis provides a different route to determining it. We shall use that the symbols of the remainder functions in the various Mandelstam regions satisfy the following linear relation [20]

$$S[R_{7,(2)}^{-+-}] = S[R_{7,(2)}^{---}] - S[R_{7,(2)}^{--+}] - S[R_{7,(2)}^{+--}]\,, \tag{5.16}$$

---

[9]The analysis in [22] assumes a certain path of analytic continuation from the $(+++)$ to the $(---)$ region.

and therefore the symbols of g and $\tilde{g}$ are identical:

$$S[g(v_5, v_6)] = S[\tilde{g}(v_5, v_6)]\,. \tag{5.17}$$

Given that g and $\tilde{g}$ possess the same symbol, and that the constraints we imposed in order to obtain the expression (5.10) for g did not make any reference to a specific Mandelstam region, we conclude that the general Ansatz (5.10) is also valid for $\tilde{g}$. Of course, the values of the four free parameters within this Ansatz do depend on the Mandelstam region, and hence are expected to differ from those we stated for the Mandelstam region $\varrho = (---)$ in eq. (5.14). In other words,

$$\tilde{g}(v_4, v_5) = g(v_4, v_5)\big|_{\kappa_i \to \tilde{\kappa}_i}\,. \tag{5.18}$$

We will determine the values of the parameters $\tilde{\kappa}_0, \ldots, \tilde{\kappa}_3$ for the region $\varrho = (-+-)$ below. The collinear expansions of the relevant hexagon functions are

$$[f(\varepsilon_5, w_5)]^{\mathrm{CL}} = 2C_5 \log(\varepsilon_5) \log(r_5) + C_5 \big(4\log^2(r_5) + 8\log(r_5) + 8\big)\,, \tag{5.19}$$

$$[f(\varepsilon_6, w_6)]^{\mathrm{CL}} = 2C_6 \log(\varepsilon_6) \log(r_6) + C_6 \big(4\log^2(r_6) + 8\log(r_6) + 8\big)\,, \tag{5.20}$$

$$[f(\varepsilon_5, v_5)]^{\mathrm{CL}} = C_+ \log(\varepsilon_5)\big(2\log(r_5) + 2\log(r_6)\big) \tag{5.21}$$
$$+ C_+\big(4\log^2(r_5) + 4\log^2(r_6) + 8\log(r_6)\log(r_5) + 8\log(r_5) + 8\log(r_6) + 8\big)\,,$$

$$[f(\varepsilon_6, v_6)]^{\mathrm{CL}} = \log(\varepsilon_6)\big(-C_- + C_+(2\log(r_6) - 1) + 2C_6\log(r_6)\big) + C_-\big(-4\log(r_6) - 4\big)$$
$$+ C_+\big(4\log^2(r_6) + 4\log(r_6) + 4\big) + C_6\big(4\log^2(r_6) + 8\log(r_6) + 8\big)\,. \tag{5.22}$$

Combining the above, we find that the collinear limit of the multi-Regge remainder function in the four different Mandelstam regions is

$$[R_{7,(2)}^{--+}]^{\mathrm{CL}} = 2C_5 \log(\varepsilon_5)\log(r_5) + C_5(4\log^2(r_5) + 8\log(r_5) + 8)\,, \tag{5.23}$$

$$[R_{7,(2)}^{+--}]^{\mathrm{CL}} = 2C_6 \log(\varepsilon_6)\log(r_6) + C_6(4\log^2(r_6) + 8\log(r_6) + 8)\,, \tag{5.24}$$

$$[R_{7,(2)}^{---}]^{\mathrm{CL}} = \log(\varepsilon_5)C_+\big(2\log(r_5) + 2\log(r_6)\big) + \log(\varepsilon_6)\big(-C_- + C_+(2\log(r_6) - 1) + 2C_6\log(r_6)\big)$$
$$+ C_5\big(-2\kappa_0\zeta_2 - 8\pi i\kappa_3\log(r_5)\big) + C_6\big((8 - 8\pi i\kappa_1)\log(r_6) + 4\log^2(r_6) + 8\big)$$
$$+ C_+\big((8 - 8\pi i(\kappa_1 - \kappa_3))\log(r_5) + (6 - 8\pi i(2\kappa_1 + \kappa_2))\log(r_6)$$
$$+ 2(\kappa_0\zeta_2 + 4) + 4\pi i(\kappa_1 - \kappa_3) + 4\log^2(r_5) + 4\log^2(r_6) + 4\log(r_6)\log(r_5)\big)$$
$$+ C_-\big(4\pi i(\kappa_1 - \kappa_3) - 2\log(r_6) - 4\big)\,, \tag{5.25}$$

$$[R_{7,(2)}^{-+-}]^{\mathrm{CL}} = \log(\varepsilon_5)\big(C_+(2\log(r_5) + 2\log(r_6)) - 2C_5\log(r_5)\big) + \log(\varepsilon_6)\big(C_+(2\log(r_6) - 1) - C_-\big)$$
$$+ C_5\big((-8 - 8\pi i\tilde{\kappa}_3)\log(r_5) - 2(\tilde{\kappa}_0\zeta_2 + 4) - 4\log^2(r_5)\big) - C_6\,8\pi i\,\tilde{\kappa}_1\log(r_6)$$
$$+ C_+\big((8 - 8\pi i(\tilde{\kappa}_1 - \tilde{\kappa}_3))\log(r_5) + (6 - 8\pi i(2\tilde{\kappa}_1 + \tilde{\kappa}_2))\log(r_6)$$
$$+ 2(\tilde{\kappa}_0\zeta_2 + 4) + 4\pi i(\tilde{\kappa}_1 - \tilde{\kappa}_3) + 4\log^2(r_5) + 4\log^2(r_6) + 4\log(r_6)\log(r_5)\big)$$
$$+ C_-\big(4\pi i(\tilde{\kappa}_1 - \tilde{\kappa}_3) - 2\log(r_6) - 4\big)\,. \tag{5.26}$$

This concludes our brief review of known results on the two-loop heptagon remainder function in multi-Regge kinematics. We are now prepared to compare with what we obtain when we continue the collinear heptagon remainder function into the various Mandelstam regions.

Region	$u_{5,1}$	$u_{5,2}$	$u_{5,3}$	$u_{6,1}$	$u_{6,2}$	$u_{6,3}$	$U_{2,6}$
$(--+)$	-1	0	0	0	$-1/2$	$1/2$	0
$(+--)$	0	$1/2$	$-1/2$	-1	0	0	0
$(---)$	0	0	0	0	0	0	-1
$(-+-)$	1	$-1/2$	$1/2$	1	$1/2$	$-1/2$	-1

Table 2: Winding numbers of basis cross ratios as one continues from the $(+++)$ to into the four different non-trivial Mandelstam regions.

5.3 Analytic Continuation

As explained in Section 2, we can reach all Mandelstam regions from the $(+++)$ region by analytic continuation of some of the forward energy variables p_i^0, $i = 4, 5, 6$. For the four non-trivial regions of the heptagon, these continuations entail the windings of the seven cross ratios around the origin displayed in Table 2. The entries of this table are produced with the help of our formula (2.7). We note that in contrast to the hexagon, some of the cross ratios possess half-windings around the origin. Let us also stress that in the $(---)$ region, only the cross ratio $U_{2,6}$ possesses a non-vanishing winding number around the origin.

Generators. As in the previous section, we first need to determine a generating set of curves that can expose all the branch cuts in the collinear limit. In order to do so, let us begin by listing all the branch cuts of the two-loop collinear remainder function. The component functions in eq. (3.12) are linear combinations of products of logarithms $\log(x_i)$ and polylogarithms $\mathrm{Li}_2(1-y_i)$, $\mathrm{Li}_3(1-y_i)$. The arguments x_i are ratios with factors[10]

$$x_i \in \left\{ S_5^2, 1 + S_5^2, S_6^2, 1 + S_6^2, 1 + S_5^2 + S_5^2 S_6^2 \right\} . \qquad (5.27)$$

In addition, there are five different polylogarithm arguments y_i:

	y_1	y_2	y_3	y_4	y_5	
$y_i:$	$\dfrac{1 + S_5^2}{S_5^2}$	$1 + S_6^2$	$\dfrac{1 + S_5^2 + S_5^2 S_6^2}{1 + S_5^2}$	$\dfrac{1 + S_5^2 + S_5^2 S_6^2}{S_5^2(1 + S_6^2)}$	$\dfrac{(1 + S_5^2)(1 + S_6^2)}{1 + S_5^2 + S_5^2 S_6^2}$	(5.28)
$(1 - y_i):$	$-\dfrac{1}{S_5^2}$	$-S_6^2$	$-\dfrac{S_5^2 S_6^2}{1 + S_5^2}$	$-\dfrac{1}{S_5^2(1 + S_6^2)}$	$-\dfrac{S_6^2}{1 + S_5^2 + S_5^2 S_6^2}$	

All expressions y_i and $1 - y_i$ are ratios of x_i. Since $\mathrm{Li}_n(z)$ has branch points at $z = 1$ and $z = 0$, the space of complex S_5^2 and S_6^2 contains $r = 5$ branch points at $x_i = 0$. Consequently, the fundamental group can be generated by five elements p_ν, $\nu = 1, \ldots, 5$. We will now describe the precise curves $\mathcal{C}_\nu$ we shall use in order to represent the set of generators, see Table 3.

All curves start and end at positive values of S_5^2 and S_6^2, since all the branch points $x_i = 0$ are located where either $S_5^2 \leq 0$ or $S_6^2 \leq 0$. The first curve $\mathcal{C}_1$ keeps S_6^2 constant. In the space of S_5^2, it looks similar to the curve $\mathcal{C}_2$ we introduced in the discussion of the hexagon, see Table 1, except that now there is one more branch point at $S_5^2 = -1/(1 + S_6^2) \in (-1, 0)$, i.e. in between the two branch points at $S_5^2 = 0$ and $S_5^2 = -1$. $\mathcal{C}_2$ moves both variables S_5^2 and S_6^2 at the same time, such that their product $S_5^2 S_6^2$ stays real and positive. For $\mathcal{C}_3$, we keep S_5^2 fixed and, similarly to $\mathcal{C}_1$, S_6^2 rotates around all three branch points. $\mathcal{C}_4$ only rotates S_5^2 around 0, just like $\mathcal{C}_1$ of the hexagon in Table 1. $\mathcal{C}_5$ is the same, but with the roles of S_5^2 and S_6^2 interchanged.

---

[10]In their original form, the component functions also contain $\log(S_i)$, which we can safely rewrite as $1/2 \log(S_i^2)$. The logarithm arguments also contain factors $(S_5^2 + S_6^2)$, but these are spurious: They cancel out upon expanding all logarithms.

generator	S_5^2	S_6^2
$\mathcal{C}_1$	×−1 × ☿ × 0 × S_5^2 (loop)	fix
$\mathcal{C}_2$	×−1 × 0 × S_5^2 (loop)	×−1 × 0 × S_6^2 (loop)
$\mathcal{C}_3$	fix	× ♃ ×−1 × 0 × S_6^2 (loop)
$\mathcal{C}_4$	×−1 × ☿ × 0 × S_5^2 (loop)	fix
$\mathcal{C}_5$	fix	× ♃ ×−1 × 0 × S_6^2 (loop)

$$\text{☿} = -1/(1+S_6^2) \qquad \text{♃} = -(1+S_5^2)/S_5^2$$

Table 3: Tables of generators of the fundamental group. All generators except $\mathcal{C}_2$, move only one of the S_j^2 variables. The $\mathcal{C}_2$ generator winds both S_5^2 and S_6^2 at the same time in opposite directions, such that $S_5^2 S_6^2$ stays real and positive.

It turns out that we can model these generators $\mathcal{C}_\nu$ with just circular movements of S_5^2 and S_6^2 around 0. More importantly, the generators $\mathcal{C}_i$ are chosen such that if an argument $1-y$ of a polylogarithm winds around $y=0$ under the action of $\mathcal{C}_\nu$, then it also winds around $y=1$, along a path that is homotopically equivalent to a circle in the y_i plane. This makes it easy to consistently pick the branches of the produced logarithms. Namely, for all our generators $\mathcal{C}_\nu$:

$$\mathcal{C}_\nu \operatorname{Li}_n(1-y_i) = \operatorname{Li}_n(1-y_i) - s_\nu(y_i)\frac{2\pi i}{\Gamma(n)}\left(\log(y_i-1) + s_\nu(y_i)\,\pi i\right)^{n-1}, \qquad (5.29)$$

where $s_\nu(y_i) = \pm 1$ is the counterclockwise winding number of y_i around $y_i = 0$ under the action of the curve $\mathcal{C}_\nu$. In addition, we have the obvious continuation rule

$$\mathcal{C}_\nu \log(x) = \log(x) + s_\nu(x)2\pi i. \qquad (5.30)$$

From our description of the curves $\mathcal{C}_\nu$, it is not difficult to infer the winding numbers of the variables x_i and of the cross ratios U_{ij}. The winding numbers of the arguments x_i and y_i around zero are given in the following tables:

x_i	$\mathcal{C}_1$	$\mathcal{C}_2$	$\mathcal{C}_3$	$\mathcal{C}_4$	$\mathcal{C}_5$		$\mathcal{C}_1$	$\mathcal{C}_2$	$\mathcal{C}_3$	$\mathcal{C}_4$	$\mathcal{C}_5$
S_5^2	1	−1	0	1	0	y_1	0	1	0	−1	0
$1+S_5^2$	1	0	0	0	0	y_2	0	1	1	0	0
S_6^2	0	1	1	0	1	y_3	0	0	1	0	0
$1+S_6^2$	0	1	1	0	0	y_4	0	0	0	−1	0
$1+S_5^2+S_5^2 S_6^2$	1	0	1	0	0	y_5	0	1	0	0	0

$$(5.31)$$

Here, a "1" means that the corresponding factor winds once around the origin, in the mathematically positive sense (counterclockwise). The curves we have introduced have the virtue that each of them winds exactly one of the cross ratios (5.5) around the origin, as shown in Table 4 on the left. Each cycle begins and ends in the region $S_5^2, S_6^2 > 0$, and therefore $0 < U_{ij} < 1$ for

	$\mathcal{C}_1$	$\mathcal{C}_2$	$\mathcal{C}_3$	$\mathcal{C}_4$	$\mathcal{C}_5$		$\mathcal{C}_1$	$\mathcal{C}_2$	$\mathcal{C}_3$	$\mathcal{C}_4$	$\mathcal{C}_5$
$u_{5,1}$	-1	0	0	0	0	$1-u_{5,1}$	0	-1	0	1	0
$u_{6,1}$	0	-1	0	0	0	$1-u_{6,1}$	-1	0	0	0	1
U_{26}	0	0	-1	0	0	$1-U_{26}$	0	0	0	1	1
$u_{5,2}$	0	0	0	1	0	$1-u_{5,2}$	-1	0	-1	0	0
$u_{6,2}$	0	0	0	0	1	$1-u_{6,2}$	0	-1	-1	0	0

Table 4: Winding numbers of cross ratios under the action of generators $\mathcal{C}_i$.

all of the cross ratios (5.5). Besides winding one cross ratio around the origin, each generator also winds two other cross ratios around $U_{ij} = 1$, as shown in Table 4 on the right. The cross ratios $u_{5,3}$ and $u_{6,3}$ are not displayed, since their leading collinear term does only depend on T_5 and T_6, respectively. In addition to these full rotations of cross ratios U_{ij} that start and end on the positive real line, we also need to include possible curves that have half-integer winding numbers, as dictated by the kinematics in Table 2. That means that we allow cross ratios to move to the negative real line above (winding number $+1/2$) or below (winding number $-1/2$) the origin, and we choose to append such region-dependent continuations to the end of our curves, so that we can just specify the correction terms to discontinuities generated by $\mathcal{C}_\nu$ for each region separately (see Appendix D). For the continuation of the cross ratios $u_{5,3}$ and $u_{6,3}$, that implies substitutions of the collinear variables $T_j \to \pm i T_j$, where the sign depends on the sign of the half winding in Table 2. That way, we need to consider continuations to negative arguments only of pure logarithms produced by eq. (5.29).

Discontinuities. Now let us focus on the discontinuities relevant for continuations into the various Mandelstam regions. Using the variables (5.2, 5.6), we find the following non-zero single discontinuities of the two-loop, near-collinear remainder function in the combined multi-Regge collinear limit:

$$\Delta_1 R_{7,(2)}^{\mathrm{ope}} = 2\log(\varepsilon_5)\, C_5 \log(r_5) + C_5\big(4\log^2(r_5) + 8\log(r_5) + 8\big),$$

$$\Delta_2 R_{7,(2)}^{\mathrm{ope}} = 2\log(\varepsilon_6)\, C_6 \log(r_6) + C_6\big(4\log^2(r_6) + 8\log(r_6) + 8\big),$$

$$\Delta_3 R_{7,(2)}^{\mathrm{ope}} = \log(\varepsilon_5)\, C_+\big(2\log(r_5) + 2\log(r_6)\big)$$

$$+ \log(\varepsilon_6)\big(2 C_6 \log(r_6) + C_+\big(2\log(r_6) - 1\big) - C_-\big)$$

$$+ C_6\big(4\log^2(r_6) + 8\log(r_6) + 8\big)$$

$$+ C_+\big(4\log^2(r_5) + 4\log(r_6)\log(r_5) + 8\log(r_5) + 4\log^2(r_6) + 6\log(r_6) + 8\big)$$

$$- C_-\big(2\log(r_6) + 4\big), \tag{5.32}$$

where we have used the abbreviated notation (5.13). In particular, the discontinuities $\Delta_4 R_{7,(2)}^{\mathrm{ope}}$ and $\Delta_5 R_{7,(2)}^{\mathrm{ope}}$ vanish. That is, the generators $\mathcal{C}_4$ and $\mathcal{C}_5$ act trivially on $R_{7,(2)}^{\mathrm{ope}}$ in the multi-Regge limit, which immediately shows that the representation of the fundamental group is not faithful. Since $\mathcal{C}_4$ and $\mathcal{C}_5$ let only small cross ratios wind, this shows that the remainder function on the main $(+++)$ sheet has trivial monodromy in the combined multi-Regge collinear limit when these small cross ratios wind around the origin. This confirms earlier findings [20]. For the double discontinuities $\Delta_{i,j} \equiv \Delta_i \Delta_j R_{7,(2)}^{\mathrm{ope}}$, we find:

$$\Delta_{1,2} = -\log(\varepsilon_5)\, C_5 - \log(\varepsilon_6)\, C_+ + C_5\big(-6\log(r_5) + 4\pi i - 4\big) + C_+\big(4\log(r_5) - 2\log(r_6) - 4\pi i\big),$$

$$\Delta_{2,1} = \log(\varepsilon_5)(C_5 - C_+) + C_5(-2\log(r_5) + 4\pi i - 4) + C_+(2\log(r_5) - 4\pi i + 2) - 2C_-,$$

$$\Delta_{1,4} = \log(\varepsilon_5)\, C_5 + C_5(6\log(r_5) + 4\pi i + 4),$$

$$\Delta_{4,1} = -\log(\varepsilon_5)\, C_5 + C_5(2\log(r_5) - 4\pi i + 4),$$

$$\Delta_{2,5} = \log(\varepsilon_6)\, C_6 + C_6(6\log(r_6) + 4\pi i + 4),$$

$$\Delta_{5,2} = -\log(\varepsilon_6)\, C_6 + C_6(2\log(r_6) - 4\pi i + 4),$$

$$\Delta_{3,4} = \log(\varepsilon_5)\, C_+ + C_+(6\log(r_5) + 4\log(r_6) + 4\pi i + 4),$$

$$\Delta_{4,3} = -\log(\varepsilon_5)\, C_+ - \log(\varepsilon_6)\, C_+ + C_+(2\log(r_5) + 2\log(r_6) - 4\pi i + 4),$$

$$\Delta_{3,5} = \log(\varepsilon_5)\, C_+ + \log(\varepsilon_6)(C_6 + C_+)$$
$$+ C_6(6\log(r_6) + 4\pi i + 4) + C_+(2\log(r_5) + 6\log(r_6) + 4\pi i + 2) - 2C_-,$$

$$\Delta_{5,3} = -\log(\varepsilon_6)(C_6 + C_+) + C_+(2\log(r_6) - 4\pi i) + C_6(2\log(r_6) - 4\pi i + 4). \tag{5.33}$$

Notably, the generators $\mathcal{C}_4$ and $\mathcal{C}_5$ act non-trivially on some of the single discontinuities. The triple discontinuities $\Delta_{i,j,k} \equiv \Delta_i \Delta_j \Delta_k R_{7,(2)}^{\mathrm{ope}}$ are:

$$\Delta_{1,2,5} = \Delta_{1,5,2} = \Delta_{5,1,2} = \Delta_{5,2,1} = \Delta_{4,1,3} = \Delta_{4,3,1}$$
$$= -\tfrac{1}{2}\Delta_{3,4,4} = \tfrac{1}{2}\Delta_{4,3,3} = -\Delta_{3,4,5} = -\Delta_{3,5,4} = -2C_+,$$

$$\Delta_{1,2,4} = \Delta_{1,4,2} = 2C_+ - 4C_5, \qquad\qquad \Delta_{1,2,2} = \Delta_{2,1,1} = 4C_5 - 4C_+,$$

$$\Delta_{3,5,5} = -\Delta_{5,3,3} = 4C_6 + 4C_+, \qquad\qquad \Delta_{5,2,3} = \Delta_{5,3,2} = -2C_+ - 4C_6,$$

$$\Delta_{1,4,4} = -\Delta_{4,1,1} = 4C_5, \qquad\qquad \Delta_{2,5,5} = -\Delta_{5,2,2} = 4C_6. \tag{5.34}$$

Continuation Results. Having listed all the relevant discontinuities that remain non-trivial in multi-Regge kinematics, we can now compute the collinear remainder function in the various Mandelstam regions. For the regions $\varrho = (--+)$, $(+--)$, and $(---)$, immediate candidates for admissible continuations are those along the curves $\mathcal{C}_1$, $\mathcal{C}_2$, and $\mathcal{C}_3$, respectively. Indeed, one finds that

$$[R_{7,(2)}^{--+}]^{\mathrm{CL}} = [\mathcal{C}_1 R_{7,(2)}^{\mathrm{ope}}]^{\mathrm{MRL}}, \qquad [R_{7,(2)}^{+--}]^{\mathrm{CL}} = [\mathcal{C}_2 R_{7,(2)}^{\mathrm{ope}}]^{\mathrm{MRL}}, \tag{5.35}$$

$$[R_{7,(2)}^{---}]^{\mathrm{CL}} = [\mathcal{C}_3 R_{7,(2)}^{\mathrm{ope}}]^{\mathrm{MRL}}, \tag{5.36}$$

where we use the simple shorthand $\bar{\mathcal{C}}_i \equiv \mathcal{C}_i^{-1}$ for the inverse of the curve $\mathcal{C}_i$, i.e. the curve with opposite orientation. The right hand side of these three equations is computed from the discontinuities we listed above (and the corrections for appended half-windings that are listed in Appendix D). What one obtains reproduces exactly the expressions in eqs. (5.23)–(5.25), including the values (5.14) of the parameters $\kappa_0, \ldots, \kappa_3$ that cannot be determined by general constraints such as single-valuedness, symmetries, and collinear limits.

For the region $\varrho = (-+-)$, finally, we infer from Table 2 and Table 4 that the corresponding curves must contain $\bar{\mathcal{C}}_1$, $\bar{\mathcal{C}}_2$, and $\mathcal{C}_3$. Of course the order in which we put these generators matters for the continuation, but it cannot be determined from the winding numbers alone. It turns out that we can obtain the correct result in several ways, including

$$[R_{7,(2)}^{-+-}]^{\mathrm{CL}} = [\bar{\mathcal{C}}_2 \mathcal{C}_3 \bar{\mathcal{C}}_1 R_{7,(2)}^{\mathrm{ope}}]^{\mathrm{MRL}} = [\bar{\mathcal{C}}_2 \bar{\mathcal{C}}_1 \mathcal{C}_3 R_{7,(2)}^{\mathrm{ope}}]^{\mathrm{MRL}} = [\mathcal{C}_3 \bar{\mathcal{C}}_2 \bar{\mathcal{C}}_1 R_{7,(2)}^{\mathrm{ope}}]^{\mathrm{MRL}}. \tag{5.37}$$
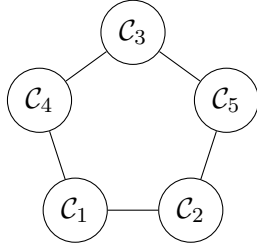
Figure 4: Commutation relations between generators. An edge between two generators $\mathcal{C}_i$ and $\mathcal{C}_j$ corresponds to a non-trivial commutator $[\mathcal{C}_i, \mathcal{C}_j]$. Notably, we find that whenever a commutator vanishes, $[\mathcal{C}_i, \mathcal{C}_j]=0$, the double discontinuities $\Delta_{i,j}$ and $\Delta_{j,i}$ also vanish.

Once again, the continuation along the three paths on the right hand side is computed with the help of the cut contributions we listed above, along with the corrections for appended half-windings from Appendix D. In all three cases, the result is the same, and it agrees with formula (5.26), with the parameters $\tilde{\kappa}_i$ given by

$$\tilde{\kappa}_0 = \tilde{\kappa}_1 = \tilde{\kappa}_2 = \tilde{\kappa}_3 - \frac{1}{2} = 0 \ . \tag{5.38}$$

These values are in agreement with the recent results in [22]. Let us note that in all three paths in (5.37), the generators $\bar{\mathcal{C}}_1$ and $\bar{\mathcal{C}}_2$ appear in the same order. But there are three more permutations in which the order of these two generators is reversed. For these remaining three paths, it is necessary to involve additional generators $\mathcal{C}_4$ and $\mathcal{C}_5$ in order to get the correct result, e. g.

$$\left[R_{7,(2)}^{-+-}\right]^{\mathrm{CL}} = \left[\bar{\mathcal{C}}_5 \mathcal{C}_4 \bar{\mathcal{C}}_1 \bar{\mathcal{C}}_2 \mathcal{C}_3 \bar{\mathcal{C}}_4 \mathcal{C}_5 R_{7,(2)}^{\mathrm{ope}}\right]^{\mathrm{MRL}} \ . \tag{5.39}$$

It turns out that the precise dressing of the path with the generators $\mathcal{C}_4$ and $\mathcal{C}_5$ can be determined by matching to the LLA on the left hand side. Once the dressing is known, one can use it to compute the NLLA, and one finds again full agreement with eqs. (5.26) and (5.38). The same is true for the remaining two orders in which we can place our three generators $\bar{\mathcal{C}}_1, \bar{\mathcal{C}}_2$ and $\mathcal{C}_5$. Some more detailed comments on the derivation of these results are collected in the final subsection.

5.4 Analysis of Continuation Paths

This final subsection contains a number of detailed comments on the results we summarized in eqs. (5.37)–(5.39) at the end of the previous subsection. As we explained above, each of the Mandelstam regions is reached by a curve that must satisfy the total winding conditions of Table 2. The latter comes purely from kinematical considerations. We view the curves as monomials in noncommutative generators $\mathcal{C}_\nu$, so that the total winding fixes the total power of each generator in these monomials. In case some cross ratios undergo half-windings, these are added at the end, after all the full windings have been carried out. The noncommutative structure of the fundamental group starts to reveal itself at the level of the double discontinuities. Let us note that some generators $\mathcal{C}_i$ commute in our two-loop analysis. In fact, two generators $\mathcal{C}_i$, $\mathcal{C}_j$ commute iff $\Delta_{A,i,j,B} = \Delta_{A,j,i,B}$ for all (possibly empty) A and B. From the tables of discontinuities (5.33) and (5.34), we see that for example $\mathcal{C}_3$ commutes with both $\mathcal{C}_1$ and $\mathcal{C}_2$. We collect the commutation relations among all generators in Figure 4. After these introductory comments, let us now briefly consider the four different Mandelstam regions.

5.4.1 The Mandelstam Regions $(--+)$ and $(+--)$

Even though the combined multi-Regge collinear limit (5.23) and (5.24) of the remainder function in the regions $(--+)$ and $(+--)$ reproduces formula (4.10) for the hexagon, the derivation

through analytic continuation from the Wilson loop OPE is not quite the same. On the one hand, the heptagon case involves some half-windings that need to be taken into account, see Table 2. On the other hand, the two-loop functions h_2, $\bar{h}_2$ in the expression (3.12) for the collinear heptagon remainder function constitute a new ingredient that does not appear for the hexagon. In addition, there are also more generators to consider for the heptagon.

It turns out that there is a natural choice of the continuation curve, dictated by the structure of the OPE prediction (3.12) that agrees with the previous analysis. In the $(--+)$ and $(+--)$ regions, as one can see from the lists of discontinuities in eq. (5.32) together with the half-winding corrections shown in (D.2) and (D.4), the contributions from h_2 and $\bar{h}_2$ to the analytic continuations along the curves $\mathcal{C}_1$ and $\mathcal{C}_2$ respectively are trivial in the combined multi-Regge collinear limit:

$$\Delta_1^{(--+)} h_2 = \Delta_1^{(--+)} \bar{h}_2 = \Delta_2^{(+--)} h_2 = \Delta_2^{(+--)} \bar{h}_2 = 0. \tag{5.40}$$

This leaves only the hexagonal functions $\tilde{f}_5$ and $\tilde{f}_6$ to contribute to these simplest continuation curves, which then leads to exactly the same form shown in eq. (5.23) and (5.24) of the heptagonal remainder function in these two regions. Hence, in the end, the results of the continuation along the simplest curves for the $(--+)$ and $(+--)$ regions do boil down to the hexagon case, albeit in a somewhat nontrivial manner.

5.4.2 The Mandelstam Region $(---)$

The collinear limit of the remainder function (5.25) contains four free parameters $\kappa_0, \ldots, \kappa_3$ that are not fixed by general considerations. Under some assumptions on the complexity of the path of continuation, we can fix these unknowns. In order to do so, we first constrain the paths using only information about the LLA in eq. (5.25). Subsequently, we can use any such LLA-admissible path to determine the free parameters in NLLA. As in the hexagon case (4.21), we accomplish this by constructing a general $\mathbb{Z}$-linear combination of discontinuities,

$$\left[R_{7,(2)}^{---} \right]^{\mathrm{CL}} = \left(2\pi i \sum_i c_i \Delta_i + (2\pi i)^2 \sum_{i,j} c_{i,j} \Delta_i \Delta_j + (2\pi i)^3 \sum_{i,j,k} c_{i,j,k} \Delta_i \Delta_j \Delta_k \right) R_{7,(2)}^{\mathrm{ope}}, \tag{5.41}$$

and match it against (5.25). Here, we include only non-zero discontinuities, see (5.32, 5.33, 5.34), which means that we need to find 5 linear coefficients c_i, 10 quadratic coefficients $c_{i,j}$ and 22 cubic coefficients $c_{i,j,k}$. The total winding conditions from Table 2, together with the dictionary in Table 4, fix the linear coefficients c_i to

$$\{c_1, c_2, c_3, c_4, c_5\} = \{0, 0, 1, 0, 0\} . \tag{5.42}$$

Matching at LLA, we obtain four constraints on the quadratic coefficients $c_{i,j}$. Next, we exploit that only special linear combinations in eq. (5.41) can actually come from some continuation curve, therefore there must be additional constraints on the coefficients $c_{i,j}$ and $c_{i,j,k}$. One such condition is discussed in eq. (2.26): One can express $c_{i,j} = c_i c_j - c_{j,i}$, which reduces the number of unknowns by 5.

We fix the remaining uncertainty in the coefficients by considering an Ansatz for the curve of continuation. From the structure of the commutation relations shown in Figure 4, we see that the most general continuation curve that has only one instance of $\mathcal{C}_3$ and does not involve $\mathcal{C}_1$ or $\mathcal{C}_2$ is

$$\gamma = \mathcal{C}_4^{\alpha_1} \mathcal{C}_5^{\alpha_2} \mathcal{C}_3 \mathcal{C}_4^{\alpha_3} \mathcal{C}_5^{\alpha_4} . \tag{5.43}$$

Assuming such a curve, all coefficients $\{c_i, c_{i,j}, c_{i,j,k}\}$ can be expressed in terms of the exponents $\{\alpha_1, \alpha_2, \alpha_3, \alpha_4\}$ via (2.22). Using the conditions (5.41) in LLA with the values (5.42) put in, the solution is unique:

$$\alpha_1 = \alpha_2 = \alpha_3 = \alpha_4 = 0\,, \tag{5.44}$$

which motivates our choice of the simplest continuation curve for the $(---)$ region in (5.36). With this curve, we can then compute the NLLA part of the remainder function $R_{7,(2)}^{---}$, and fix the four coefficients κ_i in the Ansatz (5.10) to assume the values (5.14) we stated before. Thereby, we have determined all the unknowns in our Ansatz for $R_{7,(2)}^{---}$. The numerical values for the κ_i we obtain are in full agreement with [22].

5.4.3 The Mandelstam Region $(-+-)$

After our detailed discussion of the region $(---)$, we can be rather brief for the remaining case $(-+-)$. For the latter, the winding number conditions force us to continue along a composite curve that must involve $\bar{\mathcal{C}}_1$, $\bar{\mathcal{C}}_2$ and $\mathcal{C}_3$. In addition, it can certainly also contain $\mathcal{C}_4$ and $\mathcal{C}_5$, as in the previous subsection. Table 2 shows that the Mandelstam region $\varrho = (-+-)$ also involves some half-windings, so that the continuation requires results from Appendix D in addition to the discontinuities we listed in the previous subsection.

Assuming that the generators $\mathcal{C}_3$, $\bar{\mathcal{C}}_1$, and $\bar{\mathcal{C}}_2$ each appear only once in the path-monomial, and taking into account the commutation relations of Figure 4, we find that there exist six different classes of possible curves

$$\gamma_{123} = \mathcal{C}_4^{\alpha_1} \mathcal{C}_5^{\alpha_2} \bar{\mathcal{C}}_1 \bar{\mathcal{C}}_2 \mathcal{C}_4^{\alpha_3} \mathcal{C}_5^{\alpha_4} \mathcal{C}_3 \mathcal{C}_4^{\alpha_5} \mathcal{C}_5^{\alpha_6}\,, \qquad \gamma_{213} = \mathcal{C}_4^{\alpha_1} \mathcal{C}_5^{\alpha_2} \bar{\mathcal{C}}_2 \bar{\mathcal{C}}_1 \mathcal{C}_4^{\alpha_3} \mathcal{C}_5^{\alpha_4} \mathcal{C}_3 \mathcal{C}_4^{\alpha_5} \mathcal{C}_5^{\alpha_6}\,, \tag{5.45}$$

$$\gamma_{132} = \mathcal{C}_4^{\alpha_1} \mathcal{C}_5^{\alpha_2} \bar{\mathcal{C}}_1 \mathcal{C}_4^{\alpha_3} \mathcal{C}_3 \mathcal{C}_5^{\alpha_4} \bar{\mathcal{C}}_2 \mathcal{C}_4^{\alpha_5} \mathcal{C}_5^{\alpha_6}\,, \qquad \gamma_{231} = \mathcal{C}_4^{\alpha_1} \mathcal{C}_5^{\alpha_2} \bar{\mathcal{C}}_2 \mathcal{C}_5^{\alpha_3} \mathcal{C}_3 \mathcal{C}_4^{\alpha_4} \bar{\mathcal{C}}_1 \mathcal{C}_4^{\alpha_5} \mathcal{C}_5^{\alpha_6}\,, \tag{5.46}$$

$$\gamma_{312} = \mathcal{C}_4^{\alpha_1} \mathcal{C}_5^{\alpha_2} \mathcal{C}_3 \mathcal{C}_4^{\alpha_3} \mathcal{C}_5^{\alpha_4} \bar{\mathcal{C}}_1 \bar{\mathcal{C}}_2 \mathcal{C}_4^{\alpha_5} \mathcal{C}_5^{\alpha_6}\,, \qquad \gamma_{321} = \mathcal{C}_4^{\alpha_1} \mathcal{C}_5^{\alpha_2} \mathcal{C}_3 \mathcal{C}_4^{\alpha_3} \mathcal{C}_5^{\alpha_4} \bar{\mathcal{C}}_2 \bar{\mathcal{C}}_1 \mathcal{C}_4^{\alpha_5} \mathcal{C}_5^{\alpha_6}\,. \tag{5.47}$$

By matching at LLA, for γ_{123}, γ_{132} and γ_{312} we obtain the following constraints on the exponents of the generators $\mathcal{C}_4$ and $\mathcal{C}_5$:

$$\alpha_1 = \alpha_2 = \alpha_3 = \alpha_4 = \alpha_5 = \alpha_6 = 0\,. \tag{5.48}$$

Similarly, one can also evaluate the constraints from the LLA for the paths γ_{213}, γ_{231} and γ_{321} to find that

$$-\alpha_1 = \alpha_2 = \alpha_5 = -\alpha_6 = 1 \tag{5.49}$$

$$\alpha_3 = \alpha_4 = 0\,. \tag{5.50}$$

With these constraints implemented, one can now proceed and compute the NLLA through analytic continuation of eq. (3.12). For all six curves, one obtains the same result (5.26) with the NLLA coefficients (5.38). Our analysis has indeed confirmed the paths we anticipated in eqs. (5.37, 5.39).

6 Conclusions and Outlook

In this work, we have proposed a new tool to determine the finite remainder function for all Mandelstam regions in multi-Regge kinematics. Our constraints were obtained through analytic continuation of known expressions for the remainder function on the main sheet in collinear kinematics. This input into our analysis is provided by the Wilson loop OPE, and is in principle available for any number of external gluons and any loop order. We illustrated the general

procedure in two examples, namely the hexagon and the heptagon at two loops. While the hexagon case admits only a single non-trivial Mandelstam region, there are four such regions for the heptagon. For one of these regions, the multi-Regge limit of the two-loop finite remainder was only determined quite recently in [23], though the leading logarithmic terms were known for some time [42].

Pushing this analysis to higher loops is not that difficult in principle. As we stressed above, the relevant input from the Wilson loop OPE is available. Here, we made some effort to express the two-loop collinear remainder function in terms of ordinary polylogarithms. That helped with the analytic continuation, but is not crucial. We could have been content with expressions involving Goncharov's multiple polylogarithms. The relevant expressions are considerably more bulky, but they can still be continued with computer algebra techniques [45]. For the hexagon, there is nothing new to learn, since the multi-Regge limit of the remainder function is known to all orders [10]. On the other hand, higher-loop results for the multi-Regge limit of the remainder function with more than six external gluons are scarce. For the heptagon remainder function, for example, only the LLA is known to all orders in the coupling and for all Mandelstam regions [17, 18]. It would therefore be very interesting to extend our analysis of the heptagon to higher loops. Of course, the ultimate hope would be to obtain all-loop expressions for all Mandelstam regions by analytically continuing the Wilson loop OPE at finite coupling, i. e. without expanding in the 't Hooft coupling, as done in [10] for the hexagon. Right now, this seems difficult, especially for the $\varrho = (-+-)$ region. The perturbative analysis we carried out above and its extension to higher orders is a rather pedestrian approach that could help to obtain insights into the appropriate continuation paths, and thereby valuable input for the more ambitious finite-coupling analysis.

The potential issues with finding the correct path of analytic continuation were seen at strong coupling already. At infinite 't Hooft coupling, the most non-trivial contribution to the remainder function may be interpreted as the free energy of an integrable one-dimensional quantum system [46]. For generic kinematics, this is still difficult to compute, because the elementary particles of the one-dimensional system are screened by clouds of excitations. As was shown in [15, 25], however, the multi-Regge limit in the gauge theory amounts to sending all masses in the one-dimensional auxiliary system to infinity, and hence it suppresses the difficult quantum fluctuations. As a result, in computing the free energy, one only has to solve for a finite set of Bethe roots rather than for a set of particle densities that are determined as solutions of a coupled set of non-linear integral equations [47]. Which roots contribute for a given Mandelstam region, however, depends on the continuation path. For the hexagon, and for three of the four Mandelstam regions in the heptagon, the relevant solutions were found in [15, 26]. But in the case of the region $\varrho = (-+-)$, the suggested continuation path was shown to be associated with the trivial solution of the Bethe Ansatz equations, even though its winding numbers correctly satisfy the kinematic constraints (2.7). In the light of our analysis in Section 5, and in particular the insight we gained into the choice of paths close to the collinear limit, it would be interesting to revisit this issue at strong coupling.

Our perturbative analysis above was restricted to the leading terms in the collinear limit. It would certainly be of interest to include higher-order corrections in the variables T_i. This requires to consider contributions from gluon bound-state excitations of the GKP string, extending the resummations of [34]. Continuing additional terms in the expansion around the collinear limit could provide additional information on the remainder function in the various Mandelstam regions.

There is actually another way in which our analysis may be extended to obtain further information on the multi-Regge remainder function. The combined multi-Regge collinear limit with the coordinates introduced in Section 2.1 probes the neighborhood of a particular codimension-two subregion of the heptagon multi-Regge limit. We can probe different regions by cyclically shifting
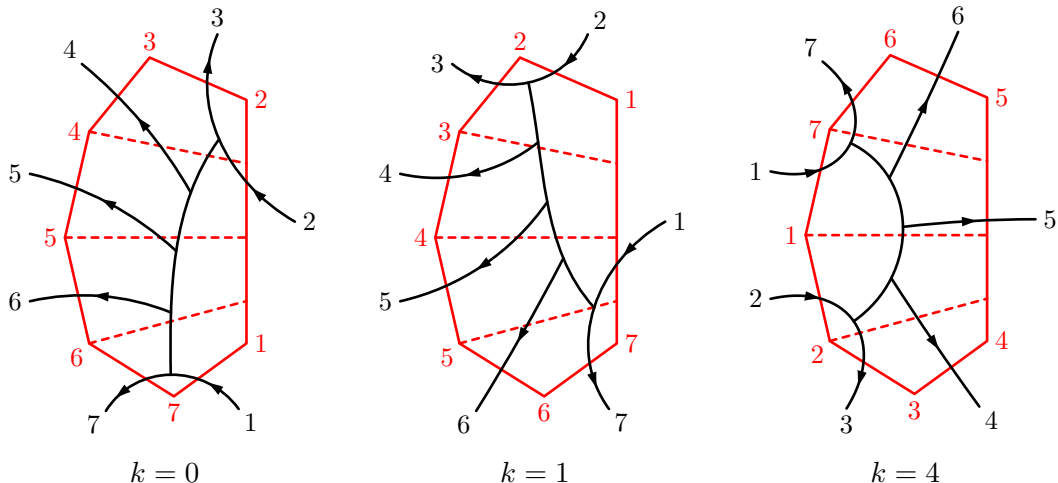
Figure 5: Shifted kinematics: The collinear limit of the Wilson-loop OPE (tessellation shown in red) has a non-trivial overlap with the multi-Regge limit (kinematics shown in black) for three different cyclic shifts $x_i \to x_{n-k}$, where $k = 0, 1, 4$. The shifts $k = 0, 1$ are related by symmetries, but the shift $k = 4$ is an independent combined multi-Regge collinear limit.

the kinematics $x_i \to x_{i-k}$ on the Wilson loop OPE side. The collinear limit described by the Wilson loop OPE will not have an overlap with the multi-Regge limit for all shifts k, but it does have a non-trivial overlap for $k = 1$ and for $k = 4$ (for a non-trivial overlap, the "small" cross ratios $u_{j,k}$, $j = 5, 6$, $k = 2, 3$ must become small when $T_5, T_6 \to 0$.). The benefit of the choice $k = 0$ described in the main text is that it has an overlap with the multi-Regge limit for all multiplicities. The kinematics with a shift $k = 1$ are related to $k = 0$ by a combination of target-projectile symmetry ($p_i \to p_{3-i}$) and reversing the OPE variables $\{F, S, T\}_i \to \{F, S, T\}_{n+4-i}$ and hence, although having a non-trivial overlap with the multi-Regge limit for any n, does not yield independent information on the Regge limit. The shift $k = 4$ is specific to the heptagon, and does contain new information. In addition, it is a very symmetric choice, see Figure 5. For the analysis in this paper, the constraints from $k = 0$ were sufficient to fix all unknowns, and we merely used the independent constraints from $k = 4$ to cross-check our results. But at higher loop orders it might be useful to combine the constraints from $k = 0$ and $k = 4$ to determine the remainder function.

Let us finally also mention the extension to higher numbers of external gluons. The multi-Regge limit of the remainder function R_8 for $n = 8$ external gluons probes a new cut that can be associated with the eigenvalue of a non-compact Heisenberg spin chain of length three [48]. While in leading logarithmic order this eigenvalue is simply the sum of eigenvalues for a spin chain of length two, higher orders give rise to terms which represent a new three-body interaction between reggeized gluons [49]. Again, the detailed composition of R_8 depends upon the kinematic region. The next extensions of the spin chain are expected to be seen in the $n = 10$ point scattering process, $2 \to 8$, the $n = 12$ point process, $2 \to 10$, etc. One of the challenges will be to find, beyond the LLA, the eigenvalues of this spin chain. The three-body interaction found in [49] raises some doubts whether they are simply obtained from the sum of two-body interactions. This issue certainly deserves further investigation.

Acknowledgments
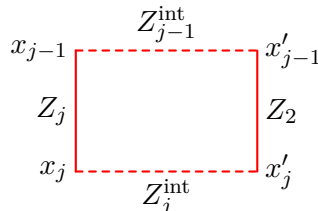
A Explicit Polygon Parametrizations

As explained in Section 2.1, we tessellate the n-point polygon with cusps $x_1, \ldots, x_n$ by drawing the unique null lines from x_j to the null line x_{12}, intersecting the line x_{12} at points x'_j, for $j = 4, \ldots, n-1$. These internal null lines dissect the polygon into two boundary and $n-5$ internal null tetragons. Each internal null tetragon formed by x_{j-1}, x_j, x'_j, and x'_{j-1} is preserved by three conformal transformations, which we parametrize by τ_j, σ_j, and ϕ_j as in [1, 2, 27, 29]. Both the external and internal null lines are conveniently parametrized by the four-component momentum twistors Z_j (see Figure 2). Using the four-bracket $\langle i, j, k, l \rangle := \det(Z_i Z_j Z_k Z_l)$ combinations of these variables, one can express the cross ratios shown in eq. (2.3) as:

$$U_{ij} = \frac{\langle i, i+1, j+1, j+2 \rangle \langle i+1, i+2, j, j+1 \rangle}{\langle i, i+1, j, j+1 \rangle \langle i+1, i+2, j+1, j+2 \rangle} \,. \tag{A.1}$$

For the j'th internal null tetragon, the relevant momentum twistors are:
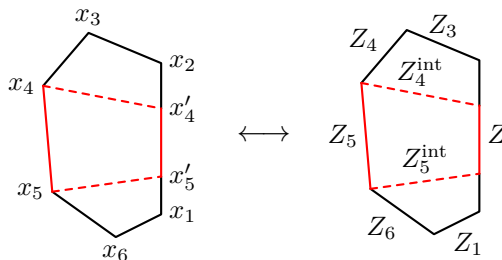

$$\tag{A.2}$$

Conformal transformations act linearly on momentum twistors. The three transformations τ_j, σ_j, and ϕ_j are defined in terms of the matrix $M_j = M_j(\tau_j, \sigma_j, \phi_j)$ via

$$\begin{pmatrix} Z_j \\ Z_2 \\ Z^{\text{int}}_{j-1} \\ Z^{\text{int}}_j \end{pmatrix} M_j = \sqrt{F_j} \begin{pmatrix} 1/(F_j S_j) & 0 & 0 & 0 \\ 0 & S_j/F_j & 0 & 0 \\ 0 & 0 & T_j & 0 \\ 0 & 0 & 0 & 1/T_j \end{pmatrix} \begin{pmatrix} Z_j \\ Z_2 \\ Z^{\text{int}}_{j-1} \\ Z^{\text{int}}_j \end{pmatrix} , \tag{A.3}$$

where the column of Z's is understood as a 4×4 matrix, and

$$T_j = e^{-\tau_j} \,, \qquad S_j = e^{\sigma_j} \,, \qquad F_j = e^{i\phi_j} \,. \tag{A.4}$$

Let us illustrate how all conformally inequivalent null polygons are constructed from the parameters $\{\tau_j, \sigma_j, \phi_j\}$ by considering the hexagon. In this case, there is only one internal tetragon:

$$\tag{A.5}$$

Because conformally inequivalent null hexagons have three degrees of freedom, and because all null tetragons are conformally equivalent, all conformally inequivalent hexagons are generated by starting with an arbitrary fixed reference hexagon, and acting with the conformal transformations

M_5 that preserve the inner tetragon on the upper part of the hexagon, i.e. on the momentum twistors Z_3 and Z_4. Concretely, we use:

$$Z_2 = (1, 0, 0, 0) \,,$$
$$Z_3 = (1, 0, 1, 1) \,,$$
$$Z_4 = (0, 1, 0, -1) \,,$$
$$Z_5 = (0, 1, 0, 0) \,, \qquad M_5 = \sqrt{F_5} \begin{pmatrix} S_5/F_5 & 0 & 0 & 0 \\ 0 & 1/(F_5 S_5) & 0 & 0 \\ 0 & 0 & 1/T_5 & 0 \\ 0 & 0 & 0 & T_5 \end{pmatrix} \,, \qquad (A.6)$$
$$Z_6 = (0, 1, -1, 0) M_5 \,,$$
$$Z_1 = (-1, 0, 1, 1) M_5 \,,$$
$$Z_4^{\text{int}} = (0, 0, 0, 1) \,,$$
$$Z_5^{\text{int}} = (0, 0, 1, 0) \,,$$

where M_5 is the solution to eq. (A.3). We construct the heptagon by extending the hexagon at the bottom, such that Z_1 of the hexagon becomes Z_6^{int} of the heptagon:

$$(A.7)$$

Concretely, we choose:

$$Z_2 = (1, 0, 0, 0) \,,$$
$$Z_3 = (1, 0, 1, 1) \,,$$
$$Z_4 = (0, 1, 0, -1) \,,$$
$$Z_5 = (0, 1, 0, 0) \,, \qquad M_5 = \sqrt{F_5} \begin{pmatrix} \frac{S_5}{F_5} & 0 & 0 & 0 \\ 0 & \frac{1}{F_5 S_5} & 0 & 0 \\ 0 & 0 & \frac{1}{T_5} & 0 \\ 0 & 0 & 0 & T_5 \end{pmatrix} \,,$$
$$Z_6 = (0, 1, -1, 0) M_5 \,,$$
$$Z_7 = (1, 1, -2, -1) M_6 M_5 \,, \qquad (A.8)$$
$$Z_1 = (2, 0, 0, -1) M_6 M_5 \,, \qquad M_6 = \sqrt{F_6} \begin{pmatrix} \frac{S_6}{F_6} & 0 & 0 & 0 \\ 0 & \frac{1}{F_6 S_6} & T_6 - \frac{1}{F_6 S_6} & 0 \\ 0 & 0 & T_6 & 0 \\ \frac{S_6}{F_6} - \frac{1}{T_6} & 0 & \frac{1 - T_6^2}{T_6} & \frac{1}{T_6} \end{pmatrix} \,,$$
$$Z_4^{\text{int}} = (0, 0, 0, 1) \,,$$
$$Z_5^{\text{int}} = (0, 0, 1, 0) \,,$$
$$Z_6^{\text{int}} = (-1, 0, 1, 1) M_5 \,,$$

where again M_5 and M_6 are the solutions to eq. (A.3), and we have chosen to act with the transformation M_6 on Z_1 and Z_7 instead of acting with M_6^{-1} on Z_3, Z_5, Z_5, and Z_4^{int}, the difference being just an overall conformal transformation.

Of course the choice of numerical reference polygon in eqs. (A.6) and (A.8) is arbitrary. Our choice is constructed in such a way that the "large" and "small" cross ratios (2.4)

$$u_{j,i} \,, \qquad j = 5, \ldots, n - 1 \,, \qquad i = 1, 2, 3 \,, \qquad (A.9)$$

when expressed in terms of T_j, S_j, and F_j, in the multi-Regge limit take the canonical form (2.16), with the simple identifications (2.15)

$$S_j^2 = \frac{T_j^2}{w_j \bar{w}_j} \,, \qquad F_j^2 = \frac{w_j}{\bar{w}_j} \,. \qquad (A.10)$$

For all $j \geq 0$:

$\boldsymbol{Z}_{6j+4} = (6j, 1, 0, -1)$,

$\boldsymbol{Z}_{6j+5} = (6j, 1, 0, 0)$,

$\boldsymbol{Z}_{6j+6} = (6j, 1, -1, 0)$,

$\boldsymbol{Z}_{6j+7} = (6j+1, 1, -2, -1)$,

$\boldsymbol{Z}_{6j+8} = (6j+3, 1, -2, -2)$,

$\boldsymbol{Z}_{6j+9} = (6j+5, 1, -1, -2)$,

$$
\begin{pmatrix} \boldsymbol{Z}_3 \\ \boldsymbol{Z}_4^{\text{int}} \\ \boldsymbol{Z}_5^{\text{int}} \\ \boldsymbol{Z}_6^{\text{int}} \\ \vdots \\ \boldsymbol{Z}_{n-1}^{\text{int}} \\ \boldsymbol{Z}_1 \end{pmatrix} = \begin{pmatrix} (1,0,1,1) \\ (0,0,0,1) \\ (0,0,1,0) \\ (-1,0,1,1) \\ (2,0,0,-1) \\ (2,0,1,0) \\ \vdots \\ \text{cyclic rep.} \\ \vdots \end{pmatrix}, \qquad \boldsymbol{Z}_2 = (1,0,0,0),
$$

$$
Z_j = \begin{cases} \boldsymbol{Z}_j & 2 \leq j \leq 5, \\ \boldsymbol{Z}_j M_{j-1} \ldots M_6 M_5 & 6 \leq j \leq n, \end{cases} \qquad Z_j^{\text{int}} = \begin{cases} \boldsymbol{Z}_j^{\text{int}} & 4 \leq j \leq 5, \\ \boldsymbol{Z}_j^{\text{int}} M_{j-1} \ldots M_6 M_5 & 6 \leq j \leq n-1, \end{cases}
$$

$$
Z_1 = \boldsymbol{Z}_1 M_{n-1} \ldots M_6 M_5.
$$

Table 5: Parametrization of the n-point polygon for any $n \geq 6$. The boldface momentum twistors $\boldsymbol{Z}_j$ define a fixed reference polygon, where "cyclic rep." stands for cyclic repetitions of the six given momentum twistors. All conformally inequivalent polygons are parametrized by the Z in normal face. They are obtained from the reference polygon by acting with each matrix M_j stabilizing the j'th internal tetragon on all momentum twistors below that tetragon (see eqs. (A.6) and (A.8) for examples). For reference, the matrices M_j are given in Table 6. This specific choice of reference polygon is engineered to satisfy the relations (2.16) with eq. (A.10) in the multi-Regge limit.

For other choices of reference polygons, the relation between $w_j, \bar{w}_j$ and T_j, S_j, F_j might get more complicated. More concretely, extending the $(n-1)$-gon to the n-gon requires adding two momentum twistors (that will become Z_n and the new Z_1), which have six degrees of freedom. Three of those degrees of freedom are fixed by consistency with the $(n-1)$-gon, namely by requiring that the equation (see Figure 2)

$$
Z_j^{\text{int}} = \langle 1, 2, 3, j \rangle Z_{j+1} - \langle 1, 2, 3, j+1 \rangle Z_j \tag{A.11}
$$

for the internal twistor Z_{n-1}^{int} (which was Z_1 in the $(n-1)$-gon) is satisfied. The three remaining degrees of freedom are fixed by imposing the multi-Regge limit relations (2.16) with (A.10).

This construction can be iterated to any number of points. We have solved the constraints explicitly for up to $n = 18$, and then recognized the pattern shown in Table 5. Here, the transformation matrices M_j, $j = 5, \ldots, n-1$, are defined via eq. (A.3) with all other M_i, $i \neq j$ set to 1. For completeness, we explicitly list these matrices in Table 6. We have checked the consistency of this parametrization with eqs. (2.16), (A.10), and (A.11) up to $n = 30$. In order to avoid overly complicated expressions, one can alternatively choose to act with the global conformal transformation $M_5^{-1} \ldots M_{2+\lfloor n/2 \rfloor}^{-1}$ on the full polygon, which evenly distributes the action of the matrices M_j on the top and bottom of the polygon and thus renders expressions a bit simpler.

The parametrization in Table 5 also entails uniform expressions for the cross ratios (A.9). We quote their expansions in the multi-collinear limit $T_j \to 0$, $j = 5, \ldots, n-1$:

$$
u_{j,1} = \frac{1}{(1+S_{j-1}^2)(1+S_j^2)} \left[1 + S_{j-1}^2(1+S_j^2) - \frac{2\cos(\phi_{j-1}) S_{j-1}^3 S_j^2 T_{j-1}}{1+S_{j-1}^2} - \frac{2\cos(\phi_j) S_j T_j}{1+S_j^2} \right.
$$

$$
\left. - \frac{S_{j-1}^2 [1 - 2\cos(2\phi_{j-1}) S_{j-1}^2 + S_{j-1}^4] S_j^2 T_{j-1}^2}{(1+S_{j-1}^2)^2} - \frac{[1 - 2\cos(2\phi_j) S_j^2 + S_j^4] T_j^2}{(1+S_j^2)^2} \right.
$$

38

$$M_j = \sqrt{F_j} \begin{pmatrix} \frac{S_j}{F_j} & 0 & 0 & 0 \\ \frac{(j-5)(1-S_j^2)}{F_j S_j} & \frac{1}{F_j S_j} & 0 & 0 \\ 0 & 0 & \frac{1}{T_j} & 0 \\ 0 & 0 & 0 & T_j \end{pmatrix} , \qquad\qquad j \in 6\mathbb{Z} - 1 \,,$$

$$M_j = \sqrt{F_j} \begin{pmatrix} \frac{S_j}{F_j} & 0 & 0 & 0 \\ \frac{(j-6)(1-S_j^2)}{F_j S_j} & \frac{1}{F_j S_j} & T_j - \frac{1}{F_j S_j} & 0 \\ 0 & 0 & T_j & 0 \\ \frac{S_j}{F_j} - \frac{1}{T_j} & 0 & \frac{1}{T_j} - T_j & \frac{1}{T_j} \end{pmatrix} , \qquad\qquad j \in 6\mathbb{Z} \,,$$

$$M_j = \sqrt{F_j} \begin{pmatrix} \frac{S_j}{F_j} & 0 & 0 & 0 \\ -\frac{(j-6)(S_j^2-1)}{F_j S_j} - 2T_j + \frac{2}{T_j} & \frac{1}{F_j S_j} & 2T_j - \frac{2}{F_j S_j} & 2T_j - \frac{1}{F_j S_j} - \frac{1}{T_j} \\ -\frac{S_j}{F_j} - T_j + \frac{2}{T_j} & 0 & T_j & T_j - \frac{1}{T_j} \\ \frac{2S_j}{F_j} - \frac{2}{T_j} & 0 & 0 & \frac{1}{T_j} \end{pmatrix} , \quad j \in 6\mathbb{Z} + 1 \,,$$

$$M_j = \sqrt{F_j} \begin{pmatrix} \frac{S_j}{F_j} & 0 & 0 & 0 \\ -\frac{(j-5)(S_j^2-1)}{F_j S_j} - 4T_j + \frac{4}{T_j} & \frac{1}{F_j S_j} & \frac{2}{T_j} - \frac{2}{F_j S_j} & 2T_j - \frac{2}{F_j S_j} \\ \frac{2}{T_j} - \frac{2S_j}{F_j} & 0 & \frac{1}{T_j} & 0 \\ \frac{2S_j}{F_j} - 2T_j & 0 & 0 & T_j \end{pmatrix} , \qquad\qquad j \in 6\mathbb{Z} + 2 \,,$$

$$M_j = \sqrt{F_j} \begin{pmatrix} \frac{S_j}{F_j} & 0 & 0 & 0 \\ -\frac{(j-4)(S_j^2-1)}{F_j S_j} - 2T_j + \frac{2}{T_j} & \frac{1}{F_j S_j} & -T_j - \frac{1}{F_j S_j} + \frac{2}{T_j} & \frac{2}{T_j} - \frac{2}{F_j S_j} \\ 2T_j - \frac{2S_j}{F_j} & 0 & T_j & 0 \\ \frac{S_j}{F_j} - 2T_j + \frac{1}{T_j} & 0 & \frac{1}{T_j} - T_j & \frac{1}{T_j} \end{pmatrix} , \quad j \in 6\mathbb{Z} + 3 \,,$$

$$M_j = \sqrt{F_j} \begin{pmatrix} \frac{S_j}{F_j} & 0 & 0 & 0 \\ -\frac{(j-4)(S_j^2-1)}{F_j S_j} & \frac{1}{F_j S_j} & 0 & \frac{1}{T_j} - \frac{1}{F_j S_j} \\ T_j - \frac{S_j}{F_j} & 0 & T_j & T_j - \frac{1}{T_j} \\ 0 & 0 & 0 & \frac{1}{T_j} \end{pmatrix} , \qquad\qquad j \in 6\mathbb{Z} + 4 \,.$$

Table 6: Matrices M_j, $5 \le j \le (n-1)$ appearing in Table 5 that stabilize the j'th internal tetragon of the reference polygon. Each of these matrices is a solution to the defining equation (A.3) with all other matrices set to $M_i = 1$.

$$+ \frac{2S_{j-1}S_j\big[\cos(\phi_{j-1}+\phi_j)(1+S_j^2+S_{j-1}^2S_j^2)-\cos(\phi_{j-1}-\phi_j)S_{j-1}^2\big]T_{j-1}T_j}{(1+S_{j-1}^2)(1+S_j^2)}\Bigg] + \mathcal{O}(T_i^3)\,,$$

$$u_{j,2} = \frac{A_j}{1+A_j} + \frac{2}{(1+A_j)^2}\Bigg[-\cos\phi_j A_j S_j T_j + \sum_{i=j+1}^{n-1}\cos\phi_i \prod_{k=j}^{i-1} S_k^2 S_i T_i\Bigg] + \mathcal{O}(T_i^2)\,, \tag{A.12}$$

$$u_{j,3} = T_j^2\Bigg[1 + (T_{j-1}^2+T_{j+1}^2) + (T_{j-2}^2T_{j-1}^2+T_{j-1}^4+T_{j-1}^2T_{j+1}^2+T_{j+1}^4+T_{j+1}^2T_{j+2}^2) + \mathcal{O}(T_{i\neq j}^6)\Bigg]$$

The leading terms in these expressions can be recognized in eq. (2.17). Here, $\mathcal{O}(T_i^\ell)$ stands for any products of all T_i of total order at least ℓ. The parameters A_j are defined via

$$S_j^2 = \frac{A_j}{1+A_{j+1}}\,, \qquad j = 5,\dots,n-1\,. \tag{A.13}$$

In all expressions above, we set

$$A_n = 0\,, \qquad S_j = T_j = 0 \quad\text{for}\quad j \notin \{5,\dots,n-1\}\,. \tag{A.14}$$

The last expression for $u_{j,3}$ in eq. (A.12) is exact in T_j. In fact, we can write the full expression for $u_{j,3}$ in general kinematics. It is a ratio of polynomials in the T_i^2 with unit coefficients:

$$u_{j,3} = T_j^2\frac{P_5^{j-2}\,P_{j+2}^{n-1}}{P_5^{j-1}\,P_{j+1}^{n-1}}\,, \qquad P_a^b = \sum_{I\in\mathcal{I}_a^b}\prod_{\ell=1}^{|I|}(-T_{i_\ell}^2) = 1 - \sum_{i=a}^{b}T_i^2 + \dots\,,$$

$$\mathcal{I}_a^b = \big\{(i_1,\dots,i_k)\,|\,k\geq 0\wedge a\leq i_\ell\leq b\wedge i_\ell+2\leq i_{\ell+1}\big\}\,. \tag{A.15}$$

In the multi-Regge limit, where all $T_i\to 0$ with $r_i = S_i/T_i$ fixed, we find the expansions

$$u_{j,2}\,u_{j,3} = \Big[1 + T_{j-1}^2 + \big(2 + 2\cos(\phi_{j+1})r_{j+1}+r_{j+1}^2\big)T_{j+1}^2 + \mathcal{O}(T_{i\neq j}^4)\Big]r_j^2T_j^4 + \mathcal{O}(T_j)^6\,, \tag{A.16}$$

$$\frac{u_{j,2}}{1-u_{j,1}} = \frac{r_j^2}{1+2\cos(\phi_j)r_j+r_j^2}\Bigg[1 + \Big(2\frac{\cos(\phi_{j-1})+\cos(\phi_{j-1}+\phi_j)r_j}{1+2\cos(\phi_j)r_j+r_j^2}r_{j-1}+r_{j-1}^2\Big)T_{j-1}^2$$

$$- T_j^2 + \Big(1+2\cos(\phi_{j+1})r_{j+1}+r_{j+1}^2\Big)T_{j+1}^2\Bigg] + \mathcal{O}(T_i^4)\,,$$

$$\frac{u_{j,3}}{u_{j,2}} = \frac{1}{r_j^2}\Bigg[1 + T_{j-1}^2 + \Big[1+2\cos(\phi_j)r_j+r_j^2\Big]T_j^2 - \Big[2\cos(\phi_{j+1})r_{j+1}+r_{j+1}^2\Big]T_{j+1}^2\Bigg] + \mathcal{O}(T_i^4)\,.$$

Besides providing an unambiguous parametrization of conformally inequivalent null polygons, the variables τ_j, σ_j, and ϕ_j explained above are of course designed for the application of the OPE for null polygon Wilson loops [1–3,5,27,29]. To this end, note that the reference n-point polygon of Table 5 is somewhat singular: For $T_j = S_j = F_j = 1$, several internal distances $x_i - x_j$ among cusps are null, and some others are timelike. The reference polygon therefore lies outside the Euclidean region where the Wilson loop OPE is applicable. However, all internal distances become spacelike when approaching the multi-collinear limit, i.e. when all parameters T_j are small, and hence the Wilson loop OPE can be applied in this region. In fact, we find experimentally that all internal distances $x_i - x_j$ are spacelike as long as all $T_i \leq 1/2$, $i = 5,\dots,n-1$.

B Performing the One-Loop Sums

In this appendix, we fill in some details about the evaluation of the sums in the one-loop contribution of the one-gluon excitation shown in eq. (3.25), which we split into double sums Σ_2 and single sums Σ_1:

$$h_1^{(0,0)} = g^2\frac{S_6}{S_5}\big(\Sigma_2 + \Sigma_1\big)\,. \tag{B.1}$$

We begin with the double sum,

$$\Sigma_2 := \sum_{k_{5,6}\in\mathbb{Z}_{\geq 1}} \frac{(-S_5^{-2})^{k_5}(-S_6^2)^{k_6}}{(k_5+1)(k_6+1)k_5 k_6} \times \frac{\Gamma(1+k_5+k_6)}{\Gamma(k_5)\Gamma(k_6)} = \sum_{j=2}^{\infty}\sum_{k_5=1}^{j-1} \frac{(S_5^2 S_6^2)^{-k_5}(-S_6^2)^j}{(k_5+1)(j-k_5+1)}\binom{j}{k_5}.$$
(B.2)

To reach the right hand side, we have introduced the summation index $j = k_5 + k_5$. Now we can split the denominators in the following way:

$$\frac{1}{(k_5+1)(j-k_5+1)} = \frac{1}{j+2}\Big(\frac{1}{k_5+1} + \frac{1}{j-k_5+1}\Big).$$
(B.3)

Note that if we let $k_5' = j - k_5$ and make use of $\binom{j}{j-k_5'} = \binom{j}{k_5'}$, we can decompose eq. (B.2) into two sums that only differ by the replacement $S_5 \leftrightarrow 1/S_6$,

$$\Sigma_2 = \sum_{j=2}^{\infty} \frac{(-S_6^2)^j}{j+2}\left(\sum_{k_5=1}^{j}(S_5^2 S_6^2)^{-k_5}\binom{j}{k_5}\frac{1}{k_5+1} - (S_5^2 S_6^2)^{-j}\frac{1}{j+1}\right) + (S_5 \leftrightarrow 1/S_6).$$
(B.4)

Next, we eliminate the $(+1)$ offset in the denominator of the inner sum. This can be done with the help of the binomial identity $\binom{j}{k-1} = \frac{k}{j+1}\binom{j+1}{k}$ (for a more general treatment, see eq. (44) in [35]),

$$\sum_{k_5=1}^{j}(S_5^2 S_6^2)^{-k_5}\binom{j}{k_5}\frac{1}{k_5+1} = \sum_{k=2}^{j+1}(S_5^2 S_6^2)^{-(k-1)}\binom{j}{k-1}\frac{1}{k} = \left(1+\frac{1}{S_5^2 S_6^2}\right)^{j+1} S_5^2 S_6^2 \frac{1}{j+1} - 1.$$
(B.5)

After these steps, the outer summation over j may be performed straightforwardly:

$$\Sigma_2 = \frac{1+S_5^2+S_5^2 S_6^2}{S_6^2}\log\frac{1+S_5^2+S_5^2 S_6^2}{(1+S_5^2)(1+S_6^2)} + 1.$$
(B.6)

Having evaluated the sum in the first line of eq. (B.2), it remains to look at the single sum,

$$\Sigma_1 := \sum_{k_5\in\mathbb{Z}_{\geq 1}} \frac{(-S_5^{-2})^{k_5}+(-S_6^2)^{k_5}}{k_5+1} + 1 = S_5^2 \log\left(1+S_5^{-2}\right) + S_6^{-2}\log\left(1+S_6^2\right) - 1.$$
(B.7)

Combining these Σ_1 and Σ_2 sums back into eq. (B.1), we obtain (up to an overall sign) eq. (125) from [2] that was stated in eq. (3.26).

C The Function g

At LLA, the MRL two-loop remainder function for all multiplicities and in all kinematic regions can be expressed in terms of the six-point function (4.7). At NLLA, further functions g and $\tilde{g}$ are required to express the seven-point remainder function in the kinematic regions $(---)$ and $(-+-)$. Writing out the expressions (5.8) and (5.15), one finds

$$R_{7,(2)}^{---} = \log(\varepsilon_5)f_1(v_5) + \log(\varepsilon_6)f_1(v_6) + f_0(v_5) + f_0(v_6) + g(v_5, v_6),$$
(C.1)

$$R_{7,(2)}^{-+-} = \log(\varepsilon_5)\big(f_1(v_5) - f_1(w_5)\big) + \log(\varepsilon_6)\big(f_1(v_6) - f_1(w_6)\big)$$
$$+ f_0(v_5) - f_0(w_5) + f_0(v_6) - f_0(w_6) + \tilde{g}(v_5, v_6).$$
(C.2)

At symbol level, the remainder functions in the various regions satisfy the identity [20]

$$S[R_{7,(2)}^{-+-}] = S[R_{7,(2)}^{---}] - S[R_{7,(2)}^{--+}] - S[R_{7,(2)}^{+--}],$$
(C.3)

41

and therefore the symbols of g and $\tilde{g}$ are identical:

$$S[g(v_5, v_6)] = S[\tilde{g}(v_5, v_6)] \,. \tag{C.4}$$

Based on its symbol as well as symmetry arguments, the function g was determined up to 25 unfixed rational coefficients [20]. Subsequently, the function g was fully determined in [22]. The latter result assumes a specific path of continuation from the Euclidean to the $(---)$ region, and is justified by Regge factorization. In the following, we independently refine the determination of the functions g and $\tilde{g}$. Without making assumptions on the path of continuation, we are able to determine both g and $\tilde{g}$ up to a few coefficients.

Function Space. Maximally helicity-violating amplitudes in $\mathcal{N} = 4$ super Yang–Mills theory are rational polynomials in multiple polylogarithms, $i\pi$, and (multiple) zeta values, where all occurring monomials have the same (uniform) transcendental weight [50]. Multiple polylogarithms, also called Goncharov polylogarithms [44], can be defined recursively as iterated integrals

$$G(a_1, \ldots, a_n; z) \equiv \begin{cases} \dfrac{1}{n!} \log^n z & \text{if } a_1 = \ldots = a_n = 0 \,, \\ \displaystyle\int_0^z \dfrac{dt}{t - a_1} G(a_2, \ldots, a_n; t) & \text{otherwise,} \end{cases} \tag{C.5}$$

with $G(; z) = 1$. The sequence of parameters $(a_1, \ldots, a_n)$ is called the weight vector, and the length of the weight vector equals the transcendental weight (or transcendentality) of the function $G(a_1, \ldots, a_n; z)$. The parameters a_i are also called letters, and the set of all multiplicatively independent letters that occur in a given function is called the alphabet of that function. Multiple zeta values are defined in terms of multiple polylogarithms evaluated at unity, and inherit their transcendental weight: ζ_k has weight k, $\zeta_{j,k}$ has weight $j + k$, and so forth. π has weight 1.

As noted in [20], using the variables (5.9), the alphabet of the seven-point remainder function in all Mandelstam regions becomes

$$\aleph_{xy} = \{x, 1 - x, y, 1 - y, 1 - xy\} \cup \{\text{c.c.}\} \,. \tag{C.6}$$

Multiple polylogarithms whose symbols draw their entries from this alphabet belong to the class of two-dimensional harmonic polylogarithms (2dHPLs) [51]. An independent basis for these is given by [52][11]

$$\{G(\vec{a}, x) \,|\, \vec{a}_i \in \text{Lyn}\{0, 1\}\} \cup \{G(\vec{a}, 1/y) \,|\, \vec{a}_i \in \text{Lyn}\{0, 1, x\}\} \cup \{\text{c.c.}\} \,, \tag{C.7}$$

where $\{\text{c.c.}\}$ stands for the complex conjugates of the previous sets, and $\text{Lyn}\{0, 1\}$ and $\text{Lyn}\{0, 1, x\}$ denote the sets of Lyndon words formed from the ordered sets of letters $\{0, 1\}$ and $\{0, 1, x\}$, respectively.

Single-Valuedness. Besides the consistency with the known symbol, the functions g and $\tilde{g}$ have to satisfy various constraints. One of them is single-valuedness: Due to unitarity, a physical amplitude can only have branch points where one of the cross ratios vanishes (or becomes infinite). Since the cross ratios are expressed in terms of absolute squares of the complex variables w_5 and w_6, see eq. (2.5), a rotation $(w_5 - z, \bar{w}_5 - \bar{z}) \to (e^{+2\pi i}(w_5 - z), e^{-2\pi i}(\bar{w}_5 - \bar{z}))$ around any point z in the complex plane can never let a cross ratio wind around zero (or infinity). The same is true for rotations of w_6, and therefore also for rotations of x and y. The conclusion is that the remainder function in the multi-Regge limit must be a single-valued function of the

---

[11] The choice of basis is not unique. We used a different basis in [20], but found the choice (C.7) more suitable for the present analysis.

complex variables x and y, and thus the same must be true for the functions g and $\tilde{g}$. This property has been essential for the determination of the six-point multi-Regge limit to high loop orders [13, 14, 53, 54].

It turns out that the single-valuedness constraint can be satisfied directly at the level of the basis: Single-valued multiple polylogarithms were constructed by Brown [43]. A suitable basis of such functions for multi-Regge amplitudes of any multiplicity was proposed in [21]. The single-valued basis can be constructed purely algebraically from the basis of ordinary multiple polylogarithms (C.7) using the Hopf algebra structure that underlies the multiple polylogarithm algebra [44]: Each holomorphic element G of the ordinary basis (C.7) gets promoted to a single-valued function $G^{\mathbf{s}}$ by the single-valued map [43]

$$\boldsymbol{s} : G(\vec{a}, z) \mapsto G^{\mathbf{s}}(\vec{a}, z) \equiv (-1)^{|\vec{a}|} \mu(\bar{S} \otimes \mathrm{id}) \Delta G(\vec{a}, z) \,, \tag{C.8}$$

where Δ is the coproduct, id is the identity, $\bar{S}$ is the complex conjugate of the antipode map of the Hopf algebra, and μ denotes the multiplication operator $\mu(a \otimes b) = a \cdot b$. All details of the single-value map are spelled out in Section 3.4.3 of [21], and we will not reproduce them here. For example, one finds[12]

$$\begin{aligned}
G^{\mathbf{s}}(0, x, 1/y) = {} & -G(0, x)G(\bar{x}, 1/\bar{y}) - G(0, \bar{x})G(\bar{x}, 1/\bar{y}) + G(0, 1/y)G(\bar{x}, 1/\bar{y}) \\
& + G(0, 1/\bar{y})G(\bar{x}, 1/\bar{y}) + G(0, x, 1/y) - G(0, \bar{x}, 1/\bar{y}) \,. \tag{C.9}
\end{aligned}$$

The anti-holomorphic elements of (C.7) can equally be promoted to single-valued functions, which however are not independent from the single-valued functions generated from the holomorphic elements. A full basis of single-valued 2dHPLs is therefore provided by the single-valued completions of the holomorphic elements of the ordinary basis (C.7). Since this halves the size of the algebra basis, it significantly reduces the number of linearly independent elements in a general Ansatz at any fixed weight.

To summarize, the single-valued algebra basis that we will employ is

$$\left\{ G^{\mathbf{s}}(\vec{a}, x) | \vec{a} \in \mathrm{Lyn}\{0, 1\} \right\} \cup \left\{ G^{\mathbf{s}}(\vec{a}, 1/y) | \vec{a} \in \mathrm{Lyn}\{0, 1, x\} \right\} , \tag{C.10}$$

where every single-valued function $G^{\mathbf{s}}(\vec{a}, z)$ is constructed from the ordinary multiple polylogarithm $G(\vec{a}, z)$ according to the algebraic prescription (C.8).

The Ansatz and Symbol Constraints. Here and in the following, we use the condensed notation $G^{\mathbf{s}, z}_{a_1, \dots, a_n} \equiv G^{\mathbf{s}}(a_1, \dots, a_n; z)$, and $\breve{y} \equiv 1/y$. For up to weight three, the basis (C.10) has 19 elements and reads

$$\begin{aligned}
\{ & G^{\mathbf{s}, x}_0, G^{\mathbf{s}, x}_1, G^{\mathbf{s}, \breve{y}}_0, G^{\mathbf{s}, \breve{y}}_1, G^{\mathbf{s}, \breve{y}}_x, G^{\mathbf{s}, x}_{0,1}, G^{\mathbf{s}, \breve{y}}_{0,1}, G^{\mathbf{s}, \breve{y}}_{0,x}, G^{\mathbf{s}, \breve{y}}_{1,x}, \\
& G^{\mathbf{s}, x}_{0,0,1}, G^{\mathbf{s}, x}_{0,1,1}, G^{\mathbf{s}, \breve{y}}_{0,0,1}, G^{\mathbf{s}, \breve{y}}_{0,0,x}, G^{\mathbf{s}, \breve{y}}_{0,1,1}, G^{\mathbf{s}, \breve{y}}_{0,1,x}, G^{\mathbf{s}, \breve{y}}_{0,x,1}, G^{\mathbf{s}, \breve{y}}_{0,x,x}, G^{\mathbf{s}, \breve{y}}_{1,1,x}, G^{\mathbf{s}, \breve{y}}_{1,x,x} \} \tag{C.11}
\end{aligned}$$

There are 65 different weight-three products of the above basis functions. At leading weight, the function $g(v_1, v_2)$ therefore has to be a linear combination of these 65 terms, with rational coefficients. Taking the symbol of this general linear combination, and equating it to the known symbol of g fixes all 65 coefficients, the result being

$$g(x, y) = -1/2\, G^{\mathbf{s}, x}_0 G^{\mathbf{s}, \breve{y}}_0 G^{\mathbf{s}, \breve{y}}_1 + 1/2\, G^{\mathbf{s}, x}_0 G^{\mathbf{s}, x}_1 G^{\mathbf{s}, \breve{y}}_1 + 1/2\, G^{\mathbf{s}, \breve{y}}_0 G^{\mathbf{s}, x}_1 G^{\mathbf{s}, \breve{y}}_1 - 1/2\, G^{\mathbf{s}, x}_0 G^{\mathbf{s}, x}_1 G^{\mathbf{s}, \breve{y}}_x$$

---

[12] After the completion of this computation, the MATHEMATICA package POLYLOGTOOLS appeared [55], which can perform many of the required manipulations of single-valued and ordinary multiple polylogarithms. For example, single-valued MPLs can be expanded in ordinary MPLs via the function `cGToG` of that package. The expansion typically contains non-basis functions. Most of these can be related back to basis functions via shuffle identities, all others can be mapped to combinations of basis functions by numerical comparison, e.g. via GINAC [56] (as done by the function `ToFibrationBasis` of POLYLOGTOOLS).

	$g^{(1)}$	$g^{(2)}$	$i\pi\zeta_2$	ζ_3
Ansatz (C.12)	19	5	1	1
Parity invariance	15	5	1	1
TP-symmetry	9	3	1	1
Collinear limit 1	6	2	0	0
Collinear limit 2	4	1	0	0
Second entry	3	1	0	0

Table 7: The table shows the numbers of undetermined coefficients in the different parts of the initial Ansatz (C.12) (first line), as well as their reduction upon imposing various consistency constraints.

$$
\begin{aligned}
&+ 1/2\, G_0^{\mathbf{s},\breve{y}} G_1^{\mathbf{s},\breve{y}} G_x^{\mathbf{s},\breve{y}} - G_1^{\mathbf{s},\breve{y}} G_{0,1}^{\mathbf{s},x} + G_x^{\mathbf{s},\breve{y}} G_{0,1}^{\mathbf{s},x} + G_0^{\mathbf{s},x} G_{0,1}^{\mathbf{s},\breve{y}} - G_1^{\mathbf{s},x} G_{0,1}^{\mathbf{s},\breve{y}} - G_x^{\mathbf{s},\breve{y}} G_{0,1}^{\mathbf{s},\breve{y}} \\
&+ G_1^{\mathbf{s},x} G_{0,x}^{\mathbf{s},\breve{y}} - G_0^{\mathbf{s},\breve{y}} G_{1,x}^{\mathbf{s},\breve{y}} - G_1^{\mathbf{s},x} G_{1,x}^{\mathbf{s},\breve{y}} + G_1^{\mathbf{s},\breve{y}} G_{1,x}^{\mathbf{s},\breve{y}} + 2\, G_{0,1,x}^{\mathbf{s},\breve{y}} - 2\, G_{1,1,x}^{\mathbf{s},\breve{y}} \\
&+ \zeta_2\, g^{(1)}(x,y) + d_0\zeta_3 + i\pi\, g^{(2)}(x,y) + i\pi d_1\zeta_2\,,
\end{aligned}
\tag{C.12}
$$

where $g^{(2)}$ and $g^{(1)}$, at this point, are general linear combinations of the 19 and 5 possible weight-two and weight-one products of basis functions, and d_0 and d_1 are rational constants. These terms are not constrained by the symbol of g.

Symmetries. While the terms with subleading functional weight are not seen by the symbol, they can be constrained by symmetry requirements. Firstly, MHV amplitudes are invariant under parity (spatial reflection), which is realized by $w_i \leftrightarrow \bar{w}_i$ in the multi-Regge limit [19], that is $x \leftrightarrow \bar{x}$ and $y \leftrightarrow \bar{y}$. Secondly, the multi-Regge limit amplitude should be invariant under target-projectile symmetry (exchange of the two incoming momenta), which amounts to symmetry under $w_5 \leftrightarrow 1/w_6$ [26], that is $x \leftrightarrow y$ and $\bar{x} \leftrightarrow \bar{y}$. The sums of six-point terms in the expressions (C.1)–(C.2) are separately invariant under these transformations, and hence we can require parity as well as target-projectile symmetry for the function g by itself, and equally for $\tilde{g}$. These symmetries significantly reduce the number of free parameters, as summarized in Table 7.

Both parity and target-projectile symmetry are not trivially implemented: The parity map replaces all holomorphic weight vectors and arguments of our single-valued basis functions $G^{\mathbf{s}}$ with their complex conjugates. Again using the Hopf algebra antipode, these conjugate single-valued functions can be re-expressed in terms of single-valued functions with holomorphic arguments [21], but those will not necessarily be elements of the basis (C.10). Similarly, the target-projectile inversion map $x \leftrightarrow y$ produces non-basis functions. In order to derive constraints for our Ansatz coefficients, all non-basis functions need to be re-expressed in terms of basis functions, which is possible due to the many relations among multiple polylogarithms. The single-valued map (C.8) is an algebra homomorphism, hence every identity among ordinary multiple polylogarithms lifts to a corresponding identity among single-valued multiple polylogarithms. In this way, single-valued multiple polylogarithms inherit the shuffle and stuffle algebra relations from their ordinary counterparts, as well as the simpler rescaling property

$$
G^{\mathbf{s}}(a_1,\ldots,a_n;z) = G^{\mathbf{s}}(ca_1,\ldots,ca_n;cz) \qquad \text{for } a_n \neq 0 \text{ and } c \neq 0\,.
\tag{C.13}
$$

We list all relations among single-valued polylogarithms with holomorphic arguments that are needed to evaluate parity and target-projectile symmetry:

$$
G_0^{\mathbf{s},\breve{x}} = -G_0^{\mathbf{s},x}, \qquad\qquad G_0^{\mathbf{s},y} = -G_0^{\mathbf{s},\breve{y}}, \qquad\qquad G_1^{\mathbf{s},y} = G_1^{\mathbf{s},\breve{y}} - G_0^{\mathbf{s},\breve{y}},
$$
$$
G_x^{\mathbf{s},1} = G_1^{\mathbf{s},x} - G_0^{\mathbf{s},x}, \qquad\qquad G_{\tilde{x}}^{\mathbf{s},x} = G_1^{\mathbf{s},\breve{y}} - G_0^{\mathbf{s},\breve{y}}, \qquad\qquad G_{\tilde{x}}^{\mathbf{s},\breve{y}} = G_1^{\mathbf{s},x} - G_0^{\mathbf{s},x},
$$

$$G_{0,x}^{\mathbf{s},1} = \tfrac{1}{2}((G_0^{\mathbf{s},x})^2 - G_{0,1}^{\mathbf{s},x}, \qquad G_{0,\tilde{x}}^{\mathbf{s},x} = \tfrac{1}{2}(G_0^{\mathbf{s},\check{y}})^2 - G_{0,1}^{\mathbf{s},\check{y}}, \qquad G_{0,\tilde{x}}^{\mathbf{s},\check{y}} = \tfrac{1}{2}(G_0^{\mathbf{s},x})^2 - G_{0,1}^{\mathbf{s},x},$$

$$G_{x,0}^{\mathbf{s},1} = G_{0,1}^{\mathbf{s},x} - \tfrac{1}{2}(G_0^{\mathbf{s},x})^2, \qquad G_{x,1}^{\mathbf{s},1} = G_{0,1}^{\mathbf{s},x} + \tfrac{1}{2}(G_1^{\mathbf{s},x})^2 - G_0^{\mathbf{s},x}G_1^{\mathbf{s},x},$$

$$G_{\tilde{x},x}^{\mathbf{s},\check{y}} = G_{0,x}^{\mathbf{s},\check{y}} - G_{1,x}^{\mathbf{s},\check{y}} - G_0^{\mathbf{s},x}G_1^{\mathbf{s},\check{y}} + G_1^{\mathbf{s},x}G_1^{\mathbf{s},\check{y}},$$

$$G_{0,0,\tilde{x}}^{\mathbf{s},x} = G_{0,0,1}^{\mathbf{s},\check{y}} - \tfrac{1}{6}(G_0^{\mathbf{s},\check{y}})^3, \qquad G_{0,0,\tilde{x}}^{\mathbf{s},\check{y}} = G_{0,0,1}^{\mathbf{s},x} - \tfrac{1}{6}(G_0^{\mathbf{s},x})^3,$$

$$G_{0,\tilde{x},x}^{\mathbf{s},\check{y}} = -G_1^{\mathbf{s},\check{y}}G_{0,1}^{\mathbf{s},x} - G_1^{\mathbf{s},\check{y}}G_{0,x}^{\mathbf{s},\check{y}} + G_{0,0,x}^{\mathbf{s},\check{y}} + G_{0,1,x}^{\mathbf{s},\check{y}} + G_{0,x,1}^{\mathbf{s},\check{y}} + \tfrac{1}{2}(G_0^{\mathbf{s},x})^2G_1^{\mathbf{s},\check{y}},$$

$$G_{\tilde{x},\tilde{x},x}^{\mathbf{s},\check{y}} = -G_0^{\mathbf{s},x}G_{0,1}^{\mathbf{s},\check{y}} + G_1^{\mathbf{s},x}G_{0,1}^{\mathbf{s},\check{y}} - G_1^{\mathbf{s},\check{y}}G_{0,x}^{\mathbf{s},\check{y}} + G_{0,0,x}^{\mathbf{s},\check{y}} + G_{0,x,1}^{\mathbf{s},\check{y}} + G_{1,1,x}^{\mathbf{s},\check{y}} + \tfrac{1}{2}(G_0^{\mathbf{s},x})^2G_1^{\mathbf{s},\check{y}}$$

$$+ \tfrac{1}{2}G_0^{\mathbf{s},x}(G_1^{\mathbf{s},\check{y}})^2 - G_1^{\mathbf{s},x}G_0^{\mathbf{s},x}G_1^{\mathbf{s},\check{y}} - \tfrac{1}{2}G_1^{\mathbf{s},x}(G_1^{\mathbf{s},\check{y}})^2 + \tfrac{1}{2}(G_1^{\mathbf{s},x})^2G_1^{\mathbf{s},\check{y}} \qquad \text{(C.14)}$$

where $\check{x} := 1/x$ and $\tilde{x} := x/y$. The weight-one single-valued basis functions are individually parity invariant, hence parity symmetry only affects the Ansatz for the weight-two part $g^{(2)}$. It reduces the number of undetermined coefficients from 19 to 15. Target-projectile symmetry further reduces the uncertainty in $g^{(2)}$ and $g^{(1)}$ to 9 and 3 coefficients, respectively.

Collinear Limit. Next, we want to expand our Ansatz function in the collinear limit. One way to do so is: First write the single-valued 2dHPLs in terms of ordinary Goncharov polylogarithms according to (C.8), then rewrite the Goncharov polylogarithms in terms of classical polylogarithms, for example using [38], and finally expand in large r_5 and r_6, using (5.9), and (5.6), which combine to

$$x = -\frac{F_6(F_5 + r_5)}{r_5 r_6}, \qquad \bar{x} = -\frac{1 + F_5 r_5}{F_5 F_6 r_5 r_6},$$

$$y = -\frac{r_5(F_6 + r_6)}{F_5 F_6}, \qquad \bar{y} = -F_5 r_5(1 + F_6 r_6). \qquad \text{(C.15)}$$

While the Regge limit sits at $T_j \to 0$, $S_j \to 0$ with $r_j \equiv S_j/T_j$ fixed, the collinear limit is defined by $T_j \to 0$ with S_j finite. From the Regge limit, the combined Regge collinear limit is therefore attained by letting $r_j \to \infty$, that is

$$x \approx -\frac{F_6}{r_6} \to 0, \quad \bar{x} \approx -\frac{1}{F_6 r_6} \to 0, \quad y \approx -\frac{r_5 r_6}{F_5 F_6} \to \infty, \quad \bar{y} \approx -F_5 F_6 r_5 r_6 \to \infty. \qquad \text{(C.16)}$$

The expansion of the basis functions (C.7) in this case is simple, since all arguments x, $\bar{x}$, $1/y$, and $1/\bar{y}$ tend to zero. After writing all single-valued functions $G^{\mathbf{s}}$ in terms of ordinary multiple polylogarithms and performing the expansion, we obtain the expansions of the Ansatz (C.12) for g near the collinear limit (C.16). In doing so, one has to be careful in picking consistent branches for all occurring logarithms. Every single-valued multiple polylogarithm of the basis (C.7) expands to a power series in $\log(r_i)$ and $1/r_i$, where the series coefficients are rational functions of F_5 and F_6 as presented below:

$$G_0^{\mathbf{s},x} = -2\log(r_6) + 2C_5 + \mathcal{O}(r^{-2}), \qquad G_0^{\mathbf{s},\check{y}} = -2\log(r_5) - 2\log(r_6) - 2C_6 + \mathcal{O}(r^{-2}),$$

$$G_1^{\mathbf{s},x} = 2C_6 + 2C_+ + \mathcal{O}(r^{-3}), \qquad G_1^{\mathbf{s},\check{y}} = 2C_+ + \mathcal{O}(r^{-3}),$$

$$G_x^{\mathbf{s},\check{y}} = -2C_5 + 2C_+ + \mathcal{O}(r^{-3}),$$

$$G_{0,1}^{\mathbf{s},x} = -\frac{2\log(r_6)}{F_6 r_6}\left(1 + \frac{1}{F_5 r_5}\right) + 2C_+ + \frac{F_6}{r_6} - \frac{1}{F_6 r_6} + \mathcal{O}(r^{-3}),$$

$$G_{0,1}^{\mathbf{s},\check{y}} = -\frac{2\log(r_5)}{F_5 F_6 r_5 r_6} - \frac{2\log(r_6)}{F_5 F_6 r_5 r_6} + \frac{F_5 F_6}{r_5 r_6} - \frac{1}{F_5 F_6 r_5 r_6} + \mathcal{O}(r^{-3}),$$

$$G_{0,x}^{\mathbf{s},\check{y}} = \frac{2\log(r_5)}{F_5 r_5}\left(1 - \frac{1}{F_6 r_6}\right) - \frac{F_5}{r_5} + \frac{1}{r_5 F_5} + \frac{2F_6 C_5}{r_6} + \mathcal{O}(r^{-3}),$$

45

$$G_{1,x}^{\mathbf{s},\check{y}} = \frac{2\log(r_6)}{F_5 F_6 r_5 r_6} + \frac{2C_6}{F_5 r_5} + \mathcal{O}(r^{-3}),$$

$$G_{0,1,x}^{\mathbf{s},\check{y}} = \frac{-4\log^2(r_6) - 4\log(r_5)\log(r_6) - 2\log(r_5)(F_6^2 + 1) - 4\log(r_6) - 2}{F_5 F_6 r_5 r_6} + \mathcal{O}(r^{-3}),$$

$$G_{1,1,x}^{\mathbf{s},\check{y}} = -\frac{2\log(r_6)}{F_5 r_5 r_6^2} - \frac{F_6^2}{2F_5 r_5 r_6^2} - \frac{2}{F_5 r_5 r_6^2} + \frac{1}{2F_5 F_6^2 r_5 r_6^2} + \mathcal{O}(r^{-4}), \tag{C.17}$$

where we have used the abbreviations (5.13), and where $\mathcal{O}(r^{-n})$ stands for terms with n or more inverse powers of r_5 or r_6.

In the Mandelstam regions that we consider, the BDS amplitude correctly captures the leading behavior in the collinear limit. Hence, the remainder function has to vanish in this limit. That is, there should be no terms that are free of $1/r_i$ factors in the collinear expansion of the remainder function. Moreover, we can require consistency with the general form of the Wilson loop OPE that governs the remainder function in the collinear limit [1, 2]. The general systematics of the Wilson loop OPE predicts that the remainder function in the combined Regge collinear limit (at two loops and in any kinematic region) takes the form shown in eq. (3.12), whose multi-Regge expansion via (5.6) has the form

$$\begin{aligned}
R_7^{\mathrm{MRL-coll}} &= \frac{\cos(\phi_5)}{r_5}\tilde{f}_5\big(\log(\varepsilon_5), \log(r_5)\big) + \frac{\cos(\phi_6)}{r_6}\tilde{f}_6\big(\log(\varepsilon_6), \log(r_6)\big) \\
&\quad + \frac{\cos(\phi_5 + \phi_6)}{r_5 r_6}h\big(\log(\varepsilon_5), \log(\varepsilon_6), \log(r_5), \log(r_6)\big) \\
&\quad + \frac{\cos(\phi_5 - \phi_6)}{r_5 r_6}\bar{h}\big(\log(\varepsilon_5), \log(\varepsilon_6), \log(r_5), \log(r_6)\big) + \mathcal{O}(r^{-2}), \tag{C.18}
\end{aligned}$$

where $F_i = e^{i\phi_i}$, and $\tilde{f}_5$, $\tilde{f}_6$, h, and $\bar{h}$ are polynomials in the respective logarithms. In particular, the dependence on ϕ_5 and ϕ_6 is very restricted.[13] A general combination of multiple polylogarithms would also produce sine functions of ϕ_5, ϕ_6, and $\phi_5 \pm \phi_6$. It turns out that our parity and target-projectile symmetric Ansatz is already free of such sine terms, which is an important cross-check of our result. Moreover, terms where $\cos(\phi_5)$ multiplies $\log(\varepsilon_6)$ or $\log(r_6)$ should be absent, and the same is true for products of $\cos(\phi_6)$ with $\log(\varepsilon_5)$ or with $\log(r_5)$. Imposing these constraints reduces the number of parameters in $g^{(2)}$ and $g^{(1)}$ to 6 and 2 coefficients, respectively, and moreover sets

$$d_0 = 0, \qquad d_1 = 0. \tag{C.19}$$

When considering the above constraints, one has to keep in mind that the remainder function in the $(---)$ region (C.1) consists of the function g as well as two copies of the six-point $(--)$ region remainder function (4.7). In principle, there could be cross-terms between the six-point functions and the function g, such that only their sum vanishes and satisfies eq. (C.18) in the collinear limit. However, the two instances of the six-point function separately vanish and satisfy eq. (C.18) in the seven-point Regge collinear limit, for both arguments $v_5 = -x$ and $v_6 = -y$. Hence also g has to satisfy these constraints by itself.

In fact, the combined Regge collinear limit is not unique: By cyclically rotating the tessellation of the heptagon that defines the OPE variables (5.2) and taking appropriate limits in the variables S_i, we can probe different limits in the space of multi-Regge kinematics. Not all collinear limits

---

[13]The form (C.18) is valid in the Euclidean region as well as the $(+++)$ region. We assume that all other Mandelstam regions are connected to the Euclidean region through analytic continuation. Moreover, the remainder function is a function of the cross ratios. The cross ratios in general kinematics (5.3) depend on the variables ϕ_5 and ϕ_6 only through the entire functions $\cos(\phi_5)$, $\cos(\phi_6)$, and $\cos(\phi_5 + \phi_6)$, and this dependence drops out in the collinear limit. Hence the general form (C.18) is preserved under the analytic continuation into the various Mandelstam regions, including the $(---)$ and the $(-+-)$ regions.

have an overlap with the multi-Regge limit: The requirement is that the vanishing of "small" cross ratios $u_{j,2}$, $u_{j,3}$ is compatible with the collinear limit $T_5, T_6 \to 0$. One further case where this is satisfied is the cyclic rotation of our polygon variables by 4 sites, that is, we use the momentum twistors $Z_i^{+4} \equiv Z_{i+4}$, where Z_i are the momentum twistors (A.8) used throughout the rest of this work.[14] In this case, the Regge limit is attained by setting $S_5 = 1/(r_5 T_5)$, $S_6 = r_6 T_6$, and letting $T_5, T_6 \to 0$. The multi-Regge parameters w_5, w_6 are then related to the OPE variables by

$$r_5 = \sqrt{w_6 \bar{w}_6}\,, \qquad r_6 = \frac{1}{\sqrt{w_5 \bar{w}_5}}\,, \qquad F_5 = \frac{\sqrt{w_6}}{\sqrt{\bar{w}_6}}\,, \qquad F_6 = \frac{\sqrt{w_5}}{\sqrt{\bar{w}_5}}\,, \qquad \text{(C.20)}$$

or equivalently

$$
\begin{aligned}
x &= -\frac{r_5(F_6 + r_6)}{F_5 r_6}\,, & \bar{x} &= -\frac{F_5 r_5(1 + F_6 r_6)}{F_6 r_6}\,, \\
y &= -\frac{(F_5 + r_5) r_6}{F_6 r_5}\,, & \bar{y} &= -\frac{F_6(1 + F_5 r_5) r_6}{F_5 r_5}\,.
\end{aligned}
\qquad \text{(C.21)}
$$

The combined Regge collinear limit is attained from the multi-Regge limit by letting $r_5, r_6 \to \infty$, which implies

$$x \approx -\frac{r_5}{F_5} \to \infty\,, \qquad \bar{x} \approx -r_5 F_5 \to \infty\,, \qquad y \approx -\frac{r_6}{F_6} \to \infty\,, \qquad \bar{y} \approx -r_6 F_6 \to \infty\,. \qquad \text{(C.22)}$$

In this limit, the basis functions of eq. (C.7) expand as follows (see eq. (C.17) for the notation):

$$
\begin{aligned}
G_0^{\mathbf{s},x} &= 2\log(r_5) + 2C_6 + \mathcal{O}(r^{-2}), & G_0^{\mathbf{s},\check{y}} &= -2\log(r_6) - 2C_5 + \mathcal{O}(r^{-2}), \\
G_1^{\mathbf{s},x} &= 2\log(r_5) + 2C_5 + 2C_6 - 2C_+ + \mathcal{O}(r^{-3}), & G_1^{\mathbf{s},\check{y}} &= 2C_6 - 2C_+ + \mathcal{O}(r^{-3}), \\
& & G_x^{\mathbf{s},\check{y}} &= -2C_+ + \mathcal{O}(r^{-3}),
\end{aligned}
$$

$$G_{0,1}^{\mathbf{s},x} = 2\log^2(r_5) + 2\log(r_5)\left(\frac{1}{F_5 r_5} - \frac{1}{F_5 F_6 r_5 r_6} + 2C_6\right) - \frac{F_5}{r_5} + \frac{1}{F_5 r_5} + \frac{2 F_6 C_5}{r_6} + \mathcal{O}(r^{-3}),$$

$$G_{0,1}^{\mathbf{s},\check{y}} = -\frac{2\log(r_6)}{F_6 r_6}\left(1 - \frac{1}{F_5 r_5}\right) + \frac{F_6}{r_6} - \frac{1}{F_6 r_6} - \frac{2 F_5 C_6}{r_5} + \mathcal{O}(r^{-3}),$$

$$G_{0,x}^{\mathbf{s},\check{y}} = \frac{2\log(r_5) + 2\log(r_6) + 1}{F_5 F_6 r_5 r_6} - \frac{F_5 F_6}{r_5 r_6} + \mathcal{O}(r^{-3}),$$

$$G_{1,x}^{\mathbf{s},\check{y}} = \frac{2\log(r_5)}{F_5 F_6 r_5 r_6} + \frac{2 C_5}{F_6 r_6} + \mathcal{O}(r^{-3}),$$

$$G_{0,1,x}^{\mathbf{s},\check{y}} = -\frac{2\log^2(r_5) + 2\log(r_5)\big(2\log(r_6) + 1\big)}{F_5 F_6 r_5 r_6} - \frac{2 C_5\big(2\log(r_6) + 1\big)}{F_6 r_6} + \mathcal{O}(r^{-3}),$$

$$G_{1,1,x}^{\mathbf{s},\check{y}} = -\frac{2\log(r_5)\big(\log(r_5) + 1\big)}{F_5 F_6 r_5 r_6} + \frac{F_5}{F_6 r_5 r_6} - \frac{1}{F_5 F_6 r_5 r_6} + \mathcal{O}(r^{-3})\,. \qquad \text{(C.23)}$$

Expanding the Ansatz (C.12) for g in the limit (C.22), we can again require *(i)* vanishing in the collinear limit, and *(ii)* agreement with the general form (C.18) of the Wilson loop OPE. Imposing these constraints further reduces the number of parameters in $g^{(2)}$ and $g^{(1)}$ to 4 and 1 coefficients, respectively, as shown in Table 7.

---

[14]Another independent Regge collinear limit is defined by $Z_i^{+1} \equiv Z_{i+1}$, with $S_5 = 1/(r_5 T_5)$, $S_6 = 1/(r_6 T_6)$, and $r_i^2 = w_i \bar{w}_i$, $F_i^2 = w_i/\bar{w}_i$, that is $x = -F_6(1 + F_5 r_5) r_6$, $y = -(1 + F_6 r_6)/(F_5 F_6 r_5 r_6)$. However, this limit is related to the unshifted kinematics by a combination of target-projectile symmetry and a permutation of the OPE variables $\{F_i, S_i, T_i\}$, and thus does not imply further independent constraints.

The Constrained Ansatz. Combining all the above constraints, the full Ansatz (C.12) for the function g reduces to

$$g(x,y) = -1/2\, G_0^{\mathbf{s},x} G_0^{\mathbf{s},\breve{y}} G_1^{\mathbf{s},\breve{y}} + 1/2\, G_0^{\mathbf{s},x} G_1^{\mathbf{s},x} G_1^{\mathbf{s},\breve{y}} + 1/2\, G_0^{\mathbf{s},\breve{y}} G_1^{\mathbf{s},x} G_1^{\mathbf{s},\breve{y}} - 1/2\, G_0^{\mathbf{s},x} G_1^{\mathbf{s},x} G_x^{\mathbf{s},\breve{y}}$$
$$+ 1/2\, G_0^{\mathbf{s},\breve{y}} G_1^{\mathbf{s},\breve{y}} G_x^{\mathbf{s},\breve{y}} - G_1^{\mathbf{s},\breve{y}} G_{0,1}^{\mathbf{s},x} + G_x^{\mathbf{s},\breve{y}} G_{0,1}^{\mathbf{s},x} + G_0^{\mathbf{s},x} G_{0,1}^{\mathbf{s},\breve{y}} - G_1^{\mathbf{s},x} G_{0,1}^{\mathbf{s},\breve{y}} - G_x^{\mathbf{s},\breve{y}} G_{0,1}^{\mathbf{s},\breve{y}}$$
$$+ G_1^{\mathbf{s},x} G_{0,x}^{\mathbf{s},\breve{y}} - G_0^{\mathbf{s},\breve{y}} G_{1,x}^{\mathbf{s},\breve{y}} - G_1^{\mathbf{s},x} G_{1,x}^{\mathbf{s},\breve{y}} + G_1^{\mathbf{s},\breve{y}} G_{1,x}^{\mathbf{s},\breve{y}} + 2\, G_{0,1,x}^{\mathbf{s},\breve{y}} - 2\, G_{1,1,x}^{\mathbf{s},\breve{y}}$$
$$+ \kappa_0 \zeta_2\, G_x^{\mathbf{s},\breve{y}} + 2\pi i \big[\kappa_1 \big((G_0^{\mathbf{s},x} - G_1^{\mathbf{s},x}) G_1^{\mathbf{s},x} + (G_0^{\mathbf{s},\breve{y}} - G_1^{\mathbf{s},\breve{y}}) G_1^{\mathbf{s},\breve{y}} \big)$$
$$+ \kappa_2 (G_0^{\mathbf{s},x} - G_1^{\mathbf{s},x}) G_1^{\mathbf{s},\breve{y}} + \kappa_3 (G_0^{\mathbf{s},x} - G_0^{\mathbf{s},\breve{y}}) G_x^{\mathbf{s},\breve{y}} + \kappa_4 (G_x^{\mathbf{s},\breve{y}})^2 \big]\,, \tag{C.24}$$

The expansion of this function in the collinear limit (C.16) takes the form

$$[g(x,y)]^{\mathrm{CL}} = -\frac{\cos(\phi_5)}{r_5} \Big(8i\pi\kappa_3 \log(r_5) + 2\kappa_0\zeta_2 \Big) - \frac{\cos(\phi_6)}{r_6} 8i\pi\kappa_1 \log(r_6)$$
$$- \frac{\cos(\phi_5 + \phi_6)}{r_5 r_6} 2 \Big(2\log(r_6)^2 + 2\log(r_5)\log(r_6) + 4i\pi(\kappa_1 - \kappa_3)\log(r_5)$$
$$+ (3 + 4i\pi(2\kappa_1 + \kappa_2))\log(r_6) + 2 - \kappa_0\zeta_2 - 2\pi i(\kappa_1 - \kappa_3) \Big)$$
$$+ \frac{\cos(\phi_5 - \phi_6)}{r_5 r_6} 2 \Big(\log(r_6) + 2\pi i(2\kappa_1 - \kappa_3) \Big)$$
$$+ \mathcal{O}(r_5^{-2}) + \mathcal{O}(r_6^{-2})\,. \tag{C.25}$$

Except for κ_4, all remaining coefficients in the constrained Ansatz (C.24) should be fixed by the expansion of the true remainder function in this combined Regge collinear limit.

All constraints considered above equally apply to the function $\tilde{g}$, and hence the constrained Ansatz for g equally holds for $\tilde{g}$. Of course, the undetermined coefficients may assume different values for $\tilde{g}$ than for g.

Second Symbol Entry Constraints. Next, we will derive further constraints on the functions g and $\tilde{g}$ by looking at the second entry of the known remainder function's symbol [57]. While the first entry of the symbol encodes the positions of all branch points on the main sheet, the first and second entries together determine the positions of all branch points on all sheets adjacent to the main sheet. We denote the symbol of the heptagon remainder function by

$$\mathrm{S}[R_7^{(2)}] = \sum_{i \in I,\, j \in J} (a_i, a_j, X_{ij})\,. \tag{C.26}$$

Letters a_i, $i \in I$ in the first entry are drawn from the six cross ratios (2.4) as well as the seventh cross ratio U_{26}. The second entry includes further letters that cannot be reduced to cross ratios. Every pair of first and second entry is followed by a two-letter symbol X_{ij}. Writing the continuation of the remainder function along some path $\mathcal{C}$ as:

$$\mathcal{C} R_7^{(2)} = (1 + \Delta^{\mathcal{C}}) R_7^{(2)}\,, \qquad \Delta^{\mathcal{C}} R_7^{(2)} = 2\pi i h_1 + (2\pi i)^2 h_2 + \dots\,, \tag{C.27}$$

the coefficients h_1 and h_2 are functions of weight 3 and 2, respectively. Their symbols have the form

$$\mathrm{S}[h_1] = \sum_{i \in I,\, j \in J} n_i\, (a_j, X_{ij})\,, \qquad \mathrm{S}[h_2] = \sum_{i \in I,\, j \in J} n_{ij} X_{ij}\,, \tag{C.28}$$

where n_i and n_{ij} are numbers that depend on the chosen path $\mathcal{C}$ (n_i is the winding number of a_i around zero).

We can now constrain the function h_2 by inspecting the known symbol (C.26): We first collect all X_{ij}, and compute their multi-Regge limits at symbol level. In the multi-Regge limit, the entries of the symbols X_{ij} are rational functions of our Regge variables T_i, w_i, and $\bar{w}_i$, $i = 5, 6$. There are 73 symbols X_{ij}, but not all of them are independent in the multi-Regge limit. We note that the six-point function f (4.7) is free of terms proportional to $2\pi i$, hence h_2 only contributes to the functions g or $\tilde{g}$. We can therefore set the LLA part of h_2 to zero. We do so by first unshuffling the variables T_5 and T_6 from the symbol, then identifying the symbol (T_i) with the function $1/4(\log \varepsilon_i + \log(w_i \bar{w}_i))$ (using eqs. (2.15)), and requiring that the coefficients of $\log \varepsilon_5$ and $\log \varepsilon_6$ must vanish. This imposes 8 linear constraints on the 73 numbers n_{ij}.

Next, we match the symbol of h_2 to the symbol of a generic weight-two combination of single-valued MPLs constructed from the basis $G^{\mathbf{s}}$ (C.10). This implies 28 further constraints on the n_{ij}, and leaves us with a six-parameter combination of single-valued MPLs. Further matching this combination against the function multiplying $2\pi i$ in eq. (C.24) (i.e. imposing parity-invariance, target-projectile symmetry, and consistency with the Wilson loop OPE in the collinear limit) eliminates 3 coefficients, and imposes the constraint

$$\kappa_4 = 0 \tag{C.29}$$

on our Ansatz (C.24). Since the analysis leading to eq. (C.29) was independent on the choice of path $\mathcal{C}$, we conclude that eq. (C.29) has to hold for both functions g and $\tilde{g}$. We note that the constraints on the numbers n_{ij} are consistent with

$$n_{ii} = 1 \quad \text{where} \quad a_i = U_{26}, \tag{C.30}$$

which follows if the path $\mathcal{C}$ winds U_{26} around zero once (in the negative sense), as is the case for the paths leading from the $(+++)$ into the $(---)$ and $(-+-)$ regions, see Table 2.

If we require in addition that $u_{5,1} = U_{25}$ and $u_{6,1} = U_{36}$ are held fixed, which is consistent with the continuation into the $(---)$ region, then it follows that

$$n_{ij} = 0 \quad \text{if} \quad a_i \in \{U_{25}, U_{36}\} \ \lor \ a_j \in \{U_{25}, U_{36}\}. \tag{C.31}$$

Combining these conditions with the previous constraints enforces that

$$\kappa_1 = \kappa_2 = \kappa_3 = 0 \tag{C.32}$$

in our Ansatz (C.24), in full agreement with [22].

D Discontinuity Tables for Half Windings

Here we list the additional contributions δ_I^{ϱ} to discontinuities Δ_I listed in eqs. (5.32), (5.33), and (5.34), that arise after appending the half-windings to the path of continuation separately for each region ϱ according to Table 2:

$$\delta_I^{\varrho} := \Delta_I^{\varrho} - \Delta_I, \qquad \varrho \in \{(+--), (--+), (-+-)\}. \tag{D.1}$$

Below, we list these corrections for single Δ_i and double $\Delta_{i,j}$ discontinuities, while the triple ones are unchanged $\delta_{i,j,k}^{\varrho} = 0$. We will use the shorthand notation (5.13).

D.1 The Region $(+--)$

The corrections to the single discontinuities for the $(+--)$ region read

$$\delta_1^{+--} = 2\pi i C_5 \log(\varepsilon_5) + C_5(8\pi i \log(r_5) - 4\pi^2 + 8\pi i),$$

$$\delta_3^{+--} = 2\pi i C_+ \log(\varepsilon_5) + C_+(8\pi i \log(r_5) + 4\pi i \log(r_6) - 4\pi^2 + 8\pi i). \tag{D.2}$$

The corrections to the double discontinuities are

$$\begin{aligned}
\tfrac{1}{3}\delta_{1,4}^{+--} &= \delta_{4,1}^{+--} = 2\pi i C_5, \\
\tfrac{1}{3}\delta_{3,4}^{+--} &= \delta_{4,3}^{+--} = \delta_{3,5}^{+--} = 2\pi i C_+, \\
\delta_{1,2}^{+--} &= -6\pi i C_5 + 4\pi i C_+, \\
\delta_{2,1}^{+--} &= -2\pi i C_5 + 2\pi i C_+.
\end{aligned} \tag{D.3}$$

D.2   The Region $(--+)$

The corrections to the single discontinuities for the $(--+)$ region read

$$\begin{aligned}
\delta_3^{--+} &= -2\pi i C_+ \log(\varepsilon_5) - (2\pi i C_+ + 2\pi i C_6)\log(\varepsilon_6) - C_6(8\pi i \log(r_6) + 4\pi^2 + 8\pi i) \\
&\quad - C_+(4\pi i \log(r_5) + 8\pi i \log(r_6) + 4\pi^2 + 6\pi i) + 2\pi i C_-, \\
\delta_2^{--+} &= -2\pi i C_6 \log(\varepsilon_6) - C_6(8\pi i \log(r_6) + 4\pi^2 + 8\pi i).
\end{aligned} \tag{D.4}$$

The corrections to the double discontinuities are

$$\begin{aligned}
\tfrac{1}{2}\delta_{3,4}^{--+} &= \delta_{4,3}^{--+} = -\delta_{1,2}^{--+} = -2\pi i C_+, \\
\tfrac{1}{3}\delta_{3,5}^{--+} &= \delta_{5,3}^{--+} = -2\pi i C_+ - 2\pi i C_6, \\
\tfrac{1}{3}\delta_{2,5}^{--+} &= \delta_{5,2}^{--+} = -2\pi i C_6.
\end{aligned} \tag{D.5}$$

D.3   The Region $(-+-)$

The corrections to the single discontinuities for the $(-+-)$ region read

$$\begin{aligned}
\delta_1^{-+-} &= -2\pi i C_5 \log(\varepsilon_5) - C_5(8\pi i \log(r_5) + 4\pi^2 + 8\pi i), \\
\delta_3^{-+-} &= (2\pi i C_+ + 2\pi i C_6)\log(\varepsilon_6) + C_6(8\pi i \log(r_6) - 4\pi^2 + 8\pi i) \\
&\quad - C_+(4\pi i \log(r_5) - 4\pi i \log(r_6) + 4\pi^2 + 2\pi i) - 2\pi i C_-, \\
\delta_2^{-+-} &= 2\pi i C_6 \log(\varepsilon_6) + C_6(8\pi i \log(r_6) - 4\pi^2 + 8\pi i).
\end{aligned} \tag{D.6}$$

The corrections to the double discontinuities are

$$\begin{aligned}
\tfrac{1}{3}\delta_{1,2}^{-+-} &= \delta_{2,1}^{-+-} = -2\pi i C_+ + 2\pi i C_5, \\
\tfrac{1}{3}\delta_{1,4}^{-+-} &= \delta_{4,1}^{-+-} = -2\pi i C_5, \\
\tfrac{1}{3}\delta_{2,5}^{-+-} &= \delta_{5,2}^{-+-} = 2\pi i C_6, \\
\delta_{3,4}^{-+-} &= -2\pi i C_+, \\
\delta_{3,5}^{-+-} &= 4\pi i C_+ + 6\pi i C_6, \\
\delta_{5,3}^{-+-} &= 2\pi i C_+ + 2\pi i C_6.
\end{aligned} \tag{D.7}$$

References

[1] B. Basso, A. Sever and P. Vieira, *"Spacetime and Flux Tube S-Matrices at Finite Coupling for $\mathcal{N} = 4$ Supersymmetric Yang–Mills Theory"*, Phys. Rev. Lett. 111, 091602 (2013), arxiv:1303.1396.

[2] B. Basso, A. Sever and P. Vieira, *"Space-time S-matrix and Flux tube S-matrix II. Extracting and Matching Data"*, JHEP 1401, 008 (2014), arxiv:1306.2058.

[3] B. Basso, A. Sever and P. Vieira, *"Space-time S-matrix and Flux-tube S-matrix III. The two-particle contributions"*, JHEP 1408, 085 (2014), `arxiv:1402.3307`.

[4] B. Basso, A. Sever and P. Vieira, *"Collinear Limit of Scattering Amplitudes at Strong Coupling"*, Phys. Rev. Lett. 113, 261604 (2014), `arxiv:1405.6350`.

[5] B. Basso, A. Sever and P. Vieira, *"Space-time S-matrix and Flux-tube S-matrix IV. Gluons and Fusion"*, JHEP 1409, 149 (2014), `arxiv:1407.1736`.

[6] Z. Bern, L. J. Dixon and V. A. Smirnov, *"Iteration of planar amplitudes in maximally supersymmetric Yang–Mills theory at three loops and beyond"*, Phys. Rev. D72, 085001 (2005), `hep-th/0505205`.

[7] J. Bartels, L. N. Lipatov and A. Sabio Vera, *"BFKL Pomeron, Reggeized gluons and Bern-Dixon-Smirnov amplitudes"*, Phys. Rev. D80, 045002 (2009), `arxiv:0802.2065`.

[8] L. F. Alday and J. Maldacena, *"Comments on gluon scattering amplitudes via AdS/CFT"*, JHEP 0711, 068 (2007), `arxiv:0710.1060`.

[9] S. Caron-Huot, L. J. Dixon, F. Dulat, M. von Hippel, A. J. McLeod and G. Papathanasiou, *"Six-Gluon Amplitudes in Planar $\mathcal{N} = 4$ Super-Yang–Mills Theory at Six and Seven Loops"*, `arxiv:1903.10890`.

[10] B. Basso, S. Caron-Huot and A. Sever, *"Adjoint BFKL at finite coupling: a short-cut from the collinear limit"*, JHEP 1501, 027 (2015), `arxiv:1407.3766`.

[11] J. Bartels, L. N. Lipatov and A. Sabio Vera, *"$\mathcal{N} = 4$ supersymmetric Yang Mills scattering amplitudes at high energies: The Regge cut contribution"*, Eur. Phys. J. C65, 587 (2010), `arxiv:0807.0894`.

[12] V. S. Fadin and L. N. Lipatov, *"BFKL equation for the adjoint representation of the gauge group in the next-to-leading approximation at $\mathcal{N} = 4$ SUSY"*, Phys. Lett. B706, 470 (2012), `arxiv:1111.0782`.

[13] L. J. Dixon, J. M. Drummond, C. Duhr and J. Pennington, *"The four-loop remainder function and multi-Regge behavior at NNLLA in planar $\mathcal{N} = 4$ super-Yang–Mills theory"*, JHEP 1406, 116 (2014), `arxiv:1402.3300`.

[14] L. J. Dixon, C. Duhr and J. Pennington, *"Single-valued harmonic polylogarithms and the multi-Regge limit"*, JHEP 1210, 074 (2012), `arxiv:1207.0186`.

[15] J. Bartels, J. Kotanski and V. Schomerus, *"Excited Hexagon Wilson Loops for Strongly Coupled $\mathcal{N} = 4$ SYM"*, JHEP 1101, 096 (2011), `arxiv:1009.3938`.

[16] J. Bartels, J. Kotanski, V. Schomerus and M. Sprenger, *"The Excited Hexagon Reloaded"*, `arxiv:1311.1512`.

[17] J. Bartels, A. Kormilitzin and L. Lipatov, *"Analytic structure of the $n = 7$ scattering amplitude in $\mathcal{N} = 4$ SYM theory in the multi-Regge kinematics: Conformal Regge pole contribution"*, Phys. Rev. D89, 065002 (2014), `arxiv:1311.2061`.

[18] J. Bartels, A. Kormilitzin and L. N. Lipatov, *"Analytic structure of the $n = 7$ scattering amplitude in $\mathcal{N} = 4$ theory in multi-Regge kinematics: Conformal Regge cut contribution"*, Phys. Rev. D91, 045005 (2015), `arxiv:1411.2294`.

[19] A. Prygarin, M. Spradlin, C. Vergu and A. Volovich, *"All Two-Loop MHV Amplitudes in Multi-Regge Kinematics From Applied Symbology"*, Phys. Rev. D85, 085019 (2012), `arxiv:1112.6365`.

[20] T. Bargheer, G. Papathanasiou and V. Schomerus, *"The Two-Loop Symbol of all Multi-Regge Regions"*, JHEP 1605, 012 (2016), `arxiv:1512.07620`.

[21] V. Del Duca, S. Druc, J. Drummond, C. Duhr, F. Dulat, R. Marzucca, G. Papathanasiou and B. Verbeek, *"Multi-Regge kinematics and the moduli space of Riemann spheres with marked points"*, JHEP 1608, 152 (2016), `arxiv:1606.08807`.

[22] V. Del Duca, S. Druc, J. Drummond, C. Duhr, F. Dulat, R. Marzucca, G. Papathanasiou and B. Verbeek, *"The seven-gluon amplitude in multi-Regge kinematics beyond leading logarithmic accuracy"*, JHEP 1806, 116 (2018), `arxiv:1801.10605`.

[23] V. Del Duca, C. Duhr, F. Dulat and B. Penante, *"All two-loop MHV remainder functions in multi-Regge kinematics"*, JHEP 1901, 162 (2019), arxiv:1811.10398.

[24] J. M. Drummond, J. Henn, G. P. Korchemsky and E. Sokatchev, *"Dual superconformal symmetry of scattering amplitudes in $\mathcal{N} = 4$ super-Yang–Mills theory"*, Nucl. Phys. B828, 317 (2010), arxiv:0807.1095.

[25] J. Bartels, V. Schomerus and M. Sprenger, *"Multi-Regge Limit of the n-Gluon Bubble Ansatz"*, JHEP 1211, 145 (2012), arxiv:1207.4204.

[26] J. Bartels, V. Schomerus and M. Sprenger, *"Heptagon Amplitude in the Multi-Regge Regime"*, JHEP 1410, 67 (2014), arxiv:1405.3658.

[27] L. F. Alday, D. Gaiotto, J. Maldacena, A. Sever and P. Vieira, *"An Operator Product Expansion for Polygonal null Wilson Loops"*, JHEP 1104, 088 (2011), arxiv:1006.2788.

[28] D. Gaiotto, J. Maldacena, A. Sever and P. Vieira, *"Bootstrapping Null Polygon Wilson Loops"*, JHEP 1103, 092 (2011), arxiv:1010.5009. ★ D. Gaiotto, J. Maldacena, A. Sever and P. Vieira, *"Pulling the straps of polygons"*, JHEP 1112, 011 (2011), arxiv:1102.0062.

[29] A. Sever and P. Vieira, *"Multichannel Conformal Blocks for Polygon Wilson Loops"*, JHEP 1201, 070 (2012), arxiv:1105.5748.

[30] S. S. Gubser, I. R. Klebanov and A. M. Polyakov, *"A semi-classical limit of the gauge/string correspondence"*, Nucl. Phys. B636, 99 (2002), hep-th/0204051.

[31] B. Basso, *"Exciting the GKP String at Any Coupling"*, Nucl. Phys. B857, 254 (2012), arxiv:1010.5237.

[32] N. Beisert, B. Eden and M. Staudacher, *"Transcendentality and crossing"*, J. Stat. Mech. 07, P01021 (2007), hep-th/0610251.

[33] G. Papathanasiou, *"Hexagon Wilson Loop OPE and Harmonic Polylogarithms"*, JHEP 1311, 150 (2013), arxiv:1310.5735.

[34] J. M. Drummond and G. Papathanasiou, *"Hexagon OPE Resummation and Multi-Regge Kinematics"*, JHEP 1602, 185 (2016), arxiv:1507.08982.

[35] S. Moch, P. Uwer and S. Weinzierl, *"Nested sums, expansion of transcendental functions and multiscale multiloop integrals"*, J. Math. Phys. 43, 3363 (2002), hep-ph/0110083.

[36] S. Moch and P. Uwer, *"XSummer: Transcendental functions and symbolic summation in form"*, Comput. Phys. Commun. 174, 759 (2006), math-ph/0508008.

[37] B. Ruijl, T. Ueda and J. Vermaseren, *"FORM version 4.2"*, arxiv:1707.06453.

[38] H. Frellesvig, D. Tommasini and C. Wever, *"On the reduction of generalized polylogarithms to Li_n and $Li_{2,2}$ and on the evaluation thereof"*, JHEP 1603, 189 (2016), arxiv:1601.02649.

[39] Y. Hatsuda, *"Wilson loop OPE, analytic continuation and multi-Regge limit"*, JHEP 1410, 38 (2014), arxiv:1404.6506.

[40] L. J. Dixon, J. M. Drummond and J. M. Henn, *"Bootstrapping the three-loop hexagon"*, JHEP 1111, 023 (2011), arxiv:1108.4461.

[41] L. J. Dixon, J. M. Drummond, M. von Hippel and J. Pennington, *"Hexagon functions and the three-loop remainder function"*, JHEP 1312, 049 (2013), arxiv:1308.2276.

[42] J. Bartels, A. Kormilitzin, L. N. Lipatov and A. Prygarin, *"BFKL approach and $2 \to 5$ maximally helicity violating amplitude in $\mathcal{N} = 4$ super-Yang–Mills theory"*, Phys. Rev. D86, 065026 (2012), arxiv:1112.6366.

[43] F. Brown, *"Single-valued Motivic Periods and Multiple Zeta Values"*, SIGMA 2, e25 (2014), arxiv:1309.5309.

[44] A. B. Goncharov, *"Multiple polylogarithms and mixed Tate motives"*, math/0103059.

[45] V. Chestnov, *"High-precision computation of observables in supersymmetric Yang–Mills theory"*, PhD thesis, DESY Hamburg, 2019.

[46] L. F. Alday, D. Gaiotto and J. Maldacena, *"Thermodynamic Bubble Ansatz"*, JHEP 1109, 032 (2011), arxiv:0911.4708.

[47] J. Bartels, V. Schomerus and M. Sprenger, *"The Bethe roots of Regge cuts in strongly coupled $\mathcal{N} = 4$ SYM theory"*, JHEP 1507, 098 (2015), `arxiv:1411.2594`.

[48] J. Bartels, *"Analytic properties of the 8-point scattering amplitude: conformal Regge pole and Regge cut contributions"*.

[49] J. Bartels, V. S. Fadin, L. N. Lipatov and G. P. Vacca, *"NLO Corrections to the kernel of the BKP-equations"*, Nucl. Phys. B867, 827 (2013), `arxiv:1210.0797`.

[50] A. V. Kotikov, L. N. Lipatov, A. I. Onishchenko and V. N. Velizhanin, *"Three-loop universal anomalous dimension of the Wilson operators in $\mathcal{N} = 4$ SUSY Yang–Mills model"*, Phys. Lett. B595, 521 (2004), `hep-th/0404092`.

[51] T. Gehrmann and E. Remiddi, *"Two loop master integrals for gamma* → 3 jets: The Planar topologies"*, Nucl. Phys. B601, 248 (2001), `hep-ph/0008287`.

[52] D. E. Radford, *"A natural ring basis for the shuffle algebra and an application to group schemes"*, Journal of Algebra 58, 432 (1979).

[53] J. Pennington, *"The six-point remainder function to all loop orders in the multi-Regge limit"*, JHEP 1301, 059 (2013), `arxiv:1209.5357`.

[54] L. J. Dixon, J. M. Drummond, C. Duhr, M. von Hippel and J. Pennington, *"Bootstrapping six-gluon scattering in planar $\mathcal{N} = 4$ super-Yang–Mills theory"*, PoS LL2014, 077 (2014), `arxiv:1407.4724`, in: *"Proceedings, 12th DESY Workshop on Elementary Particle Physics: Loops and Legs in Quantum Field Theory (LL2014)"*, pp. 077.

[55] C. Duhr and F. Dulat, *"PolyLogTools – Polylogs for the masses"*, `arxiv:1904.07279`.

[56] C. W. Bauer, A. Frink and R. Kreckel, *"Introduction to the GiNaC framework for symbolic computation within the C++ programming language"*, J. Symb. Comput. 33, 1 (2000), `cs/0004015`.

[57] S. Caron-Huot, *"Superconformal symmetry and two-loop amplitudes in planar $\mathcal{N} = 4$ super Yang–Mills"*, JHEP 1112, 066 (2011), `arxiv:1105.5606`.